Rb-Sr and Sm-Nd Study of the São Rafael Batholith, Rio Grande do Norte, NE Brazil

by

Denise H. Ketcham, B.S.

Thesis

Presented to the Faculty of the Graduate School

of The University of Texas at Austin

in Partial Fulfillment

of the Requirements

for the Degree of

Master of Arts

The University of Texas at Austin

August 1994

Rb-Sr and Sm-Nd Study of the São Rafael Batholith,

Rio Grande do Norte, NE Brazil

APPROVED BY

SUPERVISING COMMITTEE:

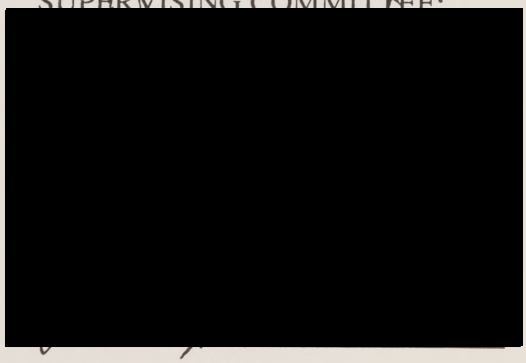

This thesis is dedicated to my two loves, my husband Rich, and my adopted country, Brazil.

ACKNOWLEDGMENTS

I wish to thank Dr. Leon E. Long most of all, for supervising me on this project and giving support, instruction and assistance, and also for being such a generous and caring person. I am indebted to Dr. Alcides N. Sial for suggesting this research project and for providing invaluable field support in Brazil. I would also like to thank Kleber de Souza for guiding me in the field and for sharing his research with me.

I am very grateful to Larry Mack, without whom I never could have completed any of my Sm-Nd research. I also thank Todd Housch for his willing assistance. Jim Connelly and Kathy Manser have provided my last hope for actually dating this pluton. The work they have done on the U-Pb zircon geochronology of my samples is greatly appreciated.

I am grateful to the Geology Foundation of the University of Texas for assistance with field expenses. I also greatly appreciate the comments and criticisms of my committee members Drs. Dan Barker and Sharon Mosher.

Finally, I would like to thank graduate students Lee Potter, Rob Reed, Stefan Boettcher and Lars Borg for their instruction and guidance. Thanks to my officemate, Alex Riter, for keeping me company these last two years. And thanks to my husband Rich for everything (i.e., help with those stupid computers, rock saws and stuff like that).

Frontispiece

The town of São Rafael, Rio Grande do Norte, Brazil with the Armando Gonçalves Ribeiro reservoir in the background.

ABSTRACT

Rb-Sr and Sm-Nd Study of the São Rafael Batholith,

Rio Grande do Norte, NE Brazil

By

Denise H. Ketcham, M.A.

The University of Texas at Austin, 1994

SUPERVISOR: Leon E. Long

During the Brasiliano (Pan-African) orogeny from 700 to 550 Ma, the geologic province of Borborema in northeast Brazil was intruded by more than 80 granitoid bodies, one of them the primary epidote-bearing São Rafael batholith located in the Seridó foldbelt. This unfoliated granite pluton is thought to be of very late Brasiliano age, perhaps between 600 and 550 Ma, based on field relations.

Twenty-four samples were analyzed isotopically, including 4 from a subtly different facies of the pluton (Serra-type), and 2 mafic enclaves. In general, the rocks have high Sr (655 ± 175 ppm) and low Rb (61 ± 9 ppm), with consequent low enrichment in radiogenic Sr. Three mineral-whole-rock isochrons provide

cooling ages of 0.49 ± 0.01 Ga. Data of the 18 epidote-bearing facies whole rocks plot as an amorphous "blob" on a Rb-Sr isochron diagram.

Inhomogeneous initial Sr ratios preclude the determination of a Rb-Sr age of crystallization. Somewhat more systematic data from the Serra samples suggest an age of about 0.6 Ga. Sr ratios of epidote-bearing facies rocks, projected back to 0.6 Ga, are high (0.713 ± 0.001), pointing to an ancient radiogenic crustal source.

Six whole-rock samples provide a Sm-Nd isochron apparent age of ~1.1 Ga, which is inconsistent with field evidence for late Brasiliano emplacement. Anomalous Sm-Nd data indicate that initial Nd ratios were also inhomogeneous, just as Sr initial ratios were. Strongly negative values of $\varepsilon Nd_{0.6Ga}$ (-18 to -21) imply a source relatively enriched in Nd, a characteristic of continental crust. Depleted mantle model ages are consistent with minimum crust-formation ages of 2.7 ± 0.3 Ga. The $\varepsilon Nd_{0.6Ga}$ values, depleted mantle model ages and high initial Sr ratios of the pluton (at 0.6 Ga) all suggest that the São Rafael source rock was ancient crust. This conclusion is also consistent with the existence of Archean basement in northeastern Brazil.

Preliminary U-Pb zircon geochronology of a single fraction yielded a highly discordant (44%) data point, with a $^{207}Pb/^{206}Pb$ age of 2.0 Ga. This result

is interpreted as indicating that relict zircon cores are present, containing an inherited component whose age is older than 2.0 Ga.

Formed at about 0.6 Ga, apparently by partial melting of Archean crust, the São Rafael magma mixed sufficiently to attain a distinctively uniform physical appearance and chemical-mineralogical composition. The magma, however, consisted of partial melts with different isotopic characters which failed to homogenize completely.

TABLE OF CONTENTS

LIST OF TABLES

LIST OF FIGURES

INTRODUCTION

During the Brasiliano/Pan-African orogeny from about 700 to 550 Ma, the geologic province of Borborema in northeast Brazil was intruded by large numbers of granitoid plutons. One of these is the São Rafael batholith, located in the Seridó Foldbelt. Although the structural geology of this foldbelt is well known, there are few geochronological data. The São Rafael pluton is thought to have been intruded very late during the Brasiliano event, perhaps between 600 and 550 Ma based on field relations. The intent of this study was to date the São Rafael batholith by the Rb-Sr and Sm-Nd methods, and to characterize the source rock of the magma.

The São Rafael batholith is particularly interesting because it contains epidote as a primary phase. Other magmatic epidote-bearing plutons in the neighboring Cachoeirinha-Salgueiro Foldbelt (CSF) have been extensively studied and suggest an existence during the Proterozoic of an LILE (Large-Ion Lithophile Element)-enriched mantle source under northeast Brazil (Sial and Ferreira, 1990). The São Rafael pluton is petrographically similar to calc-alkalic granitoid plutons of the CSF. However, trace element and oxygen-isotope data, and P-T data for São Rafael indicate that it had a significantly different origin (Sial, 1990; Sial and Ferreira, 1990; Sial and others (in press)). The chemical

disparities are the result of different source regions and/or differences in tectonic evolution of the two foldbelts.

LOCATION AND DESCRIPTION OF STUDY AREA

The study area is located between 05°40'42"S and 06°00'00"S, and between 36°45'32"W and 36°56'25"W in the state of Rio Grande do Norte, northeast Brazil (Fig. 1). It is reached by traveling 200 km west from Natal on BR 304 almost to the city of Açu and then proceeding 21 km southeast on RN-14.

The area consists mainly of a low rolling piedmont whose panorama is broken by granite inselbergs whose relief may exceed 450 meters (Figs. 2 and 3). These small mountains are important local geographic features and have given their names to many of the settlements around their bases, e.g., Serra Branca and Serra da Pindoba.

Falling within the "Polígono das secas," an area of 1.8 million km^2 subject to long droughts, the region has a harsh climate. It is semi-arid and hot, with temperatures generally higher than 25°C. Rainfall is skimpy and irregular, amounting to as little as 500 mm in a year. This northeastern triangle of Brazil is called the sertão, meaning arid and remote interior. The vegetation consists of the caatinga, made up of xerophytes such as cactus and other drought-resistant plants. In the dry season the caatinga plants lose their leaves and they sprout again at the first rain.

Economically the region is very poor. Subsistence farming, fishing and grazing of cattle and sheep are the main industries. In the past, deposits of

Figure 1. Location map of study area.

Figure 2. Serra Branca inselberg, composed of the Serra facies of the São Rafael batholith.

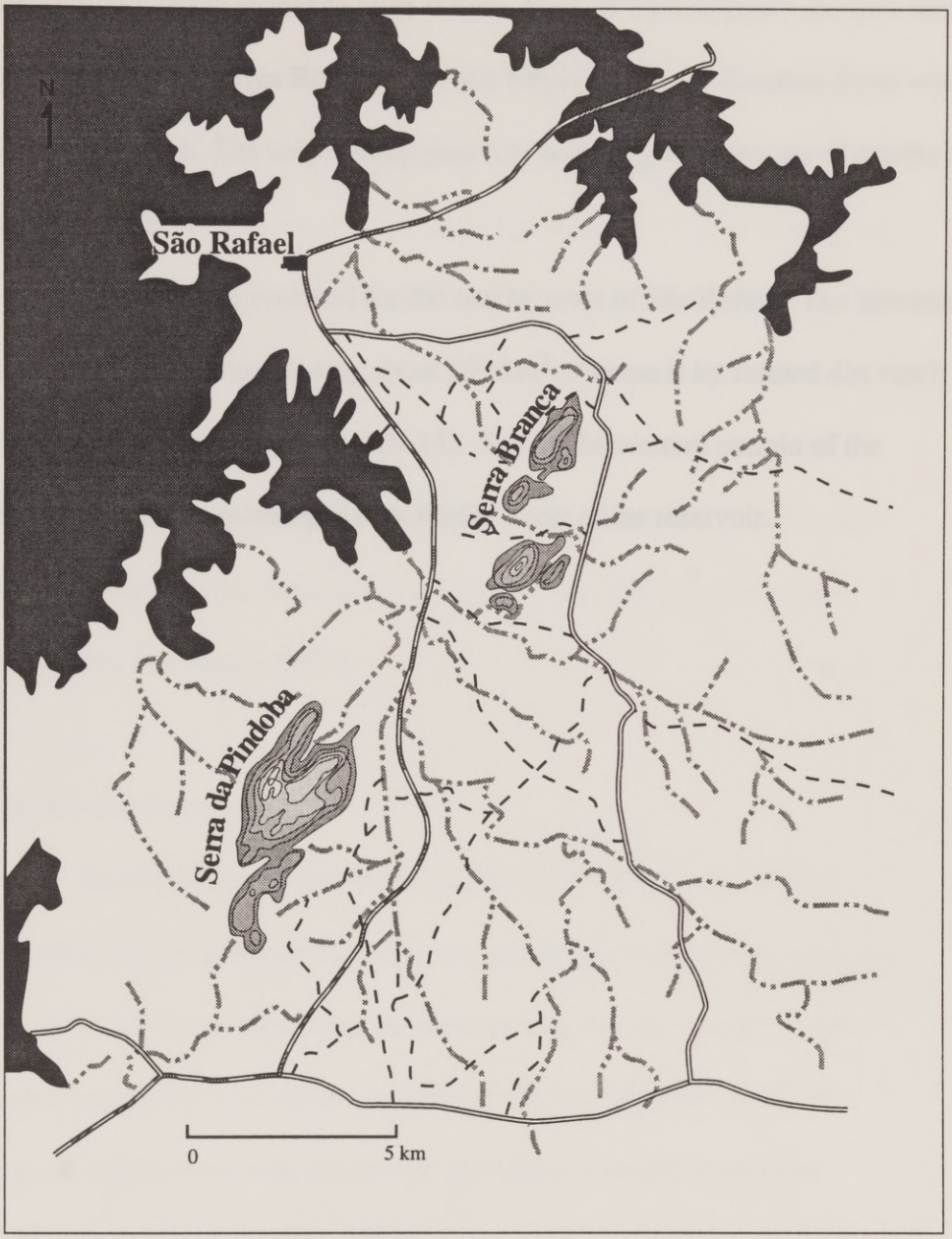

Figure 3. Map of field area. Dark shaded areas are the Armando Ribeira Gonçalves reservoir. Lighter shaded areas represent topographic highs with a contour interval of 50 m. Modified from Açu quadrangle, published by SUDENE, 1985.

scheelite, barite and monazite were mined. Most of these deposits are now under the Armando Gonçalves Ribeiro reservoir formed when the Piranhas River was dammed (Fig. 3). The only mining presently occurring is quarrying of marble and plutonic rocks.

The batholith is named for the nearby town of São Rafael. The intrusion is well-exposed, encompassing about 250 km^2. Access is by limited dirt ranch roads and one paved highway (RN-14). Part of the western margin of the batholith has been submerged beneath the water of the reservoir.

REGIONAL GEOLOGY

TECTONIC PROVINCES OF NE BRAZIL

Northeast Brazil is composed of two tectonic provinces: the Parnaíba Province which includes the Gurupi Belt and the São Luis craton, a remnant of the West African craton, and the Borborema Province (Almeida and others, 1981). The Borborema Province includes most of northeast Brazil, covering an area of 4×10^5 km^2. It is delimited by the Parnaíba province to the west, the São Francisco craton to the south, and the coastal basins and continental margin (Fig. 4) (Almeida and others, 1981; Caby and others, 1991).

Borborema Province

The Borborema Province is located on the Atlantic shield and coincides with a system of foldbelts formed during the Brasiliano orogeny, during which the province was transformed into a craton. Much of this region has a semi-arid climate, resulting in the development of areally extensive pediments with altitudes in rare places reaching more than 1000m (Almeida and others, 1981).

The most prominent tectonic feature of this province is the system of large-scale transcurrent faults that both delineate and cut juxtaposed

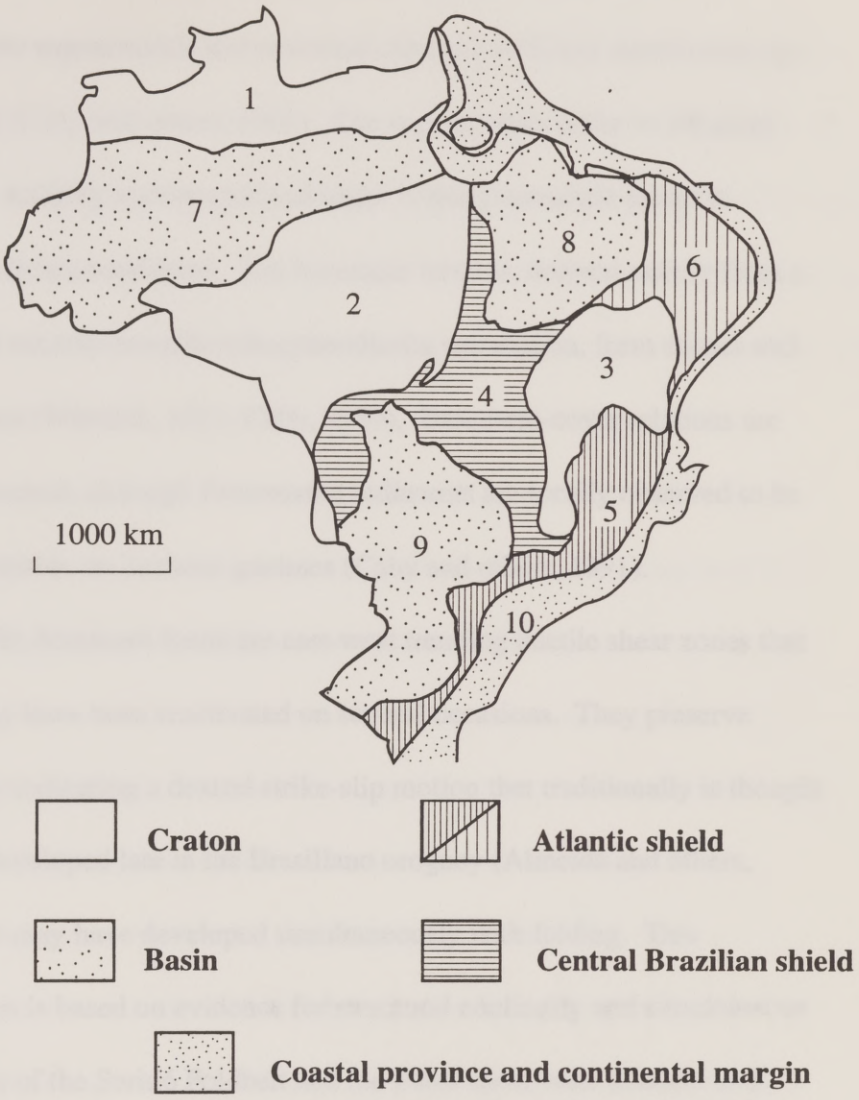

Figure 4. Structural provinces of Brazil. 1 = Rio Branco; 2 = Tapajós; 3 = São Francisco; 4 = Tocantins; 5 = Mantiqueira; 6 = Borborema; 7 = Amazonian; 8 = Parnaíba; 9 = Paraná; 10 = coastal province. From Almeida and others (1981).

domains of extensively deformed foldbelts. The latter consist of Proterozoic supracrustals and reworked Archean to Trans-Amazonian age basement (Caby and others, 1991). The supracrustals differ in lithology and were variably metamorphosed under lower greenschist-facies to granulite-facies conditions. The basement terrains, derived mainly from a reworked tonalite-trondjhemite-granodiorite association, form domes and half-domes (Wernick, 1981; Caby, 1989). Basement-cover relations are often obscured, although Proterozoic sediments are locally observed to be unconformable on Archean gneisses (Caby and others, 1991).

The dominant faults are east-west trending ductile shear zones that apparently have been reactivated on several occasions. They preserve structures indicating a dextral strike-slip motion that traditionally is thought to have developed late in the Brasiliano orogeny (Almeida and others, 1981) but may have developed simultaneously with folding. This conclusion is based on evidence for structural continuity and simultaneous formation of the Seridó Foldbelt and the Patos shear zone (Corsini and others, 1991). Also present are northeast-trending transcurrent faults associated with the northeast-trending fold belts of the central and eastern-central portions of the province.

Major Tectonic Events. Although geochonological data in the Borborema province are few and of somewhat limited geographic distribution, they suggest that northeast Brazil has experienced three major tectonothermal events at 2.6 Ga (Archean), 2.0 Ga (Trans-Amazonian), and 700-550 Ma during the Brasiliano/Pan-African orogeny. The Archean event is well documented by whole rock Rb-Sr isochrons that date the gneissification of the basement at ~2.6 Ga (Brito Neves and others, 1975; Pessoa and others, 1986).

Evidence for a 2.0 Ga orogenic event in northeast Brazil is slim. Ages of 2.0 to 1.8 Ga obtained on orthogneisses have been interpreted by Jardim de Sá and others (1987) as synkinematic to F2 generation folds of the Trans-Amazonian cycle. Caby (1989) supports an anorogenic interpretation for these plutons and suggests that they may have been misinterpreted as synkinematic; at this time, irrefutable evidence for a Trans-Amazonian event in this foldbelt remains elusive.

Almeida and others (1981) first proposed that this province had experienced a major late Proterozoic event. Caby (1989), Caby and others (1991) and Sial and Ferreira (1990) assert that the major event occurred between 700 and 550 Ma during the Brasiliano orogeny. This conclusion is supported by isotopic data. Most of the Rb-Sr and K-Ar mineral (cooling) ages lie in the range of 650-450 Ma (Caby and others, 1991). Syn- to late-

tectonic plutons that intruded the province have yielded Brasiliano Rb-Sr whole-rock isochron ages. The large volume of these granitoid plutons, whose emplacement in many instances was controlled by shear zones, indicates that the Brasiliano orogeny was a major tectonothermal event (Caby, 1989).

The Brasiliano orogeny is regarded as a thermotectonic reworking event, resulting from a collision between the West African and São Francisco/Congo cratons and a Late Proterozoic mobile domain composed of the Hoggar, Nigeria, Borborema, and Central Africa polycyclic basement provinces (Fig. 5) (Castaing and others, 1993). The resulting orogen may have resembled the Tibetan plateau, with shortening of hinterland terranes accomplished by intracontinental oblique megathrusts and lateral expulsion of blocks by deep transcurrent shear zones (Jardim de Sá and Sá, 1987). The large volume of accompanying intrusives probably represents a distal manifestation of east-directed subduction of oceanic crust under the Hoggar/Nigeria/Boborema shields. Deep magma sources caused gradual heating of shallower crustal levels that promoted metamorphism and anatexis and contributed to regional deformation (Jardim de Sa and others, 1987).

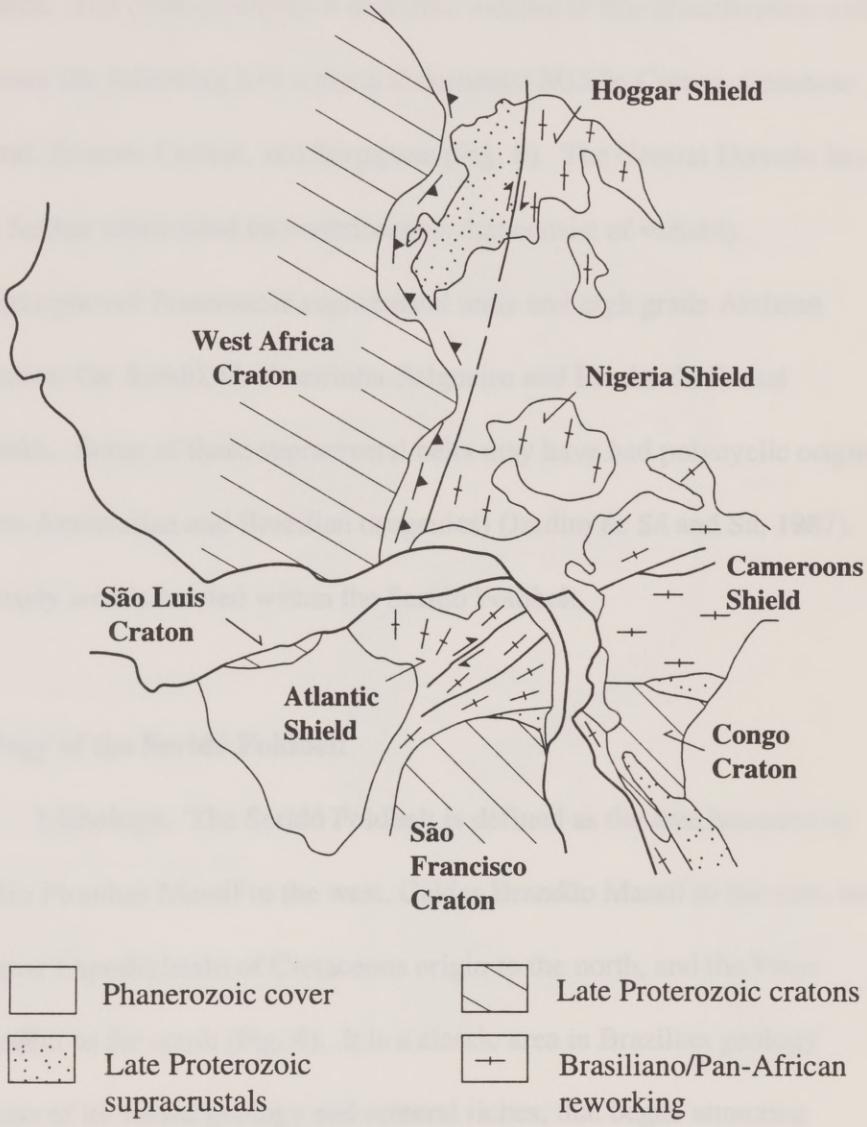

Figure 5. Tentative geologic correlations of West Africa and northeast Brazil and pre-rift plate reconstruction. After Jardim de Sá and Sá (1987).

Structural Domains of the Borborema Province. Santos and others (1984) divided the Borborema province into a number of structural domains. Sial (1987) adopted a modified version of this classification and proposes the following five structural domains: Middle Coreau, Cearense, Central, Eastern-Central, and Sergipean (Fig. 6). The Central Domain has been further subdivided into subdomains that consist of variably metamorphosed Proterozoic supracrustal units and high grade Archean basement: the Seridó, Cachoeirinha-Salgueiro and Riacho do Pontal foldbelts. Some of these supracrustal belts may have had polycyclic origins (Trans-Amazonian and Brazilian orogenies) (Jardim de Sá and Sá, 1987). My study area is located within the Seridó Foldbelt.

Geology of the Seridó Foldbelt

Lithology. The Seridó Foldbelt is defined as the area bounded by the Rio Piranhas Massif to the west, Caldas Brandão Massif to the east, the Potiguar (Apodi) basin of Cretaceous origin to the north, and the Patos lineament to the south (Fig. 6). It is a classic area in Brazilian geology because of its varied geology and mineral riches, that began attracting researchers as early as 1910. The geology is dominated by metasediments and metavolcanic rocks metamorphosed under greenschist to amphibolite

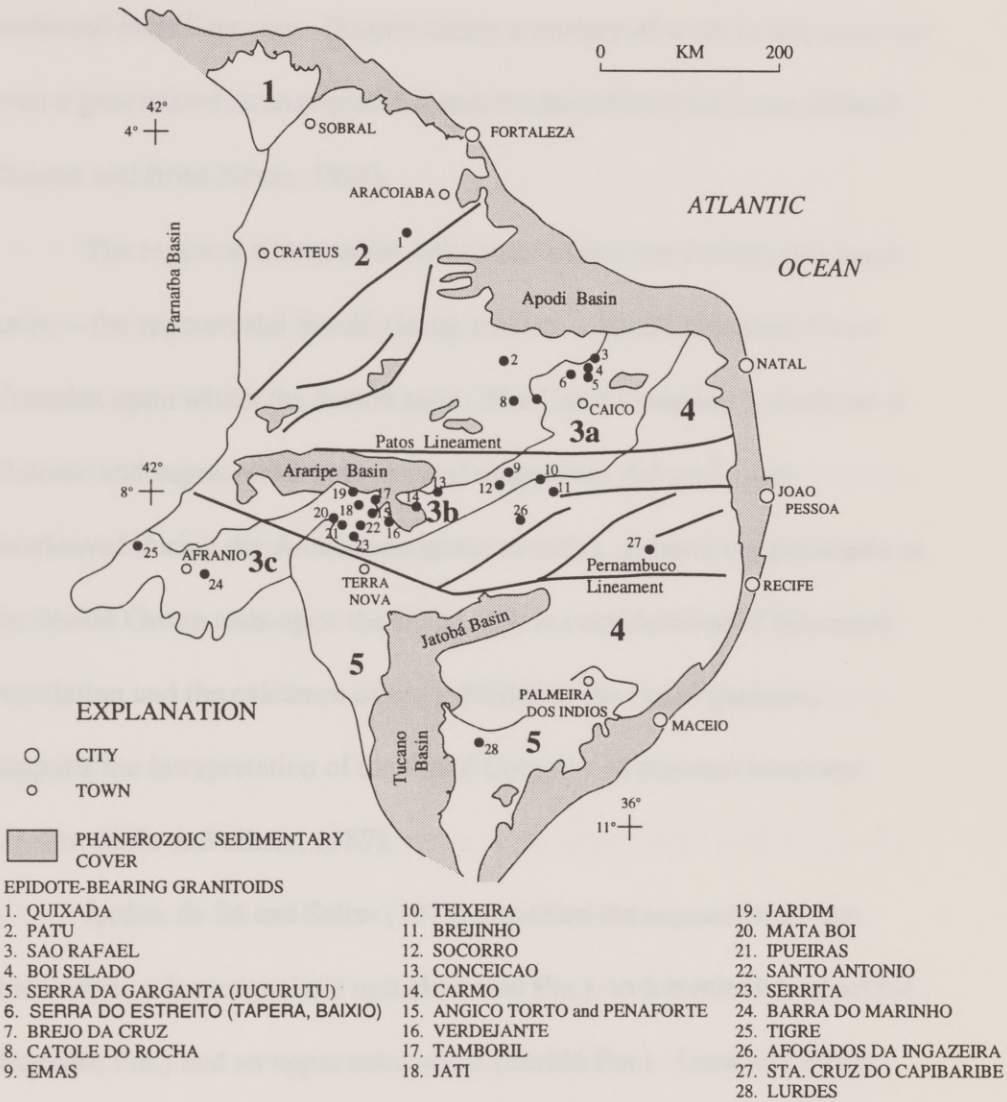

Figure 6. The structural domains of the Borborema province:
1 = Middle Coreau, 2 = Cearense, 3 = Central– 3a. Seridó Foldbelt,
3b. Cachoeirinha-Salgueiro Foldbelt, 3c. Riacho do Pontal Foldbelt,
4 = Eastern-Central, 5 = Sergipean. Modified from Sial and others (in press).

grade conditions and that rest upon Archean gneissic basement. Both the supracrustals and basement are intruded by numerous granitoid rocks of presumed Brasiliano age. Despite nearly a century of work in this area, not even a generalized stratigraphic column for the foldbelt has been defined (Santos and Brito Neves, 1984).

The regional stratigraphic column in widest use defines two major units;—the supracrustal Seridó Group and the Archean basement Caicó Complex upon which the Seridó rests. The Caicó Complex is made up of plutonic and supracrustal gneisses and migmatites deformed and interleaved during the Archean orogenic event(s). A basal conglomerate in the Seridó Group rests upon the Caicó and, in consideration of structural correlation and the existence of older fabrics in the Caicó gneisses, supports the interpretation of the Caicó Complex as regional basement (Jardim de Sa and others, 1987).

Jardim de Sá and Salim (1978) classified the supracrustals into three units: a lower gneissic unit (Jucurutú Fm.), an intermediate quartzite (Equador Fm.) and an upper mica schist (Seridó Fm.). Lima and others (1980) proposed a similar stratigraphy, but place the Equador Formation at the bottom of the supracrustal succession. The supracrustal stratigraphic columns of Jardim de Sá and Salim (1978) and Jardim de Sá (1978) have

subsequently gained the most acceptance because clasts of the Jucurutú Fm. have been found in the Equador Fm., supporting an intermediate position for the Equador (Lima, 1987).

The Jucurutú Fm. is comprised predominantly of alternating biotite-rich and quartz-feldspar-rich paragneisses, or biotite paragneisses with intercalated marble, calc-silicate, amphibolite, quartzite, iron-formation, metavolcanics, and a basal metaconglomerate. The Equador Fm. is a quartzite with minor amounts of metaconglomerate, marbles and calc-silicate. The uppermost unit, the Seridó Fm., is a mica schist with marbles and calc-silicate layers close to its base. Whereas the Jucurutú and Equador Fms. are regarded as products of pre-orogenic sedimentation, the Seridó Fm. is interpreted to represent turbidite/flysch deposits (Jardim de Sá and others, 1987).

Structure. The Seridó foldbelt is characterized by a NNE- to- NE tectonic grain of elongated basement domes, Proterozoic foldbelts, and steeply-dipping strike-slip faults that parallel the fold trends. The regional fabric becomes arcuate approaching the Patos lineament into which the subordinate shear zones converge. The shear zones are closely associated with the foldbelts, which form synformal structures (Jardim de Sá and Sá, 1987; Caby and others, 1991).

Shear zones occur on the scale of 10 to 100 meters wide and are predominantly dextral. They display retrogressive greenschist-facies mylonitic fabrics (Caby and others, 1991). Coeval shearing and injections of granodiorite veins and deformation of syntectonic granites by shear zones suggest that shearing occurred late in the deformation history and may have been active during emplacement (and indeed perhaps controlled the emplacement) of many of these granitoid bodies (Caby and others, 1991).

The basement and supracrustals show similar mineral and stretching lineation trends (Caby and others, 1991). Archean gneisses display a flat-lying foliation parallel to the S1 foliation of overlying Proterozoic rocks (Caby and others, 1991). The Seridó Fm. is characterized by upright folding with sub-horizontal axes and axial planar cleavage. Refolding of the S1 cleavage by F2 folds is common, although F2 folds vary in axial orientation (Caby and others, 1991).

Finite strain estimated from study of the fabric of a metaconglomerate suggests an intense deformation (Archanjo, 1988). Archanjo (1988) calculated horizontal extension of up to 500% and shortening normal to foliation of 50-70%.

Regional metamorphism took place under relatively low P and high T conditions. In some metapelites affected by open folding, large euhedral poikiloblastic andalusite, cordierite, staurolite, and biotite grew in connection with synkinematic emplacement of granitoid plutons (Caby and others, 1991).

Jardim de Sá (1984) and Jardim de Sá and others (1987) have continued to argue for a possible pre-Brasiliano age of the main metamorphism and a polyphase deformational history for the foldbelt. They base their arguments on relationships among pluton emplacement, cross-cutting foliations, and stratigraphic information from outside the Seridó foldbelt.

Post-Archean Granitoid Plutons. Despite an absence of geochemical data for many of the granitoid bodies in the Seridó, these intrusions are of great interest to the interpretation of the tectonic history of the region because much is known about their relation to the different regional phases of deformation. The structure and field relations of these bodies have been best studied and described by Jardim de Sá and his co-workers.

Post-Archean intrusive bodies in the region have been classified into generations G2, G3, and G4 that range from pre- to post-tectonic with

respect to two main regional folding phases (F2, F3) (Jardim de Sá, 1981; Jardim de Sá and others, 1987; Sial, 1987). Figure 7 is a schematic block diagram of the Seridó Foldbelt showing the relationships of the G2-4 bodies relative to regional structures. G1 bodies constitute basement orthogneisses of Archean age (e.g., Caicó Complex) (Sial, 1987).

Extensive gneissic foliation is developed in Jardim de Sá's G2 bodies which were previously interpreted as basement. G2 bodies consist of augen gneisses and orthogneisses formed pre- to syn-tectonically by anatexis and feldspathization of the Caicó Complex basement rocks (Sial, 1987). Where they occur within the Seridó Group, almost everywhere they are intruded at the level of the Jucurutú Fm. (Jardim de Sá and others, 1987). (Jardim de Sá and others (1987) interpret this observation as support for a turbidite/flysch origin for the Seridó Fm.) A banded appearance defined by alternating porphyritic and non-porphyritic layers, varying abundances of ferromagnesian minerals and occasional layers enriched in accessory minerals is interpreted as deformed magmatic layering (Caby and others, 1991). The G2 bodies are concordant to the S2 fabric, but commonly cross-cut the gneissic layering of Caicó Complex gneisses (Jardim de Sá and others, 1987).

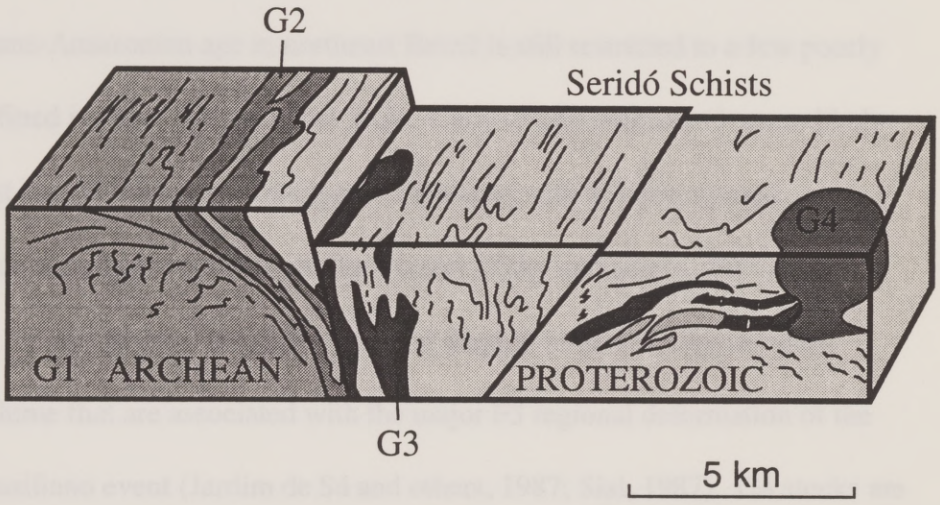

Figure 7. Schematic block diagram of the Seridó Foldbelt, illustrating the structural relationshps of G1-G4 generations. Modified from Caby et al., 1991.

The timing of emplacement of G2 bodies is somewhat ambiguous. Whole-rock Rb-Sr data for G2 orthogneisses yield poorly defined isochrons of 2.2 to 2.0 Ga (Jardim de Sá and others, 1987). Jardim de Sá and others (1987) consider the G2 granites as synorogenic bodies related to the Trans-Amazonian cycle. However, the evidence for a major orogenic event of Trans-Amazonian age in northeast Brazil is still restricted to a few poorly defined isotopic ages of about 2 Ga. Caby (1989) considers it more likely that the G2 bodies are anorogenic intrusions with a superimposed Brasiliano tectono-metamorphic imprint (Caby and others, 1991).

G3 plutons consist of younger diapiric bodies of considerable volume that are associated with the major F3 regional deformation of the Brasiliano event (Jardim de Sá and others, 1987; Sial, 1987). G4 stocks are biotite granite, granodiorite, or muscovite-biotite-leucogranite that postdate the F3 phase and are of syn- to late- F4 age. The style of emplacement of G4 aplites and pegmatites was commonly controlled by brittle or semi-brittle structures (Jardim de Sá and others, 1987).

Jardim de Sá and Sá (1987) have classified the G3 granitoid rocks into three main suites: the "diorite" suite, "horsetooth" granites, and biotite granites or muscovite-biotite leucogranites.

The diorite suite consists of mafic intrusions that range from gabbro to diorite, quartz diorite to tonalite, and hornblendite (Jardim de Sá and others, 1987). Members of this differentiated suite display a conspicuous foliation consisting of composite ballooning and regional S3 fabrics, but they are discordant to the S2 foliation and less strained than the G2 granitoid plutons and supracrustals that they intrude (Jardim de Sá and others, 1987). Based on these criteria, the suite appears to be younger than the G2s, having instead a syn-F3 intrusive origin. Most of the diorite suite bodies occur encased by younger granitoid rocks, but they also occur as isolated plutons. Contact metamorphic aureoles are present around the largest bodies (Jardim de Sá and others, 1987).

The second suite, referred to as horsetooth granites, accounts for the largest volume of G3 bodies. They range from granitic to quartz monzonitic and are characterized by 3 to 10 cm K-feldspar phenocrysts that endow the horsetooth texture for which they are named. The K-feldspar phenocrysts typically define a flow foliation that has been further modified by the regional deformation (F3) imprint. The granites display a syntectonic S3 foliation defined by mica and quartz. Contact with host rocks is generally sharp without a metamorphic aureole (Jardim de Sá and others, 1987).

Mafic inclusions in the horsetooth granites occur as amphibole-rich clasts (possible cumulates) and two kinds of dioritic mafic microgranular enclaves (MME) (Jardim de Sá and others, 1987). One family of MME contains K-feldspar phenocrysts, and the enclaves are rounded with diffuse contacts. The second consists of angular blobs that lack K-feldspar and have sharp contacts. These mafic enclaves are interpreted as reflecting a continuum of initial states of magma solidification, ranging from already solidified inclusions to blobs of viscous mafic magma that became entrained in the felsic host magma (Jardim de Sá and others, 1987). The MMEs that were apparently included as a mafic liquid indicate that mafic melts were contemporaneous with the porphyritic magmas. Some contacts show that a high degree of mechanical mixing of K-feldspar phenocrysts and matrix occurred between the MME and felsic host (Jardim de Sá and others, 1987).

The third suite of G3 rocks is characterized by the absence of modal amphibole, amphibolite inclusions, and MMEs. These syn- to late-F3 bodies consist mostly of equigranular biotite granites or muscovite-biotite leucogranites. A composite ballooning + S3 foliation is well developed. The few porphyritc plutons in this suite are characterized by sharp contacts,

whereas others are surrounded by migmatites derived from the host rocks at the time of emplacement (Jardim de Sá and others, 1987).

Geochronology of Seridó Granitoid Plutons. Except for a few Rb-Sr whole-rock data, very little isotope geochronology is available from the Seridó foldbelt. Macedo and others (1984) obtained a Rb-Sr whole-rock isochron age of 2086 ± 68 Ma and an initial Sr ratio (R_0) of 0.712 on a G2 orthogneiss located approximately 21 km to the SW of Angicos (Fig. 8). The host augen gneiss yielded an "errorchron" of 2117 ± 291 Ma (Macedo and others 1984). Jardim de Sá and others (1987) regard these as minimum emplacement ages and indicators of the timing of the regional F2 deformation, which was the first event to affect rocks of the Seridó Group and the cause of the reworking of Archean basement. G2 gneisses at Serra Negra do Norte (Fig. 8) give an age of 2030 ± 84 Ma with an initial Sr ratio of 0.707 (Macedo and others, 1984).

Caby (1989), who supports an anorogenic origin for the G2 rocks, proposes that these intrusions are rift-related. Jardim de Sá and others (1987) argued against an anorogenic origin; they favor structural reworking and rejuvenation of basement gneisses occurring at 2 Ga based on poorly defined Rb-Sr whole-rock isochron ages of ca. 2 Ga, obtained on some

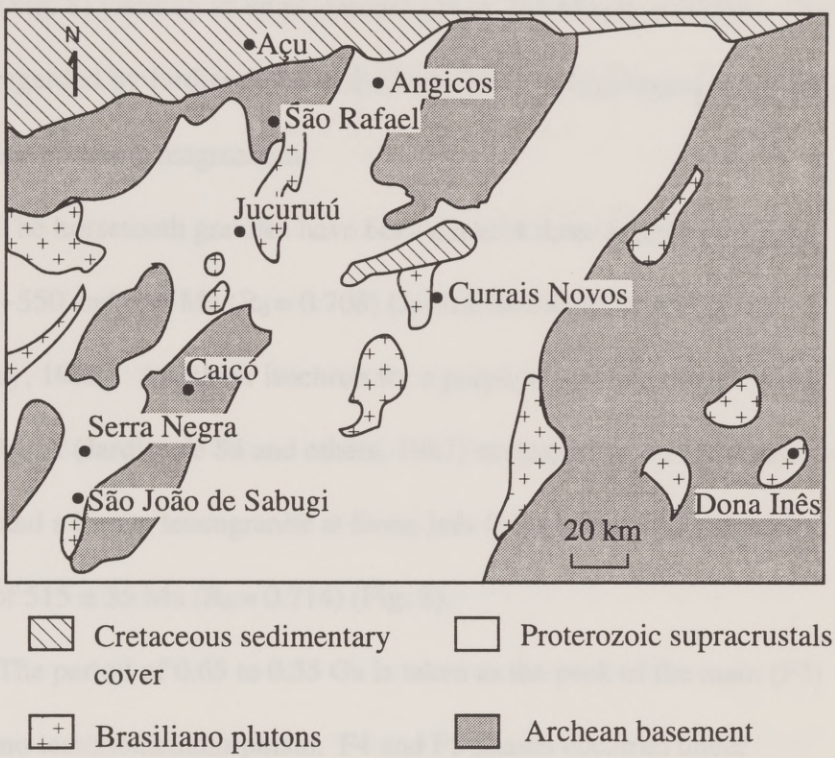

Figure 8. Generalized geologic map of the central Seridó foldbelt, with locations of towns and cities. Modified from Jardim de Sá and others (1987).

Caicó Complex orthogneisses (e.g. t =1977 ± 32 Ma, R_0 = 0.7081 ± 0.0009).

A diorite suite of the G3 generation was dated near São João de Sabugi (Fig. 8) yielding an emplacement age of 765 Ma (R_0 = 0.706). This date is regarded by Jardim de Sá and others (1987) as the beginning of the Brasiliano orogenic magmatism.

The horsetooth granites have been dated at three localities, giving ages of ~550 and 660 Ma (R_0 = 0.708) (Jardim de Sá and others, 1987; McMurry, 1982). An Rb-Sr isochron for a porphyritic leucogranite of the Acarí Massif (Jardim de Sá and others, 1987) corresponds to 575 Ma (Ro = 0.707), and a biotite leucogranite at Dona Inês (McMurry, 1982) provides an age of 515 ± 35 Ma (R_0 = 0.714) (Fig. 8).

The period of 0.65 to 0.55 Ga is taken as the peak of the main (F3) Brasiliano tectonometamorphism. F4 and F5 phases occurred under retrogressive conditions and are thought to have terminated around 0.5 Ga, the peak in the distribution of K-Ar and mineral Rb-Sr cooling ages.

Tectonic Setting. The tectonic regime under which the G2 granitoid rocks were emplaced is not well understood. For the G3 and G4 intrusions (0.75 to 0.50 Ga), much more is known. The driving force of the Brasiliano-age deformation and intrusive igneous activity in the Seridó was

the east-directed subduction of oceanic crust under the São Francisco craton. Partial melting of mantle or amphibolitic crust led to the formation of the G3 dioritic melts (Jardim de Sá and others, 1987). These may have been trapped at the base of the crust where they promoted melting and interacted with granitic magmas, resulting in magma mixing (evidenced by the association of felsic and mafic rocks and presence of inclusions of mafic magma blobs in more felsic bodies). Intrusion of these large volumes of magmas caused regional heating and metamorphism. The late porphyritic and equigranular leucogranites apparently formed from melting of lower crustal sources and metasediments (Jardim de Sá and others, 1987).

Geology of the Field Area. Geology field studies in the Seridó region began in the 1950s. Many of them were carried out by professors and students from the Federal University of Rio Grande do Norte in Natal and the Federal University of Pernambuco in Recife. Mining companies also conducted substantial exploration for molybdenum, tungsten and other ores.

Geologic mapping of the Açu quadrangle was done in 1968 by Edilton José dos Santos for SUDENE (Superintendencia de Desenvolvimento do Nordeste) and the Ministry of the Interior (Fig. 9).

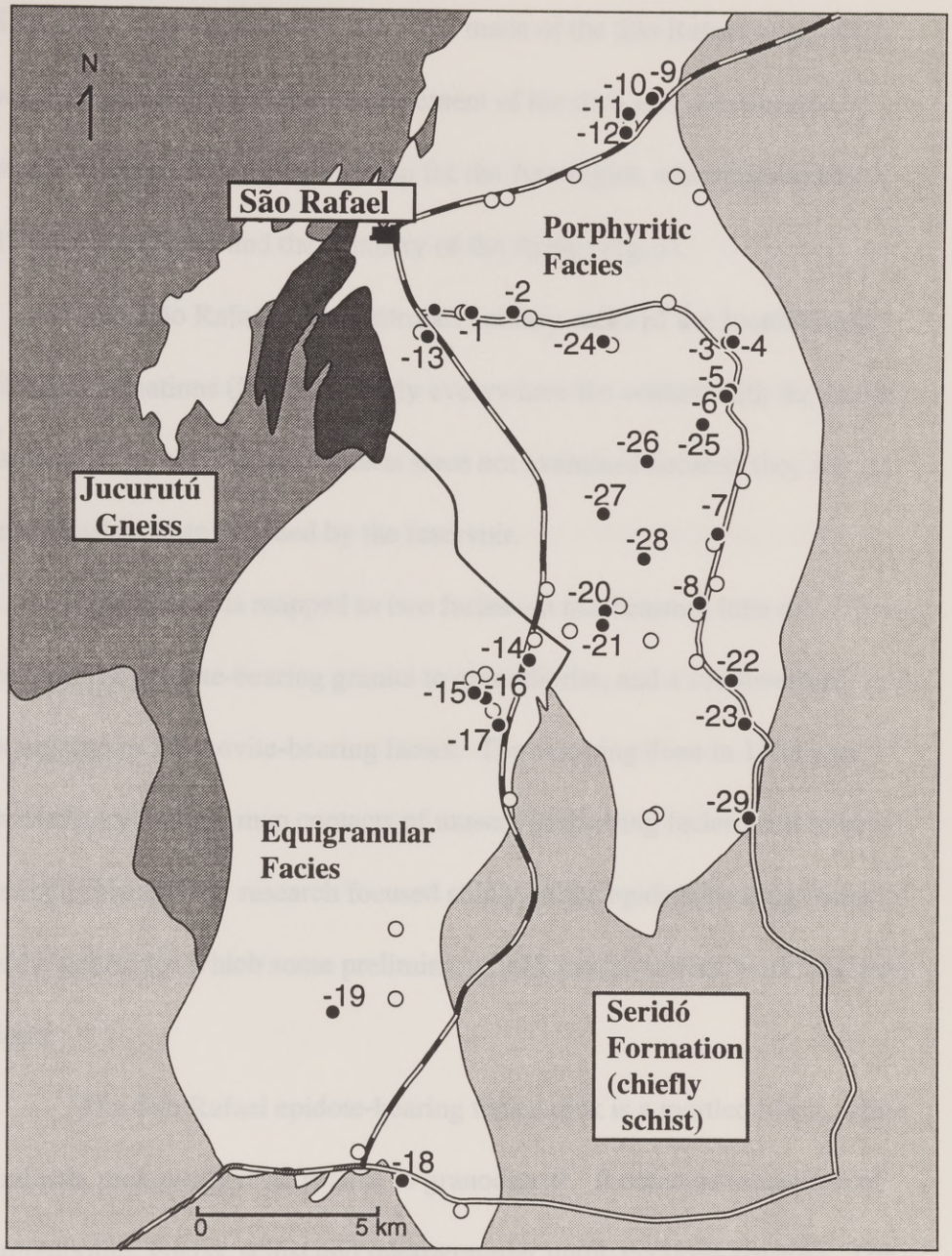

Figure 9. Geologic map of field area. Solid circles are sampling locations from this study (DSR- series). Hollow circles are de Souza's sample locations (KSR- series). Modified from Santos, 1964.

This map is the only one to have been made of the São Rafael area, and it was completed prior to the emplacement of the dam and construction of roads. The latest topographic map for the Açu region was published in 1985 by SUDENE and the Ministry of the Army (Fig. 3).

The São Rafael pluton intrudes country rocks of the Jucurutú and Seridó Formations (Fig. 9). Nearly everywhere the contact with the schist is covered by soil. Other contacts were not examined because they are inaccessible or are flooded by the reservoir.

The pluton is mapped as two facies—a northeastern lobe of porphyritic epidote-bearing granite to granodiorite, and a southwestern equigranular muscovite-bearing facies. The mapping done in 1968 was preliminary and the map contacts of muscovite-bearing facies need to be refined further. My research focused solely on the epidote-bearing facies ofthe pluton for which some preliminary field and laboratory work has been done.

The São Rafael epidote-bearing facies rock is a mottled black, white and pale pink porphyritic granite to granodiorite. It contains inclusions of amphibolite, gneiss, schist and microgranular mafic enclaves (MME). The MMEs are quartz dioritic and display pillow-like structures in several

localities, indicative of their incorporation as a ductile magma rather than as a solid.

Perhaps the most striking feature of the area consists of the Serras (inselbergs). Both in the field and on a topographic map (Fig. 3), the mutual alignment of these bodies in a consistent N-NE trend is apparent. Because they are included as part of the porphyritic epidote-bearing facies, they do not stand out on the geologic map (the petrology of the rocks that comprise these topographic highs had not been examined prior to this study). They appear to consist of a separate facies of the primary epidote-bearing magma, of similar mineralogy to that of the main facies except that overall the rock contains lower abundances of mafic minerals. The relief and aligned nature of the inselbergs, however, hint at an origin that differs at least slightly from that of the main facies. These rocks are more closely examined in this thesis.

PREVIOUS WORK

Much of the petrographic and geochemical data available for the São Rafael batholith are the result of work done by Kleber de Souza (unfinished Master's thesis from the Federal University of Pernambuco, Recife). Souza studied the petrography of the epidote-bearing facies, equigranular muscovite-bearing facies, mafic enclaves, and leucocratic dikes. He also arranged for major and minor element analyses to be made of these facies. Souza's work has never been completed and it seems unlikely that it will be published. It is very important to the characterization of the pluton, however, and thus I have included relevant portions of his work in this thesis and have added to them descriptions and geochemical data for the Serra facies. Figure 9 shows sampling locations. Souza's samples comprise the KSR- series (after Kleber São Rafael), and my samples comprise the DSR- series (Denise São Rafael). My samples were collected near many of Souza's sample localities and as often as possible from the same outcrop.

PETROGRAPHY

Primary Epidote-bearing Facies

The main facies of the São Rafael batholith consists of a light gray to white porphyritic granite to quartz monzodiorite (Fig. 10). This rock is characterized by microcline phenocrysts (3 to 5 cm, rarely 7 cm) in an equigranular, medium- to coarse-grained groundmass. It is massive and homogeneous (although in some places K-feldspar phenocrysts form aggregates).

Table 1 shows the mineral modes of main facies samples. In order of decreasing abundance, the minerals are plagioclase, quartz, microcline, biotite, amphibole, epidote, titanite, apatite, opaques, zircon, and fluorite (?). Alteration minerals consist of sericite, chlorite, and calcite.

Plagioclase occurs as subhedral to anhedral, rounded equant to prismatic crystals. The plagioclase commonly shows oscillatory zoning and polysynthetic twinning. Occasional pericline twinning also occurs. Some of the crystals show "synneusis" texture described by Vance (1969). Myrmekite, an intergrowth of vermicular quartz in plagioclase, occurs close to contacts with microcline. Plagioclase contains inclusions of apatite, biotite, and rarely amphibole and fluorite. It alters to sericite and calcite.

Quartz occurs as anhedral, equant crystals whose sizes vary from small inclusions to masses several mm across. Almost all quartz crystals are strained,

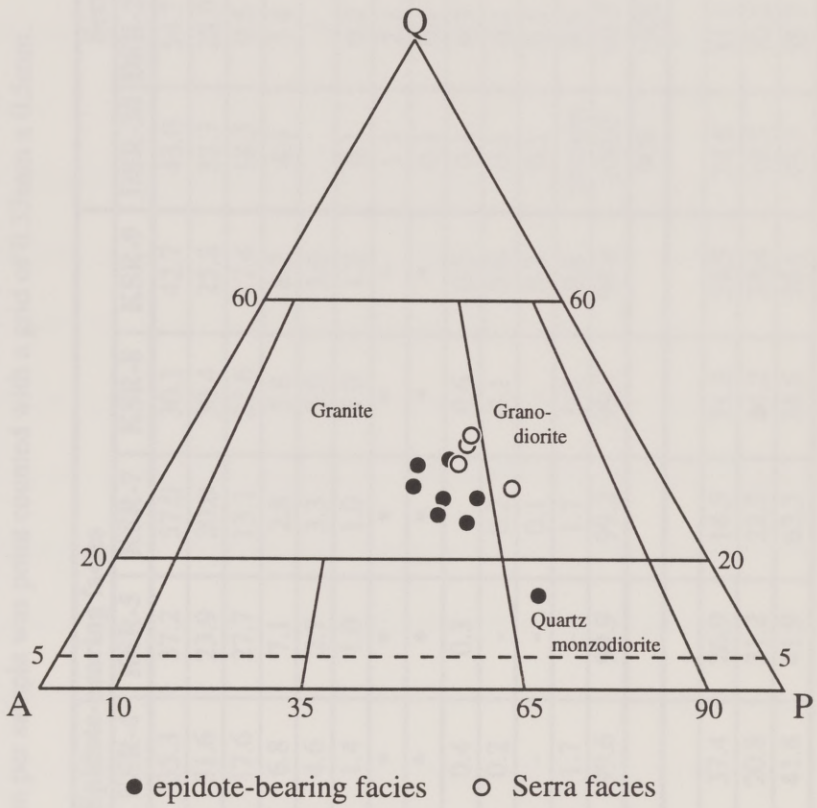

Figure 10. QAP plot of São Rafael samples. (QAP diagram based on LeMaitre, 1989.)

Table 1. Modal compositions (vol %) for samples of the epidote-bearing and Serra facies of the Sao Rafael batholith. Data for epidote-bearing facies from Souza (unpublished thesis). For Serra samples, one thinsection per sample was point counted with a grid of 0.33mm x 0.5mm.

	Epidote-bearing facies							Serra facies			
Sample ID	**KSR-2**	**KSR-3**	**KSR-4**	**KSR-5**	**KSR-7**	**KSR-8**	**KSR-9**	**DSR-20**	**DSR-25**	**DSR-26**	**DSR-28**
Plagioclase	43.1	35.4	35.3	37.2	57.0	30.1	42.7	43.0	54.7	44	47.5
Quartz	25.0	24.6	31.6	23.9	20.0	30.4	25.2	32.7	28.9	33.5	35.5
Microcline	22.9	23.6	17.6	27.7	13.1	27.6	17.4	18.3	9.5	11.2	7.6
Biotite	7.1	9.2	6.8	7.1	2.8	5.8	8.2	4.4	3.4	8.1	4.9
Hornblende	0.4	2.3	4.6	2.7	3.3	3.8	3.0	-	-	-	-
Epidote	0.6	2.8	1.4	1.0	1.0	1.0	1.2	0.1	0.2	0.5	0.9
Myrmekite	*	*	*	*	*	*	*	1.1	2.1	2.5	2.3
Allanite	*	*	*	*	*	*	*	0.1	0.1	present	0.2
Titanite	0.2	0.3	0.4	0.3	-	0.6	0.5	0.1	0.3	0.1	present
Apatite	0.1	0.5	0.2	-	0.2	0.1	0.6	0.1	0.1	present	0.2
Opaques	0.3	0.1	-	-	0.1	-	0.2	0.1	0.1	0.1	present
Alteration	-	0.8	1.7	-	1.7	0.3	0.8	present	0.5	present	0.9
Total	99.7	99.6	99.6	99.9	99.2	99.7	99.8	100.0	99.9	100.0	100.0
Points counted								908	1500	1000	1750
QAP parameters											
Q	27.5	29.4	37.4	26.9	14.5	31.3	29.5	34.8	31.1	37.8	39.2
A	25.2	28.3	20.8	31.2	22.2	34.2	20.4	19.5	10.2	12.6	8.4
P	47.4	42.3	41.8	41.9	63.3	34.5	50.1	45.7	58.7	49.6	52.4

* Not point counted in Souza's samples, but present in DSR- samples from similar or same sampling locations.

displaying undulatory extinction, with occasional extinction bands and show evidence for minor recrystallization by grain-boundary migration and bulge nucleation.

Microcline phenocrysts are euhedral prisms, displaying "tartan" twinning, and occasional Carlsbad twins. They contain inclusions of plagioclase, quartz and biotite.

Biotite forms euhedral, pleochroic light brown to green blades. Epidote, apatite, titanite, zircon, and opaques are commonly included within biotite. In some samples, biotite is partly altered to chlorite.

Amphibole occurs as small, euhedral crystals and as inclusions in plagioclase and microcline megacrysts, and as anhedral crystals in contact with biotite and epidote. It is pleochroic light green to dark green and it displays two directions of cleavage. Some of it is twinned. Amphibole can contain inclusions of apatite, biotite, and rarely epidote. The epidote textures suggest formation by reaction of amphibole with the magma. Amphibole is also observed with exsolution of opaques along cleavages.

Epidote occurs in association with mafic minerals and with mafic banding. Epidote displays two generations of formation. The first consists of well developed crystals with twins, compositional zonation, and allanite inclusions. Epidote of this generation is euhedral in relation to biotite, and occurs as

inclusions in biotite or it is associated with biotite and amphibole (Fig. 11). The common textural relationship is characterized by euhedral, prismatic to equant twinned epidote with allanite cores. The other generation of epidote is associated with plagioclase, quartz, and amphibole, and is characterized by an irregular outline, with embayments penetrated by quartz. Less commonly, epidote is seen inside microcline or plagioclase. Euhedral apatite inclusions in epidote are observed. The modal percentage of epidote varies over a wide range (0.4% to 2%) from sample to sample.

Euhedral titanite crystals with lozenge or parallelogram shapes are common (Fig. 12). In addition, titanite occurs as anhedral rounded crystals. The crystals are large enough to be seen with a hand lens. They occur as inclusions in plagioclase, quartz, biotite, microcline, or epidote, and also commonly dispersed within the matrix.

Apatite occurs as euhedral, elongate batons with hexagonal cross sections. It occasionally occurs as stubby hexagonal crystals. Apatite preferentially occurs as inclusions in biotite, plagioclase, microcline, amphibole, and rarely epidote.

Zircon with characteristic pleochroic halos appears as small grains included in biotite, amphibole, and plagioclase. Opaque minerals are rare, appearing as euhedral rectangular or equant crystals. They are well developed and of sizes similar to those of other accessory minerals. They occur among grains

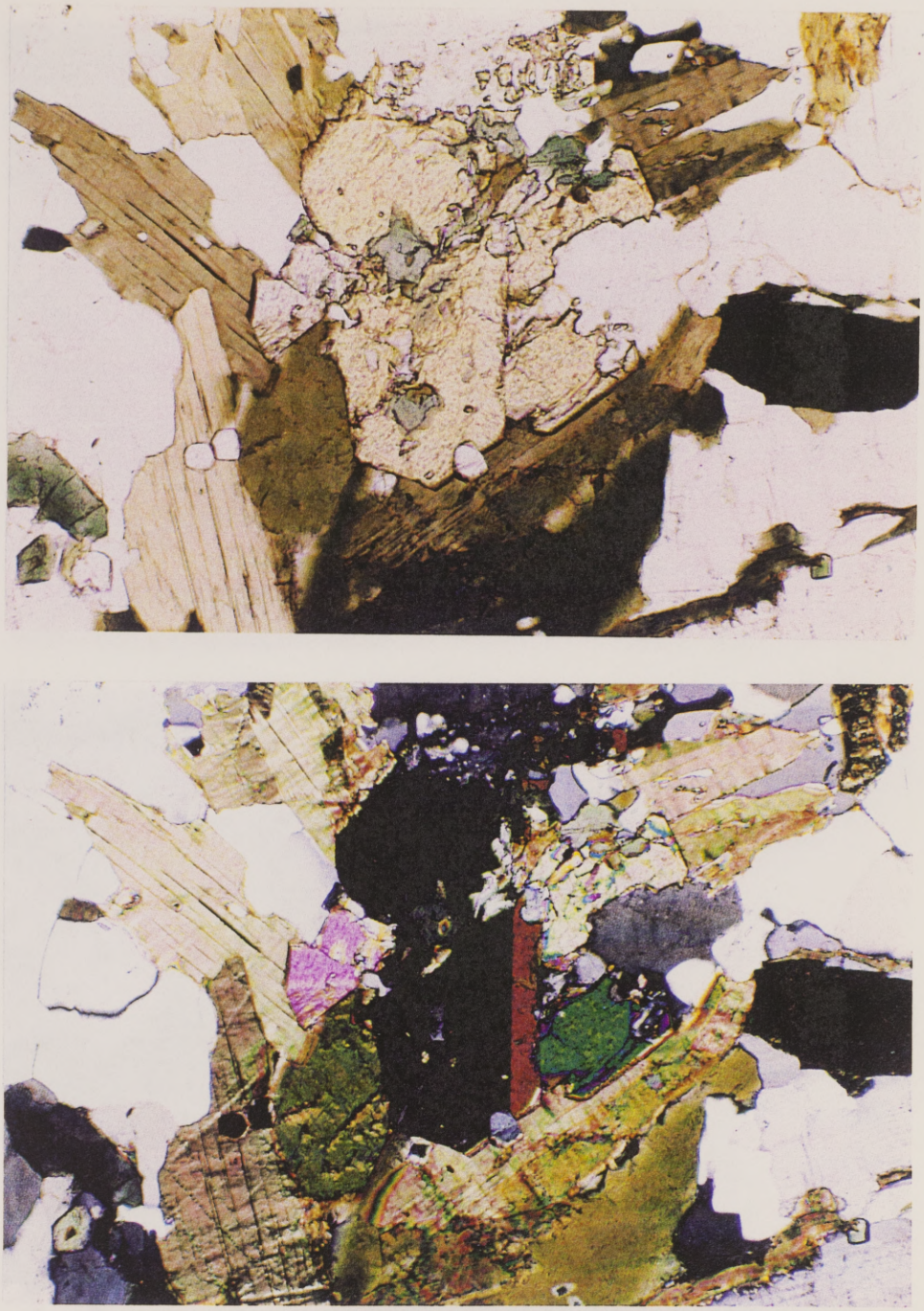

Figure 11. Twinned epidote with inclusions of amphibole remnants. Upper photomicrograph in plane light, lower with crossed polars. Long dimension 1.7 mm. (Sample DSR-10)

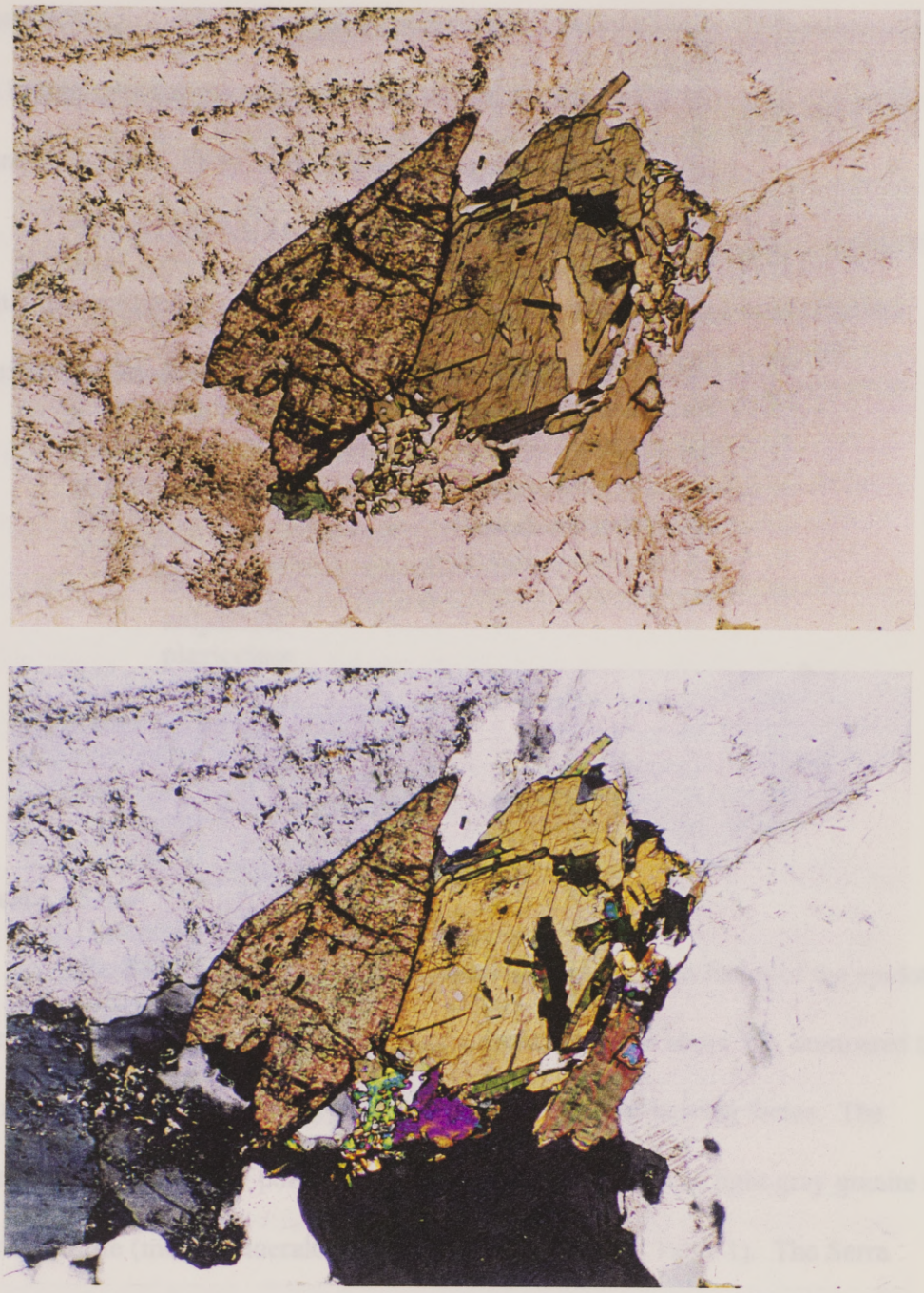

Figure 12. Large titanite wedge, amphibole cross section and epidote crystals at edge of amphibole and included within biotite lath. Upper photomicrograph in plane light, lower with crossed polars. Long dimension 1.7 mm. (DSR-10)

and as small inclusions in biotite, plagioclase, and microcline. Chlorite occurs as a biotite alteration product, whereas sericite is observed on grains of plagioclase and microcline. Rare alteration of plagioclase to calcite is seen.

The occurrence of a euhedral inclusion is normally considered to indicate that the included mineral crystallized earlier. Based upon observations of this textural relationship, the sequence of appearance of minerals might have been:

Early → **Late**
apatite
zircon
allanite
titanite
amphibole
plagioclase
epidote
biotite
quartz
microcline

Serra Facies

The Serra samples represent a paler, less epidote-rich facies of the epidote-bearing suite. A typical mafic index for a Serra sample is about 5%, compared to a mafic index of 11% for a typical sample of the epidote-bearing facies. The Serra facies consists of porphyritic, medium-grained, white to light gray granite to granodiorite (modal mineralogy of four Serra samples in Table 1). The Serra samples contain more plagioclase and quartz, and smaller, less abundant

microcline phenocrysts than the epidote-bearing facies, and thus plot farther toward the P vertex of the QAP diagram (Fig. 10).

Vitreous white to slightly pink prismatic, 1 to 2 cm microcline phenocrysts are randomly arranged in an equigranular medium-grained groundmass of gray quartz, white plagioclase, and black biotite (which gives a black speckled appearance to the rock). Other groundmass phases present in trace amounts are epidote, titanite, allanite, apatite, opaques, and zircon. Although the main porphyritic facies of the batholith is referred to as the primary epidote-bearing facies, the Serra facies also contains magmatic epidote, but in smaller abundances. The mineral assemblages of the two facies are similar except for the notable absence of amphibole in the Serra facies.

Here also, plagioclase is the most abundant mineral, occurring as oscillatory zoned subhedral to anhedral stubby prisms (Fig. 13). It commonly displays albite polysynthetic and Carlsbad twinning, and occasional pericline polysynthetic twinning (Fig. 14). "Synneusis" texture is also observed (Fig. 15). The (more calcic?) cores of plagioclase crystals invariably have sericitic alteration.

Quartz forms medium size anhedral grains, almost all of which display undulatory extinction. Some grains show minor grain boundary migration and bulge nucleation, subgrains, and extinction bands (Fig. 16 and 17).

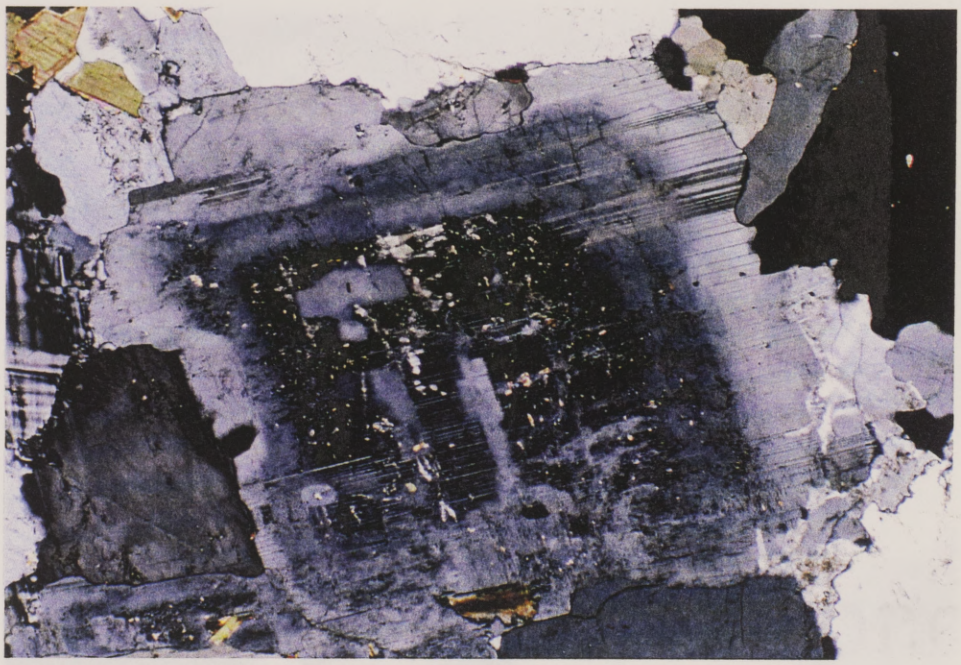

Figure 13. Photomicrograph of oscillatory zoned plagioclase with albite twinning and sericitic alteration of core. Crossed polars. Long dimension 3.3 mm. (DSR-20)

Figure 14. Photomicrograph of plagioclase displaying albite polysynthetic twinning, Carlsbad twin, and pericline polysynthetic twinning. Crossed polars. Long dimension 3.3 mm. (DSR-25)

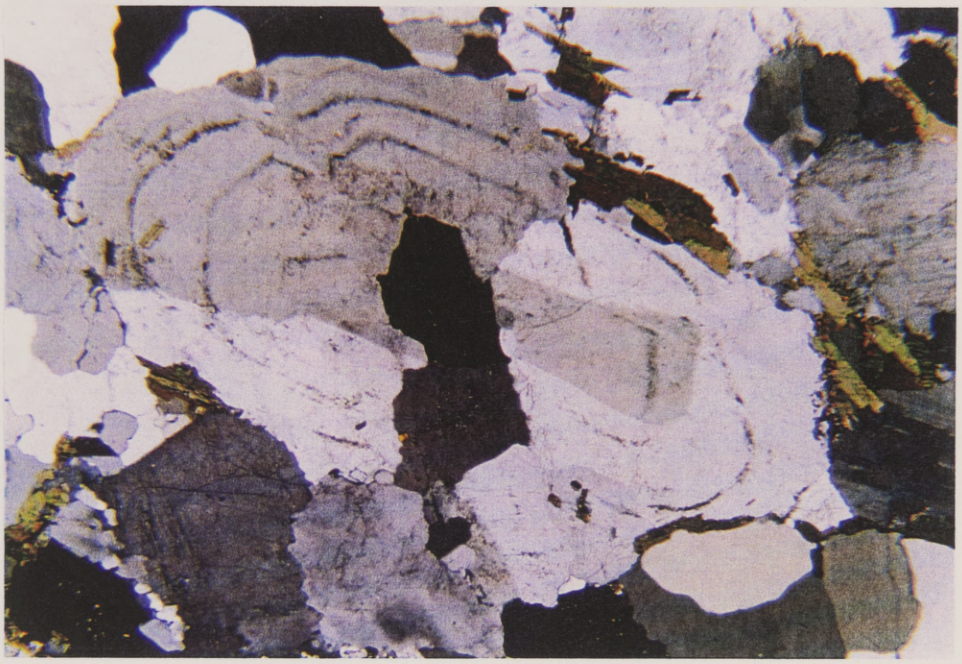

Figure 15. Synneusis texture in zoned plagioclase. Crossed polars. Long dimension 5 mm. (DSR-26)

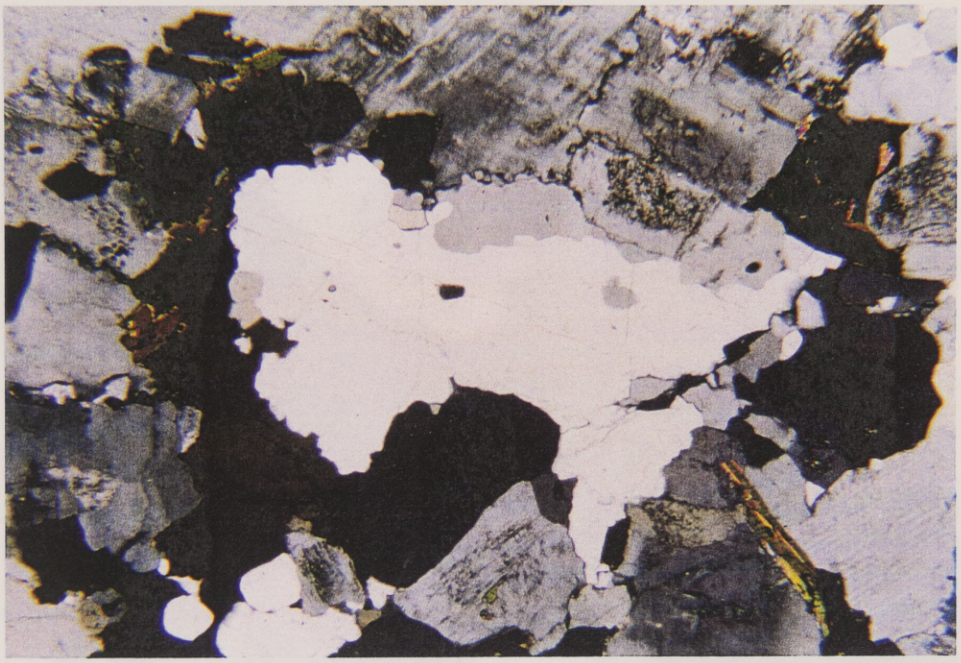

Figure 16. Quartz partially recrystallized by grain boundary migration and minor bulge nucleation. Crossed polars. Long dimension 5 mm. (DSR-20)

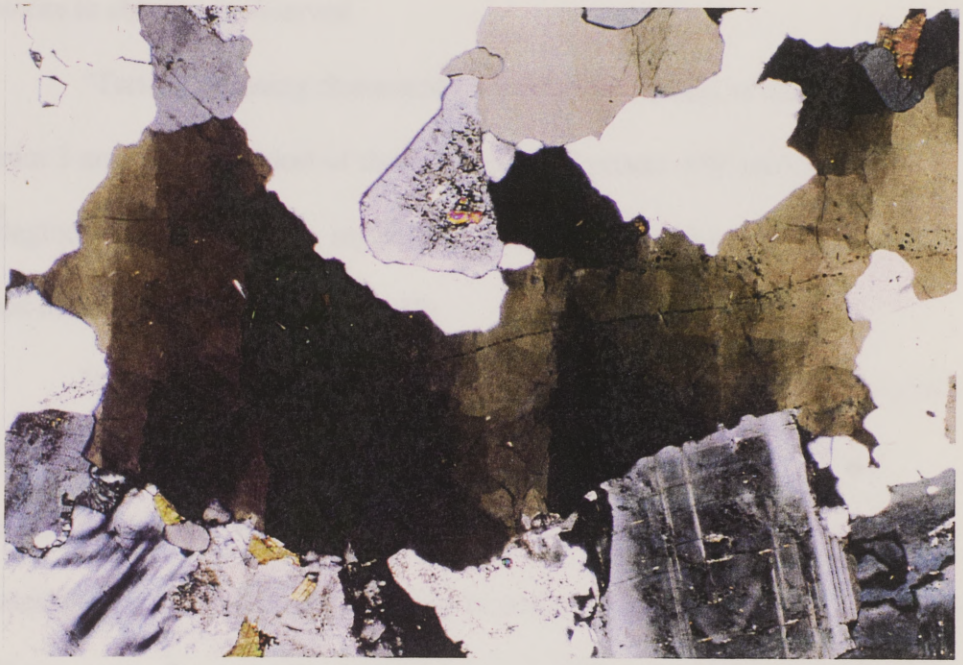

Figure 17. Strained quartz with patchy extinction, extinction bands, and subgrains. Crossed polars. Long dimension 5 mm. (DSR-20)

Pleochroic straw to dark olive-green biotite appears as subhedral laths to anhedral fragments up to 2 mm long. The trace phases epidote, titanite, apatite, and opaques commonly occur in close association with it. Some alteration of biotite to chlorite is observed.

"Tartan" twinning characterizes microcline crystals which range in size from 3 mm to 2 cm. Most of them are anhedral prisms with inclusions of plagioclase, biotite, quartz, myrmekite, and allanite. Myrmekite is very common and occurs near microcline (Fig. 18).

Epidote occurs as small (0.05 to 0.2 mm) euhedral to subhedral crystals. It displays very high relief, clear to pale green pleochroism, and occasional anomalous birefringence. It generally occurs included in biotite, with straight faces against the biotite. Epidote may be zoned, with abundant zoned euhedral allanite cores. Some epidote shows twinning. Where it occurs as inclusions in minerals other than biotite, epidote tends to be subhedral to anhedral. However, euhedral twinned crystals are also observed included in such minerals as plagioclase. Modes of occurrence of epidote are illustrated in Figures 19-24.

Titanite is deceptively similar in relief to epidote, but can be distinguished by its crystal habit and brownish color. It commonly occurs in association with biotite, epidote, and opaques. Its morphology ranges from euhedral diamond-

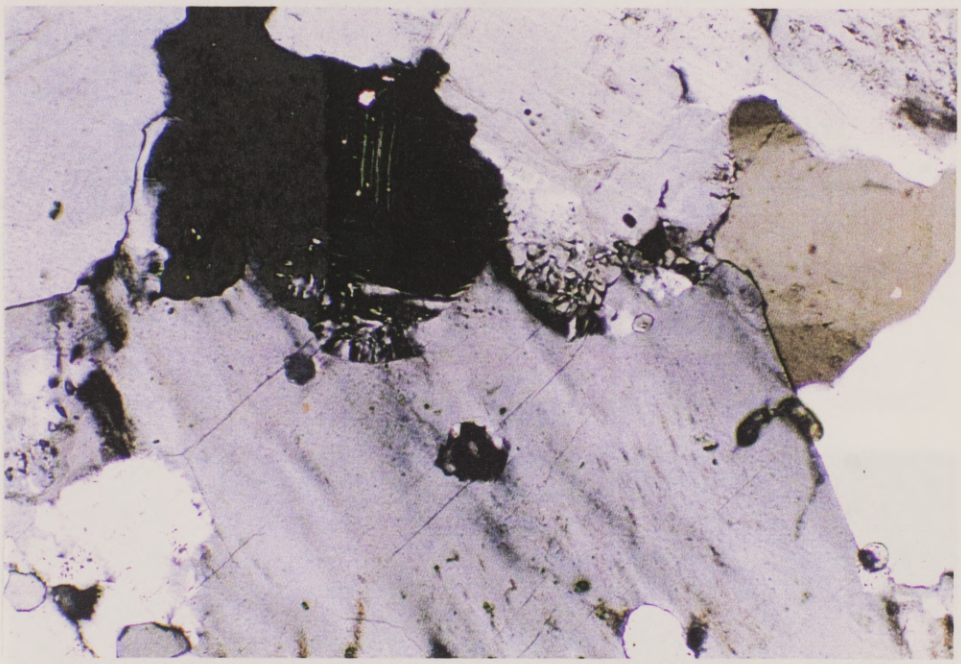

Figure 18. Myrmekitic intergrowth of quartz and plagioclase. It is commonly observed as convex bulges growing into microcline. Crossed polars. Long dimension 1.7 mm. (DSR-20)

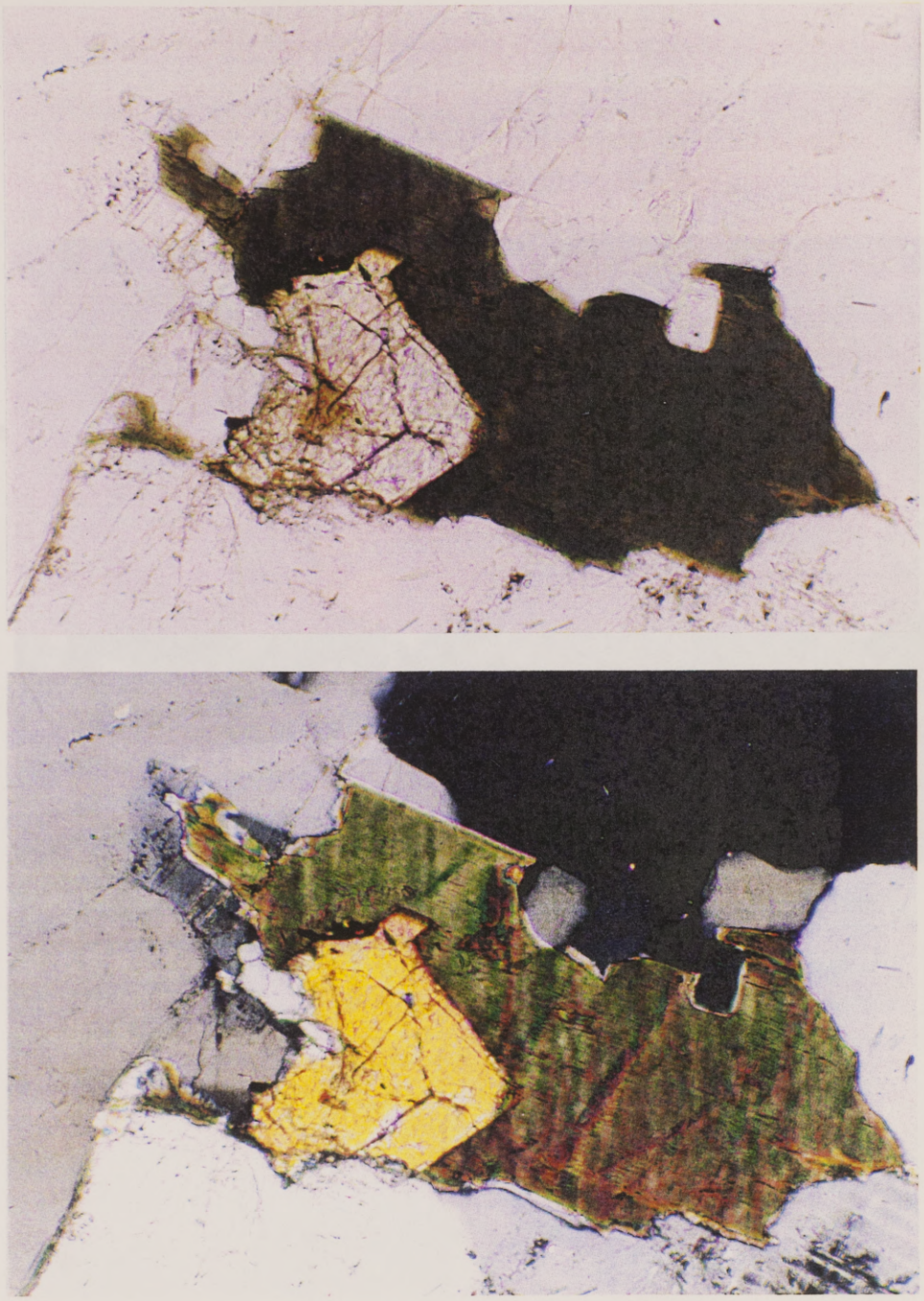

Figure 19. Epidote (type III, see later discussion) with euhedral crystal faces against biotite. Slight compositional zoning. Upper photomicrograph in plane light, lower in crossed polars. Long dimension 0.75 mm. (DSR-20)

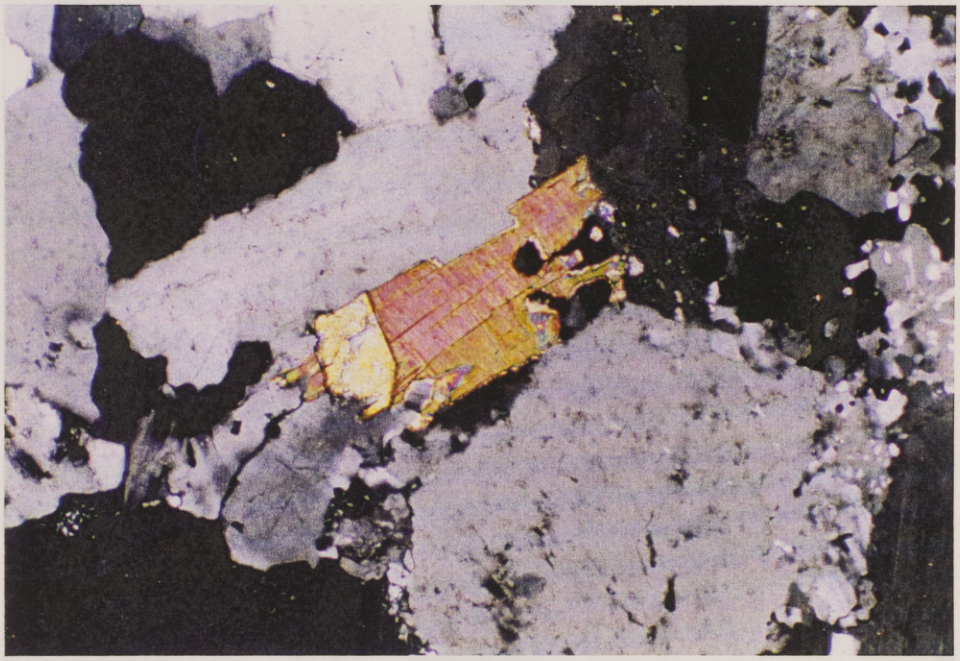

Figure 20. Euhedral epidote (type III) without a core included in biotite. Crossed polars. Long dimension 1.7 mm. (DSR-25)

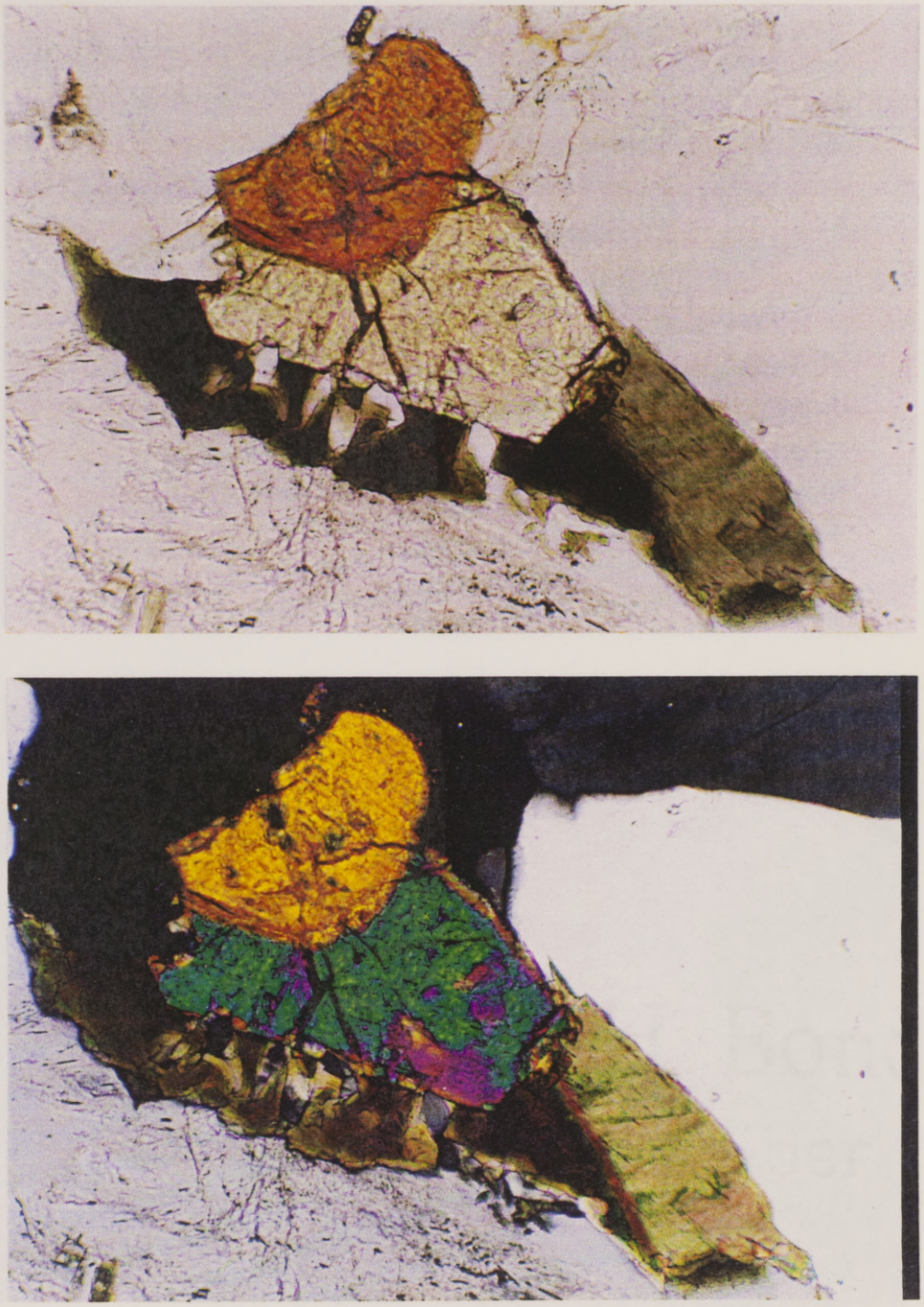

Figure 21. Type II epidote with allanite core, included in biotite. Upper photomicrograph in plane light, lower with crossed polars. Long dimension 0.75 mm. (DSR-28)

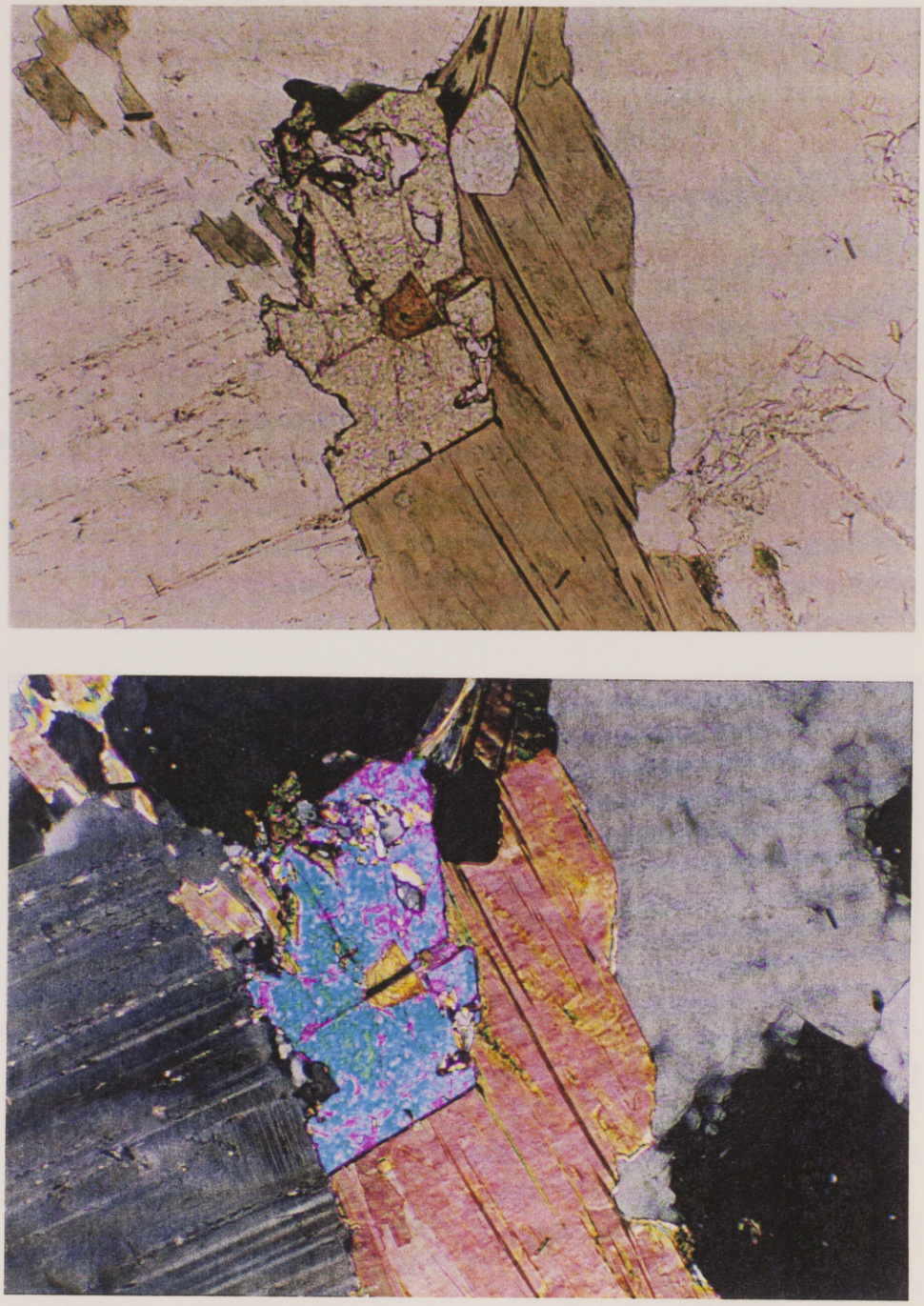

Figure 22. Euhedral epidote (type II) with twin and zoned allanite core, included in biotite. Upper photomicrograph in plane light, lower in crossed polars. Long dimension 0.75 mm. (DSR-26)

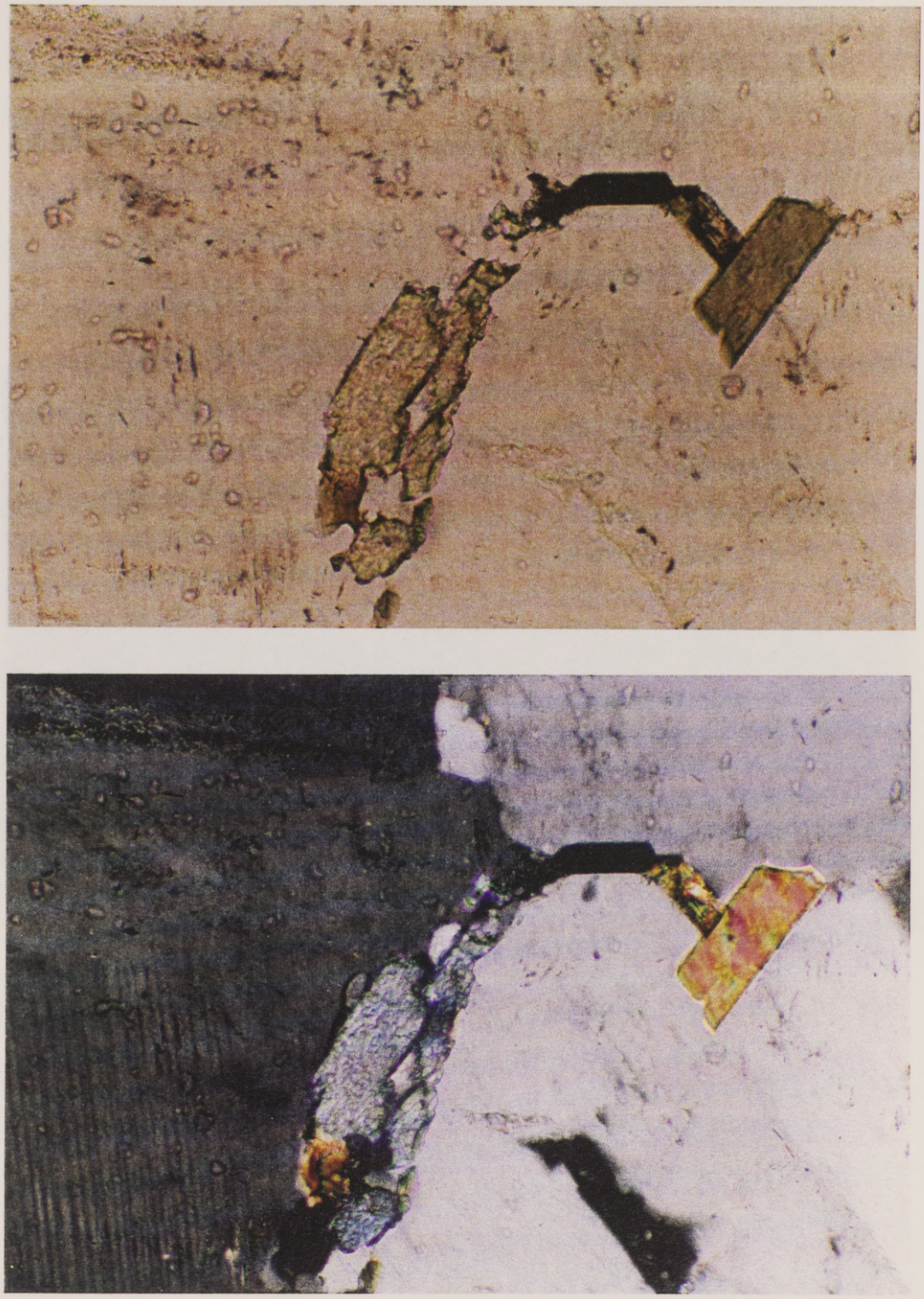

Figure 23. Subhedral epidote with anomalous blue birefringence included in plagioclase. Upper photomicrograph in plane light, lower in crossed polars. Long dimension 0.75 mm. (DSR-25)

Figure 24. Twinned euhedral epidote (type I?) with anomalous birefringence, in plagioclase. Crossed polars. Long dimension 0.75 mm. (DSR-20)

shaped parallelograms to anhedral, granular masses. Rare occurrences of biotite and opaques as inclusions in titanite are observed.

Other trace minerals include allanite, apatite, opaques, and zircon. Allanite commonly occurs as inclusions in epidote cores, but not uncommonly occurs as separate orange-colored euhedral zoned crystals in the groundmass and in feldspars (Figs. 25 and 26). Apatite appears as stubby prisms and commonly as larger hexagonal crystals. It is green in plane-polarized light, with moderately high relief. Opaque minerals can be up to a millimeter across, and display hexagonal or rectangular shapes. They are typically associated with biotite and titanite. Zircon appears as tiny inclusions in biotite, with characteristic pleochroic haloes.

Mafic Enclaves

Inclusions in the main facies of the pluton consist of amphibolites, schists, gneisses, and MMEs. The schist and gneiss inclusions are common close to the contact of the pluton with the host rock. They can be round, elongate, or angular, and display reaction aureoles of biotite and epidote. The amphibolites apparently have a cumulate origin. The MMEs, which are of quartz-diorite composition, are of the greatest interest to this study due to their apparently igneous origin; they are described below.

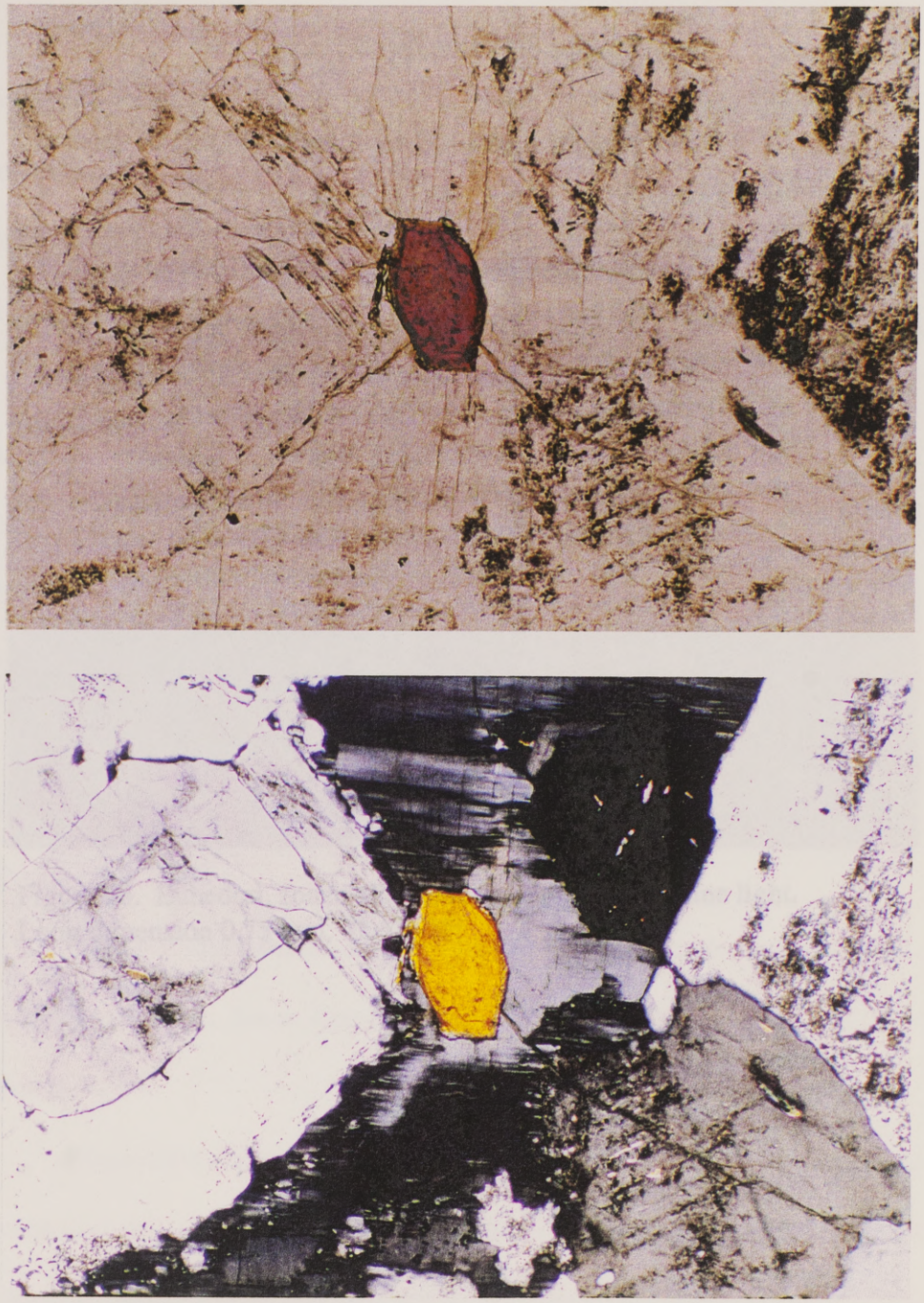

Figure 25. Euhedral allanite in microcline. Upper photomicrograph in plane light, lower in crossed polars. Long dimension 1.7 mm. (DSR-28)

Figure 26. Euhedral, zoned allanite crystal in quartz. Plane light. Long dimension 0.75 mm. (DSR-28)

The MMEs have well-defined contacts that vary from straight to undulatory, and many are sharp; diffuse contacts and rounded forms predominate, however. Some outcrops display abundant rounded enclaves resembling "pillow-like" structures suggesting that the quartz-diorite magma was not fully solid in the presence of the granitic melt (Fig. 27).

Texturally, the enclaves are equigranular, and lamellar and tabular minerals show a preferred orientation. Static recrystallization textures are seen in small aggregates of biotite, amphibole, and quartz. The enclaves are composed of biotite, amphibole, plagioclase, microcline, quartz, and the accessory minerals apatite, titanite, epidote, and opaques.

Hornblende appears as tabular euhedral to subhedral crystals that are pleochroic light brown to dark green. It contains inclusions of apatite and opaques.

Biotite is observed as euhedral to subhedral blades with cream to green-brown pleochroism. Some flexure is observed along cleavages. Biotite alters to chlorite.

Plagioclase forms anhedral, oscillatory zoned crystals with inclusions of apatite and fluorite (?). It commonly displays albite polysynthetic twins, Carlsbad twinning, and occasional pericline twins. Myrmekite occurs along contacts with microcline.

Figure 27. "Pillow-like" structures. Rounded mafic enclaves included within the main epidote-bearing facies. Six inch ruler for scale.

Quartz forms fine to medium size anhedral grains. Some quartz crystals display preferred orientations, triple junction intersections of grains indicative of static recrystallization, and minor subgrain development.

Microcline occurs as mm-scale anhedral grains. It is generally inclusion-rich, containing biotite, amphibole, titanite, apatite, and myrmekite.

Epidote is observed as euhedral to subhedral crystals preferentially located within biotite and amphibole aggregates. It displays moderate pleochroism from clear to green. Allanite cores and simple twinning suggest a magmatic origin for this epidote. Thin sections of the granite-enclave contact show that epidote is relatively concentrated close to the contact.

Trace phases include apatite, opaques, and titanite. Apatite forms euhedral batons that are included in plagioclase, microcline, and less commonly in biotite, hornblende, and quartz. Some acicular apatite crystals are observed. Opaques occur included within hornblende and biotite as euhedral cubic crystals, some with reddish borders. Euhedral to subhedral titanite is common and occurs as inclusions in plagioclase, quartz, biotite, microcline, and amphibole and it is also dispersed intergranularly.

MME samples DSR-3 and DSR-11 are very different from one another. DSR-3 is characterized by very abundant biotite and titanite (Fig. 28). Figure 29

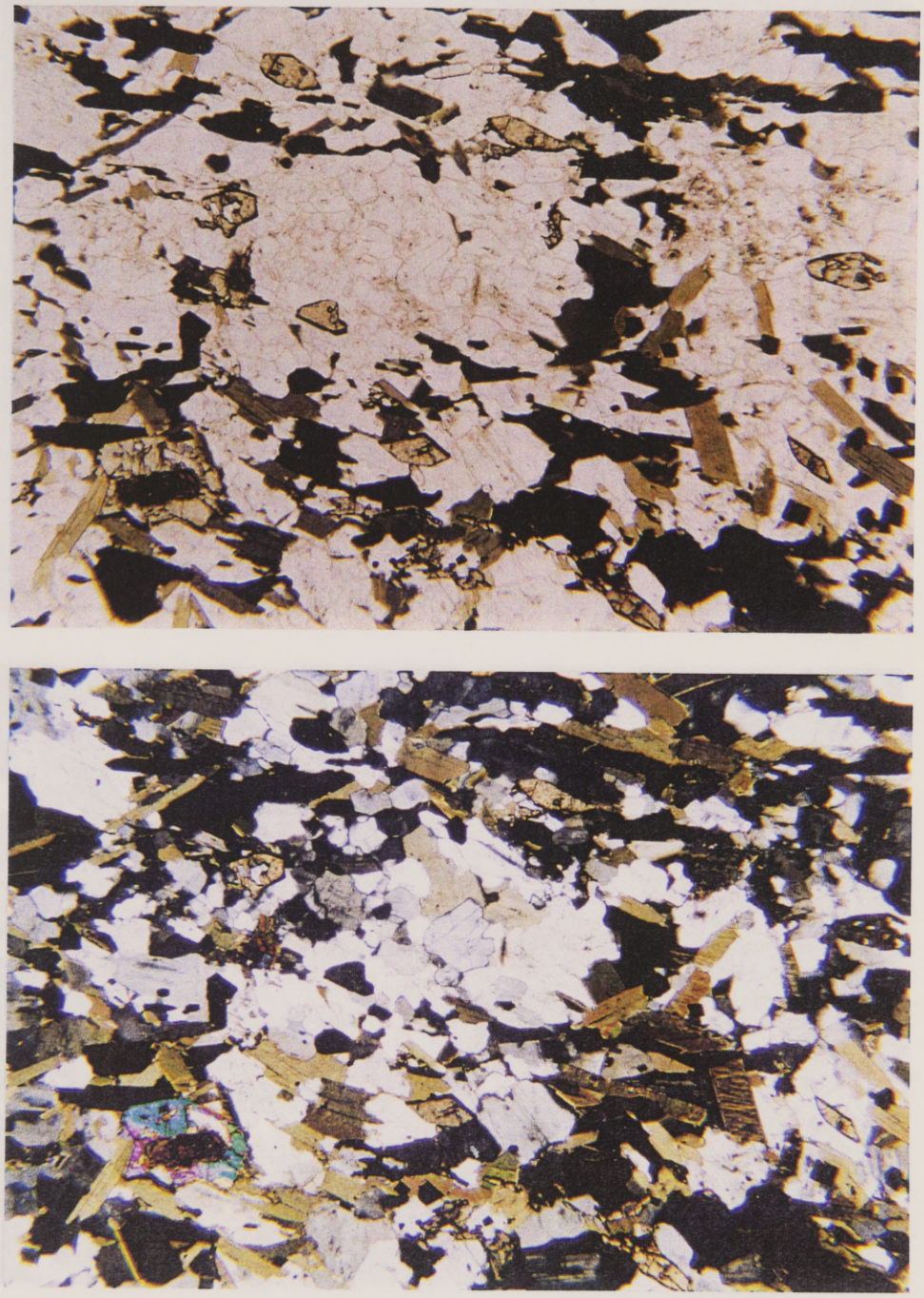

Figure 28. Photomicrograph of biotite rich MME. Note swarms of titanite crystals and the type II epidote in lower left corner. Upper photo in plane light, lower in crossed polars. Long dimension 5 mm. (DSR-3)

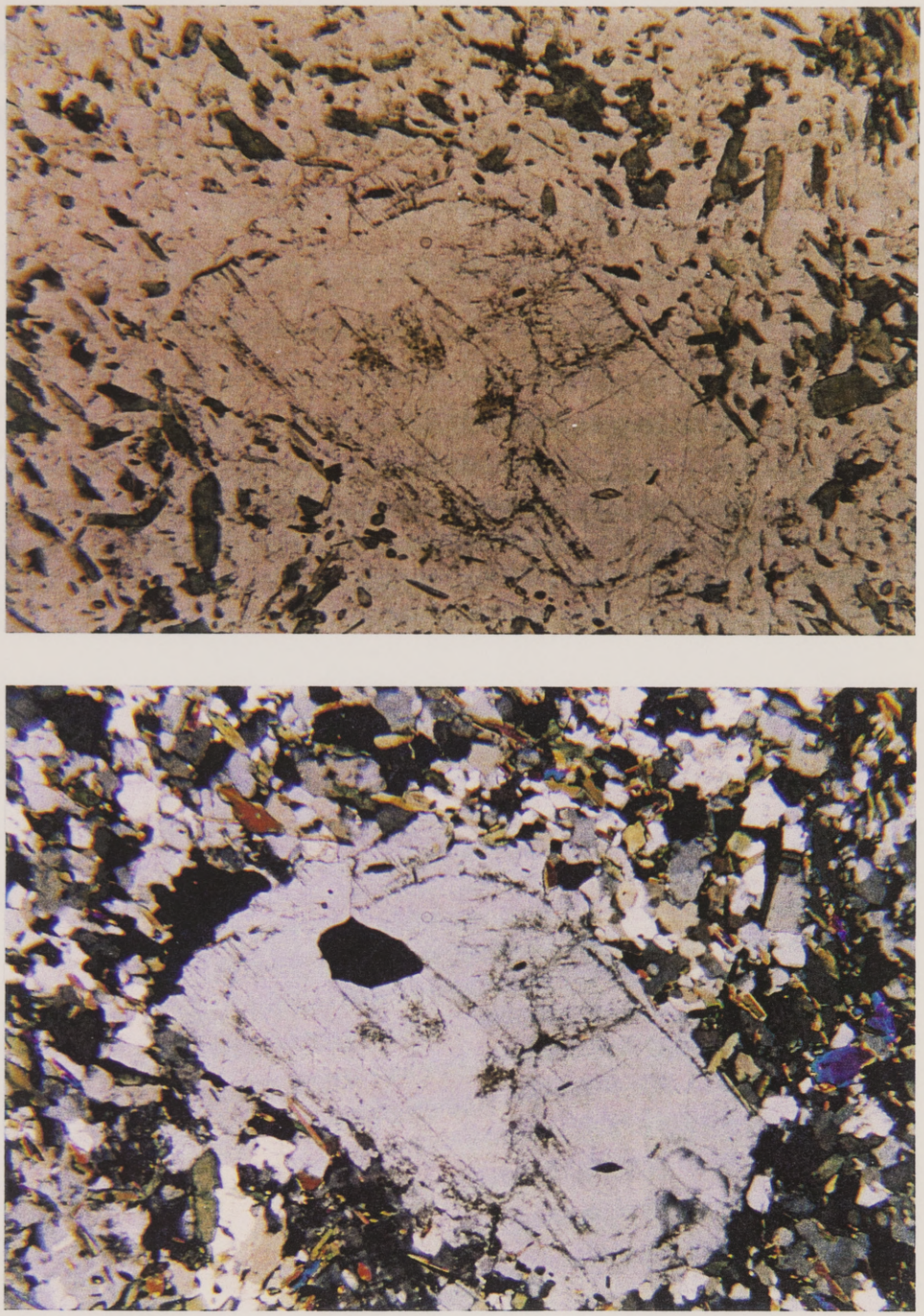

Figure 29. Photomicrograph of amphibole rich MME with plagioclase phenocrysts. Amphibole is the abundant green mineral in plane light (upper photo). Lower photo with crossed polars. Long dimension 5 mm. (DSR-11)

is a photomicrograph of DSR-11 which is amphibole-rich and contains large plagioclase phenocrysts.

GEOCHEMISTRY

Major Element Chemistry

Ten samples of the porphyritic epidote-bearing granite, and four MMEs, were analyzed for major and trace element chemistry by the GEOSOL lab in Belo Horizonte, Minas Gerais. Major and trace element chemistry of four Serra samples were analyzed by XRF at McGill University, Montreal, Canada. A representative epidote-bearing facies sample (DSR-29, taken from the same outcrop as KSR-7) was also analyzed at McGill as a check of agreement between the results of the Brazilian and Canadian laboratories. By inspection, the results for KSR-7 and DSR-29 are very similar. Table 2 contains the major oxide results for eleven of the most representative epidote-bearing samples, four MMEs, and the four Serra samples. Trace element data are presented in the Appendix, Tables A and B.

The batholith consists uniformly of silica-oversaturated rocks. Values of SiO_2 vary from 68.8 to 71.7 wt % in the epidote-bearing and Serra facies, and from 59.8 to 65.7 wt % in the quartz-diorite enclaves.

In most samples, the Al_2O_3 is greater than $Na_2O + K_2O$ and less than $Na_2O + K_2O + CaO$ (all quantities in mol %). Thus the batholith is metaluminous according to the alumina saturation classification of Shand (1951). The triangular diagram $Na_2O + K_2O$, CaO, and Al_2O_3 of Loiselle and Wones (1979), shown in

Table 2. Major oxide chemistry (wt %). (DSR- samples analyzed by XRF. Method of analysis of KSR- samples is unknown.)

Sample ID	Epidote-bearing Facies										
OXIDES	KSR-2	KSR-3	KSR-4	KSR-5	KSR-7	KSR-8	KSR-9	KSR-10	KSR-11	KSR-13	DSR-29
SiO2	70.40	68.80	70.40	69.40	71.70	71.40	69.50	68.40	69.30	69.70	71.06
TiO2	0.24	0.23	0.31	0.32	0.18	0.28	0.29	0.20	0.18	0.22	0.26
Al2O3	15.60	15.40	14.20	14.50	14.50	14.20	15.10	16.00	15.90	15.10	14.87
Fe2O3	0.48	0.93	0.94	1.30	0.58	0.85	0.74	0.36	0.59	0.21	0.69
FeO	1.10	1.50	1.50	1.40	1.10	1.40	1.50	1.30	1.00	1.70	1.35
MnO	0.02	0.04	0.03	0.03	0.03	0.03	0.03	0.04	0.02	0.04	0.03
MgO	0.60	1.00	1.30	1.30	0.52	0.80	1.20	1.00	0.82	1.10	1.05
CaO	2.90	2.70	2.80	2.90	2.10	2.40	2.70	2.40	2.80	2.20	2.33
Na2O	5.80	5.50	5.20	5.70	5.60	4.80	5.80	6.00	5.90	4.90	4.34
K2O	1.90	2.50	2.30	2.40	3.00	2.90	2.30	2.80	2.20	2.40	3.08
P2O5	0.09	0.13	0.12	0.14	0.08	0.11	0.11	0.11	0.10	0.16	0.10
H2O+	0.22	1.05	0.38	0.19	0.28	0.26	0.35	0.93	0.81	0.87	-
H2O-	0.03	0.06	0.05	0.05	0.05	0.03	0.04	0.03	0.03	0.04	-
BaO	0.12	0.13	0.14	0.14	0.13	0.15	0.15	0.13	0.14	0.18	0.15
CO2	0.25	0.10	0.25	0.25	0.25	0.25	0.25	0.25	0.10	0.10	-
LOI	-	-	-	-	-	-	-	-	-	-	0.82
Total	99.75	100.07	99.92	100.02	100.10	99.86	100.06	99.95	99.89	98.92	100.13

Table 2. Major oxide chemistry (wt %) (continued)

Serra Facies				Quartz-diorite Enclaves			
DSR-20	**DSR-25**	**DSR-26**	**DSR-28**	**KSR-5A**	**KSR-8A**	**KSR-9A**	**KSR-12A**
72.62	71.99	70.56	72.80	65.7	58.1	62.7	59.8
0.17	0.18	0.22	0.19	0.48	0.8	0.62	0.69
14.97	15.18	15.79	14.95	13.1	13.5	13.4	14.8
0.36	0.37	0.58	0.30	1.4	2.6	2	1.8
1.02	1.13	1.17	1.10	2.9	5	4.3	3.3
0.02	0.03	0.02	0.02	0.07	0.14	0.11	0.07
0.48	0.65	0.63	0.55	3.7	4.7	4.8	4.5
2.03	2.47	2.55	2.30	3.6	5.3	4.5	5.1
4.36	4.55	4.41	4.25	3.9	2.1	4.1	3.6
3.22	2.51	2.77	2.55	3.9	6.1	2.7	4.8
0.05	0.05	0.07	0.07	0.21	0.39	0.19	0.68
-	-	-	-	0.34	0.6	0.27	0.43
-	-	-	-	0.03	0.04	0.04	0.05
0.11	0.09	0.18	0.10	0.3	0.29	0.15	0.3
-	-	-	-	0.25	0.25	0.1	0.1
0.71	0.67	0.71	0.76	-	-	-	-
100.12	99.87	99.66	99.93	99.88	99.91	99.98	100.02

Fig. 30, also shows that the samples plot in the metaluminous field. With the exception of the Serra samples, which fall in the I-type field, the samples plot outside the fields delineating I- and S-type granitoid rocks as defined by Chappell and White (1974).

Figure 31 is an AFM plot of the São Rafael samples, with the calc-alkaline differentiation trend of Irvine and Baragar (1971) also illustrated. The data plot in three distinct groups and do not define a standard differentiation trend.

Normative Compositions. Table 3 lists calculated CIPW norms. The mineral phases are similar, but their relative proportions vary significantly from sample to sample. All norms present qz, the average normative composition for the epidote-bearing facies being quartz (22%), orthoclase (15%), albite (47%), anorthite (8.7%), diopside (2%) and hypersthene (3%). The average values for normative magnetite, ilmenite, apatite and calcite are each less than 1%.

The Serra facies rocks display small abundances of normative corundum and therefore lack normative diopside. The average normative composition for this facies is quartz (29%), corundum (<1%), orthoclase (16%), albite (37%), anorthite (11%), hypersthene (3%), and magnetite, ilmenite, and apatite each less than 1%.

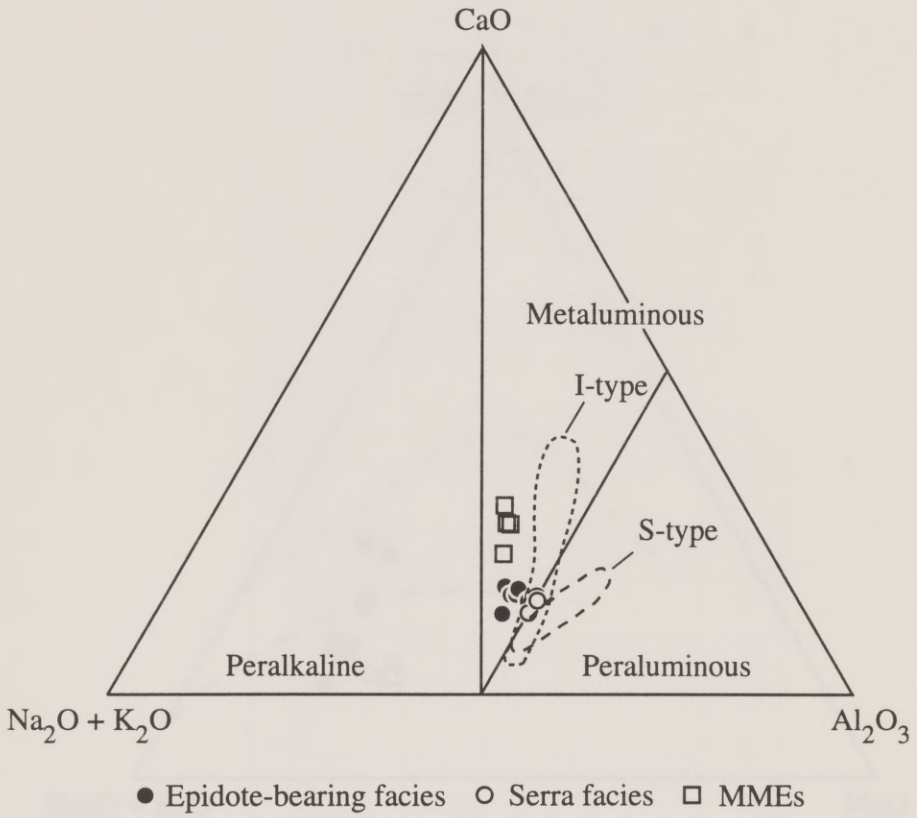

Figure 30. Alumina saturation triangular diagram of Loiselle and Wones (1979) with I- and S-type fields. Oxides are in mol %.

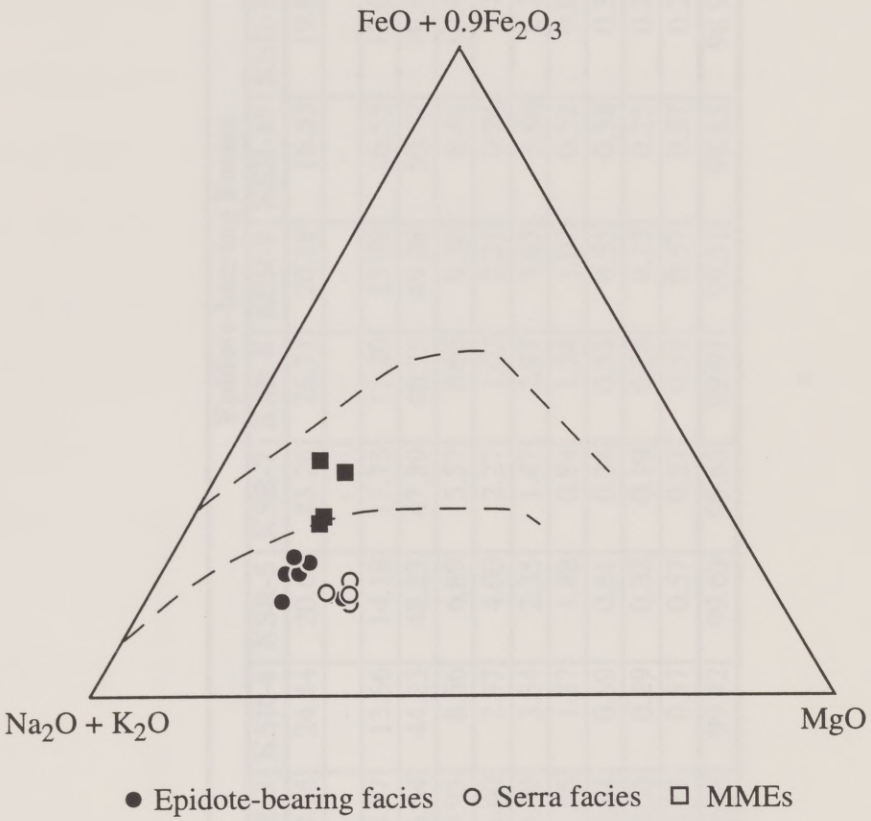

Figure 31. AFM diagram (wt %) with calc-alkaline trend of Irvine and Baragar, 1971.

Table 3. CIPW norms

Weight % Norm	Epidote-bearing Facies										
	KSR-2	KSR-3	KSR-4	KSR-5	KSR-7	KSR-8	KSR-9	KSR-10	KSR-11	KSR-13	DSR-29
Q	22.92	20.26	24.44	20.60	23.28	26.71	20.18	16.55	19.87	25.17	27.05
C	-	-	-	-	-	-	-	-	-	-	0.40
Or	11.23	14.77	13.66	14.18	17.73	17.20	13.59	16.55	13.00	14.18	18.20
Ab	49.08	46.54	44.23	48.23	47.39	40.75	49.08	50.77	49.93	41.46	36.73
An	10.92	9.95	8.66	6.89	5.57	8.66	8.38	8.46	10.40	9.24	10.91
Di	1.07	1.60	2.57	4.00	2.27	1.02	2.21	0.94	1.79	5.40	-
Hy	2.23	3.39	3.54	2.35	1.47	2.97	3.63	3.86	2.26	0.30	4.15
Mt	0.70	1.35	1.37	1.88	0.84	1.24	1.07	0.52	0.86	0.42	1.00
Il	0.46	0.44	0.59	0.61	0.34	0.53	0.55	0.38	0.34	0.37	0.49
Ap	0.21	0.30	0.29	0.32	0.19	0.26	0.25	0.25	0.23	0.23	0.24
Cc	0.57	0.23	0.57	0.57	0.57	0.57	0.57	0.57	0.23	1.06	-
Total	99.39	98.83	99.92	99.63	99.65	99.91	99.51	98.85	98.91	97.83	99.17

Table 3. CIPW norms (continued)

Serra Facies				Quartz-diorite Enclaves			
DSR-20	**DSR-25**	**DSR-26**	**DSR-28**	**KSR-5A**	**KSR-8A**	**KSR-9A**	**KSR-12A**
29.40	29.10	27.49	32.09	16.30	6.00	12.27	5.62
0.74	0.61	1.07	1.18	-	-	-	-
19.03	14.83	16.37	15.07	23.05	36.05	15.96	28.37
36.89	38.50	37.32	35.96	33.00	17.77	34.69	30.46
9.74	11.93	12.19	10.95	6.72	9.39	10.19	10.05
-	-	-	-	6.58	10.35	8.29	8.15
2.53	3.15	2.91	2.87	9.56	12.66	13.37	10.87
0.52	0.54	0.84	0.43	2.03	3.77	2.90	2.61
0.32	0.34	0.42	0.36	0.91	1.52	1.18	1.31
0.12	0.12	0.16	0.17	0.49	0.90	0.44	1.58
-	-	-	-	0.57	0.57	0.23	0.23
99.29	99.12	98.77	99.08	99.21	98.98	99.52	99.25

The quartz-diorite enclaves contain more normative orthoclase, diopside, and hypersthene than in the felsic facies, reflecting a greater modal abundance of amphibole and biotite. They are also richer in normative magnetite and ilmenite.

Variation Diagrams. Major element *vs.* silica diagrams (Harker diagrams) are shown in Figure 32. Data for the felsic facies major-element oxides are similar and tend to cluster, the data for Serra samples lying at the high-silica end of the cluster. Compositions of MMEs show more dispersion, with consistent trends of negative correlation of silica *vs.* major oxides commonly incorporated into mafic minerals (Fe_2O_3, CaO, MgO, FeO, TiO_2, and MnO). Correlations of SiO_2 with the other major oxides, calculated for the entire population of whole-rock analyses (Table 4, Fig. 32), are more negative than -0.9 for TiO_2, Fe_2O_3, FeO, MnO, MgO, and CaO; for K_2O and P_2O_5 the correlations are more negative than -0.75. Much of this strong negative correlation may be attributed to a "mineral effect" whereby a felsic component is mixed with varying abundances of Ti-, Fe-, Mn-, Mg-, and Ca-bearing minerals. A strong positive correlation between TiO_2 and CaO (Figure 33) is simply evidence that most of the Ti resides in the Ca-bearing mineral titanite. Data for mafic samples lie along the same trends as for the felsics.

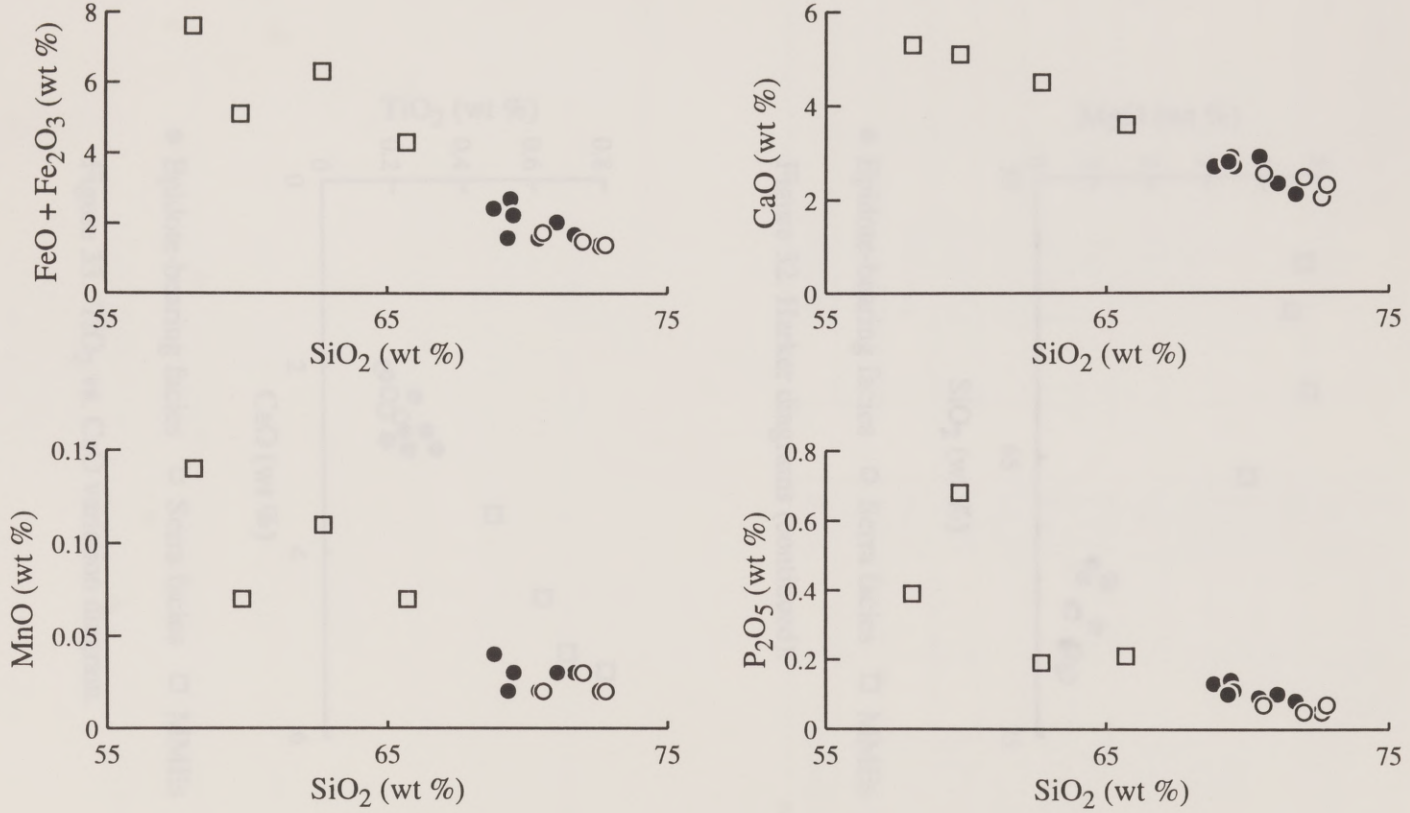

Figure 32. Harker diagrams. ● Epidote-bearing facies ○ Serra facies □ MMEs

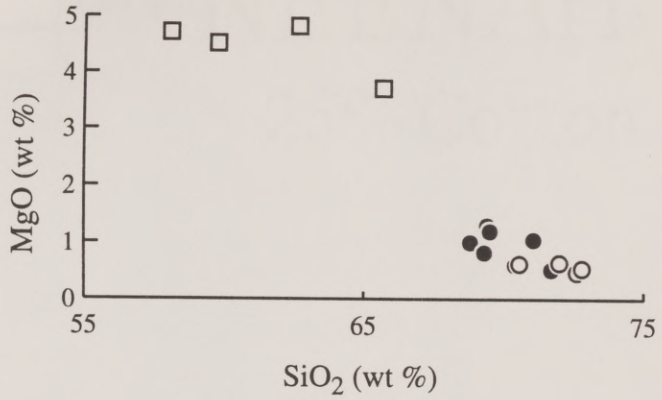

● Epidote-bearing facies ○ Serra facies □ MMEs

Figure 32. Harker diagrams (continued).

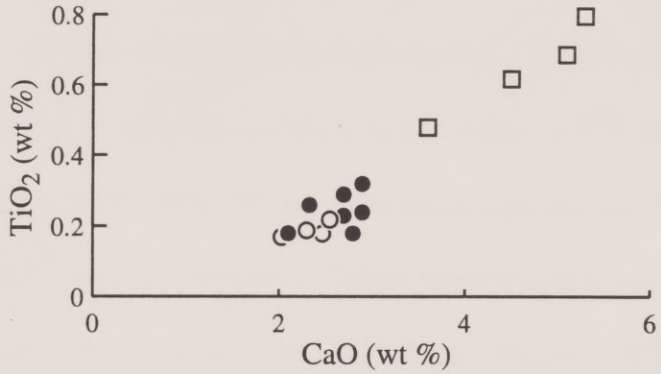

● Epidote-bearing facies ○ Serra facies □ MMEs

Figure 33. TiO_2 vs. CaO variation diagram.

Table 4. Correlation of oxide with SiO_2.

A. Entire population	
Oxide	**Correlation**
SiO_2	1
TiO_2	-0.9755
Al_2O_3	0.594665
Fe_2O_3	-0.95431
FeO	-0.9411
MnO	-0.90655
MgO	-0.94918
CaO	-0.98726
Na_2O	0.65391
K_2O	-0.77503
P_2O_5	-0.8609

B. Felsic samples	
Oxide	**Correlation**
SiO_2	1
TiO_2	-0.59917
Al_2O_3	-0.35077
Fe_2O_3	-0.75166
FeO	-0.60148
MnO	-0.41482
MgO	-0.72888
CaO	-0.82011
Na_2O	-0.73541
K_2O	0.552997
P_2O_5	-0.84818

Rare Earth Element Chemistry

Figure 34 is a chondrite normalized Coryell-Masuda rare earth element (REE) plot for samples of the epidote-bearing facies. REE data are tabulated in the Appendix, Table C. The REE trends of all of the samples are very similar with a high *y*-intercept and a steep slope that flattens out at the HREE end. The pattern of intercept and slope are indicative of a small liquid/solid ratio (small degree of partial melting or large degree of fractional crystallization). The rocks are preferentially highly enriched in light LREE, moderately enriched in middle REE, and less enriched in the HREE compared to mean C1 chondrites. The absence of Eu anomaly is notable.

Oxygen Isotope Geochemistry

Sial and Ferreira (1990), and Sial and others (in press) determined $\delta^{18}O$ in the São Rafael primary epidote-bearing facies. Values of $\delta^{18}O$ in the Seridó epidote-bearing plutons (Fig. 35) are +7 to +8 per mil (Sial and Ferreira, 1990; Sial and others, in press). In general, S-type granites tend to have heavier stable oxygen isotopes than I-type granites. O'Neil and Chappell (1977) recommend a $\delta^{18}O$ value of 10‰ as a guideline to distinguish between I-type granite (with lighter oxygen) and S-type granite (with heavier oxygen). The oxygen isotope

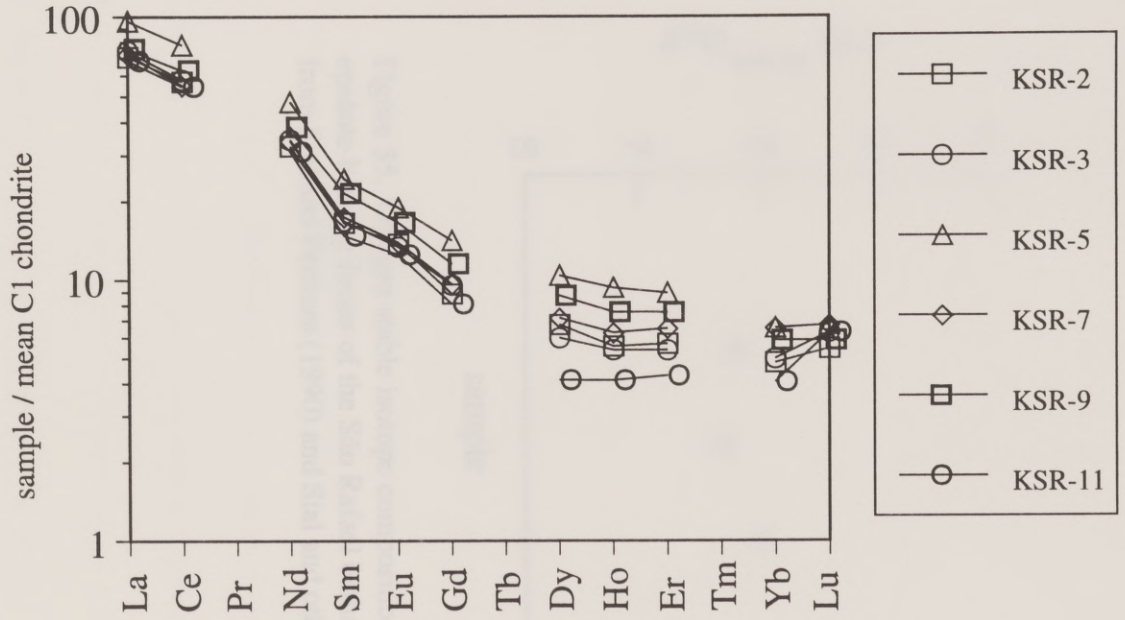

Figure 34. Coryell-Masuda (REE) plot for epidote-bearing facies. Normalized according to Anders and Grevesse (1989).

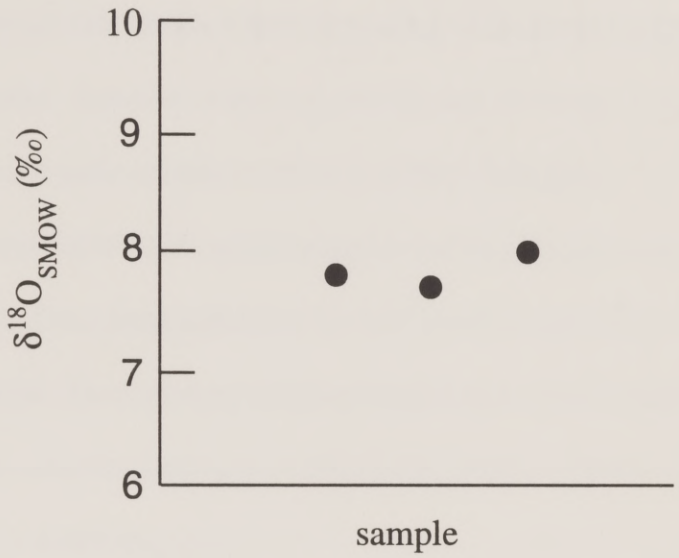

Figure 35. Oxygen stable isotope compositions for the epidote-bearing facies of the São Rafael batholith. Modified from Sial and Ferreira (1990) and Sial and others (in press).

geochemistry of the São Rafael batholith suggests that it is I-type, i.e., derived from melting of an igneous precursor.

GEOBAROMETRY AND GEOTHERMOMETRY

Magmatic Epidote

Epidote is a calcium-aluminum silicate mineral of the formula $Ca_2Al_{2+x}Fe_{1-x}Si_3O_{12}(OH)$. It has long been recognized as a common metamorphic mineral and as a subsolidus alteration product of biotite and plagioclase in igneous rocks. However, it was not until the late 1970s that workers began to recognize that some epidote occurs as a primary melt phase.

Tulloch (1979) identified occurrences of epidote as an early magmatic phase in the Cretaceous plutons of the Karamea Batholith of the South Island of New Zealand. There primary (magmatic) epidote is characterized by pale, weakly pleochroic, euhedral inclusions within biotite. It has a pistacite content [atomic $Fe^{3+}/Fe^{3+} + Al$)]of Ps_{27-29}.

Naney (1983) was the first to produce epidote experimentally in synthetic granite and granodiorite melts at 200 and 800 MPa. Epidote was observed at only 800 MPa, giving evidence for the existence of stability only at high pressures. Naney concluded that the epidote/melt equilibrium is pressure-dependent. His experiments show that epidote is stable over a range of 100 °C in a granodioritic melt at 8 kbar and $a_{H2O} = 1$.

Textural relationships indicate that magmatic epidote commonly forms through the resorption of hornblende into the melt and precipitation of epidote around the remnants of the hornblende according to the reaction:

$$2HB + 2af + 2AN + 1mt + nH_2O + mO_2 = 3EP + 3BT + 6q$$

where HB (hornblende), AN (plagioclase), EP (epidote) and BT (biotite) are solid phases, and af (alkali feldspar), mt (magnetite) and q (quartz) are implicit melt components (Zen and Hammarstrom, 1984). Magmatic epidote can also crystallize directly from a melt, even in the absence of hornblende, as shown for dacitic dikes in the Front Range of Colorado (Dawes and Evans, 1991).

Zen and Hammarstrom (1984) proposed that magmatic epidote may be identified by these criteria: 1) concentration of epidote with other mafic minerals in flow bands; 2) similarity of crystal sizes of epidote, hornblende, and biotite; 3) epidote overgrowth on euhedral allanite cores; 4) euhedral epidote crystal faces against biotite, but embayed where in contact with plagioclase and quartz; 5) zoned or twinned epidote; 6) occurrence of hornblende resorption textures, e.g., highly embayed hornblende crystals surrounded by epidote or encased within plagioclase; 7) absence of alteration minerals.

Sial (1990) identified four textural types of epidote in the epidote-bearing granitoid plutons of northeast Brazil. Type I epidote occurs as euhedral to subhedral, prismatic to elongate crystals included in cores of plagioclase phenocrysts. Type II epidote is relatively common and appears as euhedral to subhedral crystals with euhedral, oscillatory zoned allanite cores. The most common form of occurrence is Type III which is similar to Type II but which lacks the allanite core and is rimmed or included by biotite. Type IV is rare and is usually observed in mafic enclaves. It consists of granular epidote along boundaries of hornblende and biotite, in contact with plagioclase. Types II and III are magmatic, whereas type I and type IV result from the breakdown of calcic cores of plagioclase during cooling (Type I) and subsolidus reaction of hornblende with plagioclase (Type IV).

Occurrences of epidote in the main facies, Serra facies, and mafic enclaves of the São Rafael batholith exhibit many of these characteristic features of magmatic epidote. Epidote occurs most commonly in association with biotite and hornblende as euhedral to subhedral crystals with and without allanite cores (Types II and III of Sial (1990)). It also displays straight crystal faces against biotite. Minor Type IV epidote is also observed.

Magmatic Epidote as a Pressure Indicator

Zen and Hammarstrom (1984) also proposed the use of magmatic epidote as an indicator of high-pressure emplacement of plutons and conducted a study of three epidote-bearing tonalitic plutons in the North American Cordillera. They estimated a minimum pressure of emplacement of 6 kbar for the plutons (Zen and Hammarstrom, 1984; Zen, 1985).

Interpretations of high-pressure emplacement for magmatic epidote-bearing plutons are based on: 1) the phase equilibrium data of Naney (1983) and experimental data of Liou (1973); 2) the intersection of the epidote stability curve with the liquidus curve for tonalitic melts which occurs only at pressures of 6 kbar or higher; 3) high pressures of intrusion estimated from the pressure of regional tectonism and metamorphism (Zen, 1985).

Magmatic epidote by itself is not necessarily indicative of high pressure emplacement (Tulloch, 1986; Moench, 1986). One of the complications arises from the variability of pistacite content of epidote. The full range of epidote composition ranges from Ps_0 to Ps_{48} (mole %). Zen (1989) states that the presence of epidote does not indicate high pressure unless proper conditions are met, including a Ps content of 20-25, a range of Ps that includes only a very limited part of the range of magmatic epidote reported by Johnston and Wyllie

(1988). Thus only some magmatic epidote apparently is suited for use as a pressure indicator.

Magmatic epidote in the São Rafael batholith shows a narrow compositional range (Sial and others, in press). Pistacite content varies from Ps_{27-29}, within the range of igneous epidote, but higher than the 20-25 range suggested by Zen (1989) for high-pressure crystallization (Fig. 36). These epidote compositions fall between the nickel-bunsenite buffer (Ps_{25}) and magnetite-hematite buffer (Ps_{33}) curves on a Log fO_2-T diagram (Liou, 1983). Thus crystallization probably occurred at an fO_2 between these buffers.

Limitations of Application. Zen and Hammarstrom (1986) and Zen (1989) stress that magmatic epidote can be used as a pressure indicator only for rocks with a mineral assemblage (quartz, high-Al hornblende, biotite, plagioclase, K-feldspar, titanite, and/or magnetite and ilmenite) that buffers the chemical components in epidote. A reaction relationship between hornblende and epidote should also be evident to further support the magmatic hypothesis.

Many estimates of depths of emplacement for epidote-bearing plutons come from the use of the Al-in-hornblende geobarometer in conjunction with information from metamorphic mineral assemblages in the country rocks. There are a number of calibrations of geobarometers, some quite discrepant, based on a presumed linear relationship between aluminum in hornblende and total pressure.

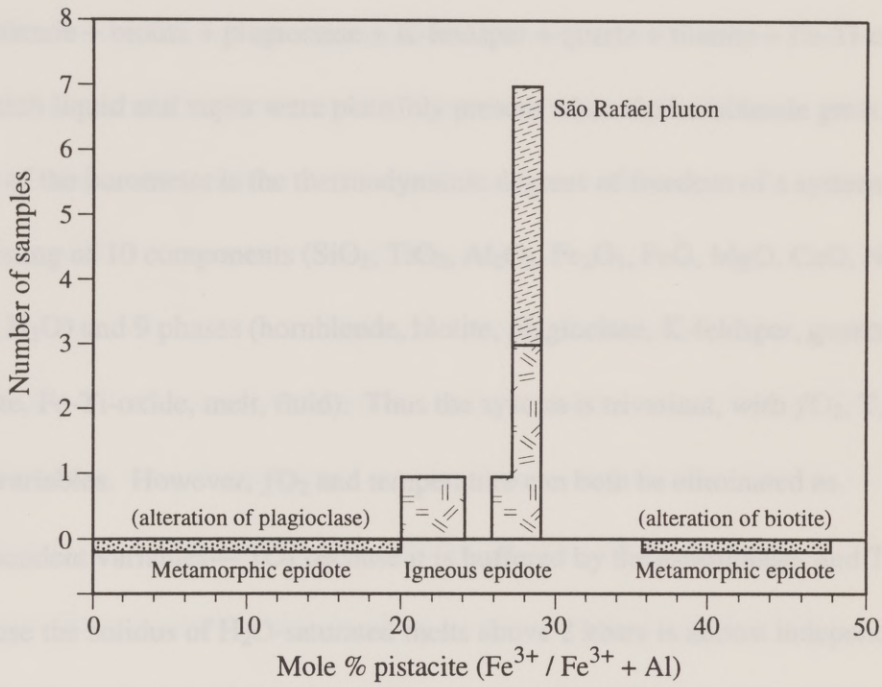

Figure 36. São Rafael epidote compositions in mol per cent pistacite, and pistacite compositions of magmatic and non-magmatic epidote. Modified from Sial and others (in press).

As much as a 2 kbar difference in the estimated pressure is possible using different calibrations applied to the same data set (Johnson and Rutherford, 1989).

Al-in-hornblende Geobarometer

As mentioned, the geobarometer applies to igneous rocks containing hornblende + biotite + plagioclase + K-feldspar + quartz + titanite + Fe-Ti-oxide, in which liquid and vapor were plausibly present when the hornblende grew. The basis of the barometer is the thermodynamic degrees of freedom of a system consisting of 10 components (SiO_2, TiO_2, Al_2O_3, Fe_2O_3, FeO, MgO, CaO, Na_2O, K_2O, H_2O) and 9 phases (hornblende, biotite, plagioclase, K-feldspar, quartz, titanite, Fe-Ti-oxide, melt, fluid). Thus the system is trivariant, with fO_2, T, and P as variables. However, fO_2 and temperature can both be eliminated as independent variables— fO_2 because it is buffered by the assemblage, and T because the solidus of H_2O-saturated melts above 2 kbars is almost independent of temperature. Under these stringently prescribed circumstances, pressure can be correlated directly to the variation of total aluminum in hornblende (Hammarstrom and Zen, 1986; Hollister and others, 1987; Schmidt, 1992).

Hammarstrom and Zen (1986) made the first empirical pressure calibration of total aluminum (Al^T) in hornblende. Since then, Hollister and others (1987), Johnson and Rutherford (1989) and Rutter and others (1989) have

produced other, somewhat different, calibrations of the Al-in-hornblende geobarometer. The most recent calibration was presented by Schmidt (1992) who performed experiments on natural tonalite at pressures in the range of 2.5-13 kbar and temperatures of 700-655 C. The resulting geobarometer is:

$$P\ (\pm 0.6\ \text{kbar}) = -3.01 + 4.76Al^{T}$$

Al^{T} is in atoms per formula unit (apfu), based on amphibole compositions normalized to $Fe^{3+}/(Fe^{3+} + Fe^{2+}) = 0.30$ and 23 oxygens. The Schmidt (1992) calibration is consistent with earlier experimental calibrations, but provides data for greater intervals of pressure and temperature.

The most important limitation of the Al-in-hornblende geobarometer is the stipulation of the necessary suite of mineral species. It is also necessary that hornblende be in equilibrium with quartz. Otherwise, total aluminum becomes a function of both pressure and silica activity, and the barometer gives a falsely low pressure (Hammarstrom and Zen, 1986; Johnson and Rutherford, 1989). Commonly, only hornblende rim analyses are used in order to ensure that the hornblende actually analyzed was indeed in equilibrium with the quartz. In general, the rock must be more mafic than a quartz diorite to contain this mineral assemblage. The amphibole must equilibrate close to the water-saturated solidus if its composition is to be independent of temperature (Poli and Schmidt, 1992).

This is usually not a problem because the presence of K-feldspar indicates that conditions must have been near the solidus.

Blundy and Holland (1990) point out that subsolidus re-equilibration can occur in amphibole; Hammarstrom and Zen (1986) contend that Al is not very mobile under subsolidus conditions, and that the method should be applied only where there is no textural evidence for disequilibrium.

Plagioclase-hornblende Thermometer. Blundy and Holland (1990) introduced a thermometer based on the Al^{iv} content of amphibole coexisting with plagioclase in silica-saturated rocks. This thermometer is valid for amphiboles with less than 7.8 apfu Si and plagioclase less calcic than An_{92}. It is claimed to be accurate to ±75°C for temperatures between 500 and 1100°C.

Geobarometry and Geothermometry of the batholith. Sial and others (in press) determined compositions of amphibole and plagioclase from four samples of the epidote-bearing facies of the São Rafael batholith by electron microprobe analysis, and applied the Al-in-hornblende geobarometer and the plagioclase-hornblende thermometer to the rocks. Figure 37 is a plot of the analyzed amphibole compositions, which are predominantly edenite to edenitic hornblende. The average plagioclase composition is Ab_{82} An_{17} $Or_{1.0}$ but ranges from Ab_{98} $An_{1.5}$ $Or_{0.5}$ to Ab_{78} An_{21} $Or_{1.0}$.

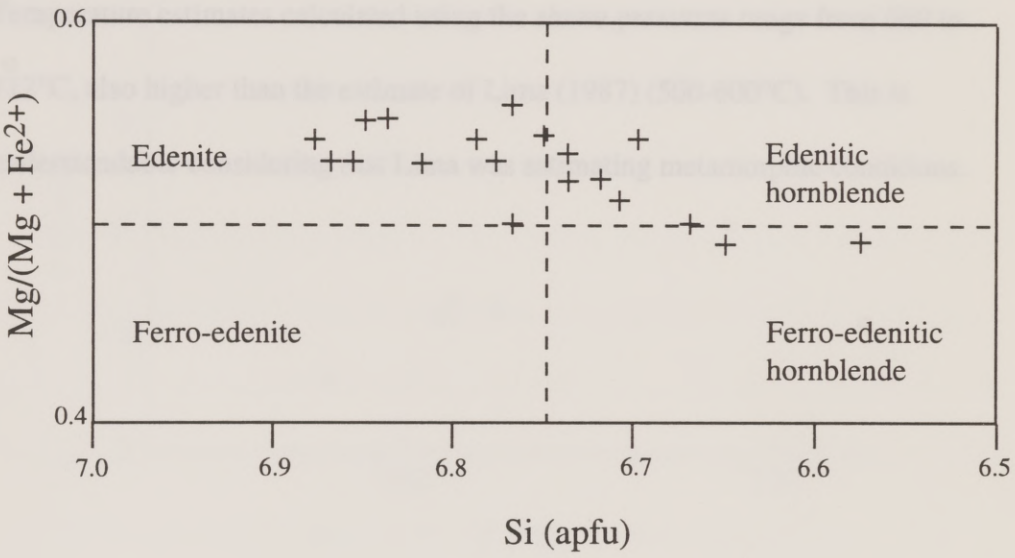

Figure 37. Amphibole compositions for the epidote-bearing facies, as determined by electron microprobe analysis. From Souza (unpublished thesis).

Figure 38 is a plot of P (Schmidt) *vs.* T (Blundy-Holland) for the batholith. Pressures were calculated using the Al-in-hornblende calibration of Schmidt (1992). The barometer yields pressures of 3.8 to 4.7 kbar (average 4.1 kbar ± 0.4), a value that is slightly higher than the pressure estimate of 2-4 kbar for the Seridó Fm. (the eastern country rocks) near Currais Novos (Lima, 1987). Temperature estimates calculated using the above pressures range from 680 to 712°C, also higher than the estimate of Lima (1987) (500-600°C). This is understandable considering that Lima was estimating metamorphic conditions.

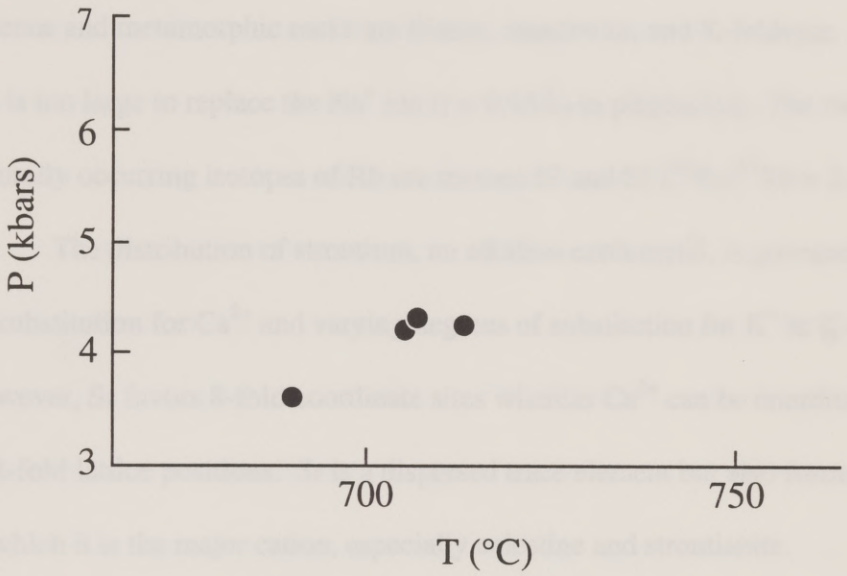

Figure 38. P vs. T plot for the São Rafael batholith based on the Al-in-hornblende geobarometer of Schmidt (1992) and the plagioclase-hornblende thermobarometer of Blundy and Holland (1990). Modified from Sial and others (in press).

Rb-Sr ISOTOPE GEOCHEMISTRY

Geochemistry of Rb and Sr

Rubidium, an alkali metal, (r = 1.48Å) fits readily into K^+ (r = 1.33Å) crystallographic sites. Rubidium does not form its own minerals, its distribution in nature being governed chiefly by this substitution. Principle carriers of K in igneous and metamorphic rocks are biotite, muscovite, and K-feldspar. The Rb ion is too large to replace the Na^+ ion (r = 0.95Å) in plagioclase. The two naturally occurring isotopes of Rb are masses 87 and 85 ($^{85}Rb/^{87}Rb = 2.6$).

The distribution of strontium, an alkaline earth metal, is governed chiefly by substitution for Ca^{2+} and varying degrees of substitution for K^+ in K-feldspar. However, Sr favors 8-fold coordinate sites whereas Ca^{2+} can be coordinated in 6- or 8-fold lattice positions. Sr is a dispersed trace element but also forms minerals in which it is the major cation, especially celestine and strontianite.

Age Determinations. ^{87}Rb decays to ^{86}Sr by beta decay:

$$^{87}Rb \rightarrow {}^{87}Sr + \beta^- + \nu + Q$$

Abundances of ^{87}Rb and ^{87}Sr are referenced to ^{86}Sr, which neither decays nor is a radioactive decay product:

$$\frac{^{87}Sr}{^{86}Sr} = \left(\frac{^{87}Sr}{^{86}Sr}\right)_{t=0} + \frac{^{87}Rb}{^{86}Sr}\left(e^{\lambda t} - 1\right) \quad [1]$$

where λ is the decay constant and t is time elapsed.

Certain assumptions must be fulfilled if a comagmatic suite is to be dated successfully by the Rb-Sr method. The rocks (or minerals) must have originated at the same time, with the same initial $^{87}Sr/^{86}Sr$ ratio. They must individually have remained chemically closed to Rb and Sr.

Because members of a comagmatic suite generally have differing mineral abundances and Rb/Sr is typically different in each mineral species, the result is that each member of the suite has a uniquely different $^{87}Rb/^{86}Sr$ ratio. For a given value of t, equation 1 above reduces to the equation of a straight line: $y = b + mx$. If a suite satisfies the initial assumptions of Rb-Sr dating, the data points corresponding to Rb-Sr isotopic analyses of the rocks or minerals will define a straight line (an *isochron*) in $^{87}Sr/^{86}Sr$ (y), $^{87}Rb/^{86}Sr$ (x) coordinate space. The slope of the isochron is related to the age of the Rb-Sr isotope system ($m \equiv$ slope $= d/p = e^{\lambda t}-1$), and the intercept is initial $^{87}Sr/^{86}Sr$. As Rb decays, points arrayed upon the isochron move along straight-line trajectories, each with slope of -1. The isochron, which is anchored at its y-intercept, rotates upward. To date comagmatic rocks or minerals, it is necessary to measure $^{87}Sr/^{86}Sr$ and $^{87}Rb/^{86}Sr$ in each sample. I have performed 29 analyses of rocks and minerals from the São Rafael batholith.

Sample Preparation

Rock crushing facilities of the SUDENE laboratory at UFPE, Recife were used for initial processing. 5 to 10 kg samples were ground to sand-size particles using a jaw crusher and a roller crusher. Small representative aliquots of sample returned to the University of Texas at Austin were further powdered using a tungsten carbide Shatterbox®. A pre-contamination technique was used to minimize the possibility of cross contamination. To ensure sample homogenization, each sample was Shatterboxed for ~6 minutes until a particle size of < 200 mesh was obtained.

Analytical Technique

Whole-rock samples typically weighed about 15 mg. Biotite samples weighed about 3 mg, and apatite separates averaged 0.6 mg. All samples were spiked with "old mixed spike" (a solution containing calibrated abundances and isotope compositions of Sr enriched in ^{84}Sr and Rb enriched in ^{87}Rb), except for biotite separates which were spiked with "superspike" which is characterized by a higher Rb/Sr ratio. Because a standard analytical balance was used to weigh the samples, serious errors are probably present in weighing milligram or submilligram masses. Parts-per-million concentrations are thus incorrect, but isotope ratios are accurate because they are determined through use of a mixed

spike in which isotope compositions and relative concentrations of Rb and Sr are known.

After being spiked, samples were digested in a mixture of concentrated HF and HNO_3 in 15ml screw-top Teflon containers. Samples were dried down and taken up in HCl, and most were centrifuged to ensure that no solid material had escaped dissociation. Residual solid was returned to acid dissolution until all had decomposed. Rb and Sr were isolated from all other elements and from one another by using a standard cation exchange column (BIO-RAD AG 50W-X8 resin) eluted with 2.3N HCl.

Rb isotope compositions were determined using an automated, 30-cm-radius, single-collector mass spectrometer equipped with double Ta filaments. Sr isotope compositions were determined using a Finnigan MAT-261 multicollector mass spectrometer operated in static acquisition mode. A more complete description of the analytical technique can be found in Awwiller (1992).

Rb-Sr Whole-rock Data

Twenty-four whole-rock samples (Table 5) were analyzed in this study, including 12 from the epidote-bearing facies, four from the Serra facies and two MMEs. Six additional analyses of the epidote-bearing facies, performed at the Federal University of Pará, Belém, were provided by Souza. In general, the rocks

Table 5. Rb-Sr data.

SAMPLE ID	ppm Rb	ppm Com Sr	$^{87}Rb/^{86}Sr$	$^{87}Sr/^{86}Sr)_T$
DSR-24	50.3	837.7	0.1736	0.7133
DSR-22	51.9	885.1	0.1697	0.7133
DSR-13	69.5	793.6	0.2534	0.7138
DSR-12	63.7	895.6	0.2058	0.7138
DSR-8	49.9	852.3	0.1695	0.7141
DSR-29	72.2	759.2	0.2753	0.7142
DSR-10	61.1	744.1	0.2377	0.7143
DSR-23	64.9	669.4	0.2806	0.7144
DSR-4	54.0	488.5	0.3199	0.7169
DSR-2	45.1	546.1	0.2388	0.7170
DSR-9	66.6	379.9	0.5075	0.7185
DSR-1	59.9	430.7	0.4023	0.7192
KSR-5	51.3	796.0	0.1860	0.7136
KSR-2	53.2	686.5	0.2240	0.7146
KSR-10	63.0	781.2	0.2340	0.7137
KSR-9	55.3	639.6	0.2500	0.7149
KSR-7	67.5	690.5	0.2830	0.7147
KSR-13	81.7	788.6	0.3000	0.7140
DSR-20 (Serra)	74.7	365.3	0.5918	0.7192
DSR-25 (Serra)	58.8	424.0	0.4014	0.7176
DSR-26 (Serra)	59.0	514.3	0.3317	0.7170
DSR-28 (Serra)	60.1	461.8	0.3764	0.7169
DSR-3 (MME)	104.7	496.1	0.6108	0.7173
DSR-11 (MME)	78.1	730.4	0.3095	0.7143
DSR-4 apatite	0.25	100.3	0.0071	0.7146
DSR-4 biotite	371.1	014.1	76.38	1.2550
DSR-13 biotite	431.1	013.4	92.95	1.3692
DSR-25 apatite	0.24	114.6	0.0059	0.7166
DSR-25 biotite	474.9	014.6	93.89	1.3756
DSR-13 repeat	61.5	785.2	0.2266	0.7137
DSR-25 repeat	57.8	420.1	0.3981	0.7176

All samples normalized to $^{86}Sr/^{88}Sr = 0.1194$.

have high Sr (655 ± 175 ppm standard deviation) and low Rb (61 ± 9 ppm) concentrations, with consequent low enrichment in radiogenic Sr.

On a whole-rock isochron diagram (Fig. 39), data from all the samples yield an errorchron of t = 1.11 ± 0.39 Ga with an initial $^{87}Sr/^{86}Sr$ ratio (R_0) of 0.711. (In the literature, the rather inappropriate term "errorchron" refers to a data pattern that deviates markedly from the anticipated linear array.) Data of the 18 epidote-bearing facies rocks plot as an amorphous "blob." Values of $^{87}Rb/^{86}Sr$ and $^{87}Sr/^{86}Sr$ in Serra samples are consistently higher than in the main blob. One MME data point plots with the Serra samples, whereas the other one plots in the midst of the "blob" for epidote-bearing facies rocks.

A plot corresponding only to the epidote-bearing facies samples gives an errorchron of t = 1.64 ± 0.53 Ga, with R_0 of 0.709 (Fig. 40). Data from the four Serra samples give a poorly-constrained isochron age of 0.612 ± 0.054 Ga, with a high initial Sr ratio of 0.714 (Fig. 41).

The ages formally calculated for the data arrays in Figures 39 and 40 have not only very large associated errors, but they are also inconsistent with the field relations and unfoliated nature of the São Rafael batholith. That is, a pluton with >1 Ga age should have experienced Brasiliano deformation and metamorphism, for which there is no evidence in São Rafael outcrop or thin section. I attribute the scatter of data, and erroneous ages, to inhomogeneity of initial Sr ratios. The

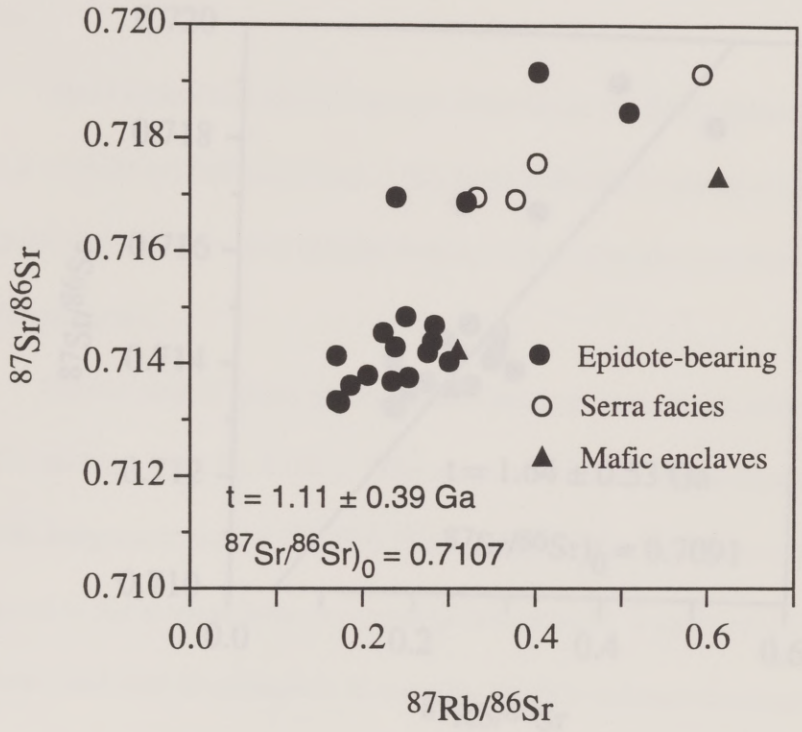

Figure 39. Plot of $^{87}Sr/^{86}Sr$ *vs.* $^{87}Rb/^{86}Sr$ for São Rafael whole-rock samples.

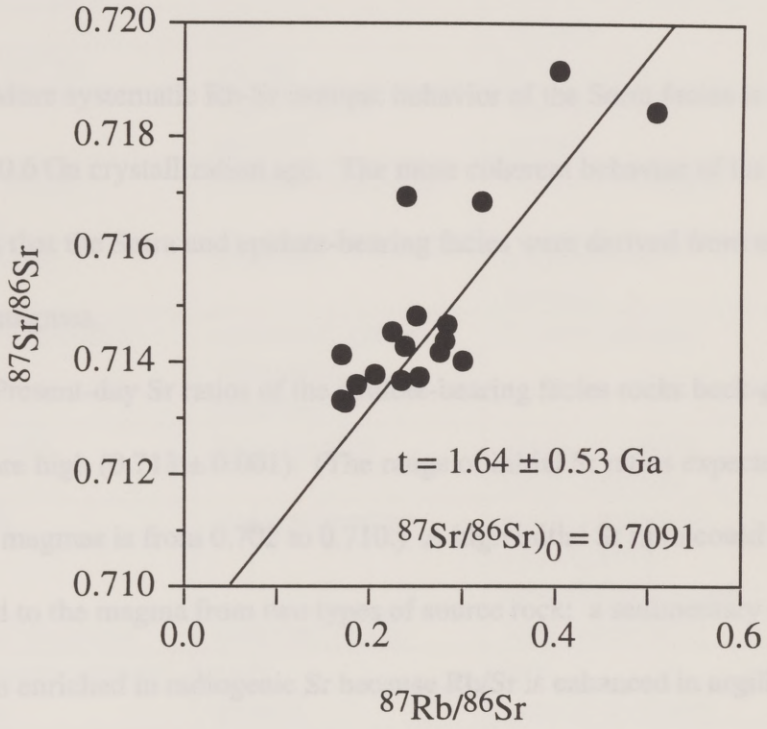

Figure 40. Rb-Sr whole-rock plot for the epidote-bearing facies.

São Rafael magma must have been generated from partial melting of at least two source rocks having different ratios of $^{87}Sr/^{86}Sr$, that later failed to homogenize. The inhomogeneity of initial Sr ratios precludes the determination of a geologically meaningful Rb-Sr age of crystallization for the epidote-bearing facies.

More systematic Rb-Sr isotopic behavior of the Serra facies is consistent with a ~0.6 Ga crystallization age. The more coherent behavior of the Serra facies suggests that the Serra and epidote-bearing facies were derived from separate, but related magmas.

Present-day Sr ratios of the epidote-bearing facies rocks back-calculated to 0.6 Ga are high (0.713 ± 0.001). (The range of initial Sr ratios expected in most granitic magmas is from 0.702 to 0.710.) A high initial Sr ratio could have been imparted to the magma from two types of source rock: a sedimentary source that had been enriched in radiogenic Sr because Rb/Sr is enhanced in argillaceous products of weathering, or a source consisting of very ancient crust in which radiogenic Sr had built up by decay of Rb over a long time interval. The first-mentioned hypothesis is unlikely because, other than for exhibiting elevated initial Sr ratios, the pluton does not have most of the characteristics of S-type granitoid rocks (those derived from rocks that had been enriched in K and Al through weathering processes at the earth's surface; see Table 6). A more likely

Table 6. Some generalized characteristics of S- and I-type granitoid plutons. From Chappell and White (1974), Chappell and White (1992), Chappell (1984), Hines and others (1978) and O'Neil and Chappell (1977).

	S-type	I-type	São Rafael
mol K/(Na +K)	>0.5	<0.5	I
alumina saturation	>1.1	<1.1	I
normative c or di	>1% c	<1% c or di present	I
SiO_2	high	variable	I
initial $^{87}Sr/^{86}Sr$	>0.708	0.704-0.712	S
$\delta^{18}O$	"heavy" (>10 permil)	"lighter" (<10 permil)	I
hydrous mafic minerals	biotite + muscovite	biotite + ca-amph.	I
Fe-Ti oxides	ilmenite	magnetite +/- ilmenite	I
accessory minerals	cordierite, garnet, sillimanite, monazite	titanite, allanite	I
apatite habit	large crystals	small, in biotite and amphibole	I
xenoliths	metasedimentary	mafic igneous or meta-igneous, amphibole-bearing	I
variation diagrams	scattered points	tight linear array	I
time of emplacement	early	late	I
foliation	present	present or absent	I

possibility is the second one, that Archean crust was partially melted to form the São Rafael pluton. The existence of Archean-age basement (Caicó Complex) adjacent to the Seridó Foldbelt supports this possibility.

Mineral-Whole-rock Data

Biotite and apatite mineral separates from three whole-rock samples (DSR-4, DSR-13, and DSR-25) were also analyzed. DSR-4 and DSR-13 are samples representative of the epidote-bearing facies; DSR-25 is a Serra sample. Three-point biotite-whole-rock-apatite isochrons for DSR-4 (Fig. 42) and DSR-25 (Fig. 44), and a two-point biotite-whole-rock isochron for DSR-13 (Fig. 43) provide cooling ages of 0.49 ± 0.01 Ga. The $^{87}Sr/^{86}Sr$ ratios at 0.49 Ga for the isochrons are high (i.e. 0.712-0.715). These data are consistent with the conclusion that initial Sr ratios were relatively high if crystallization had occurred at 0.6 Ga.

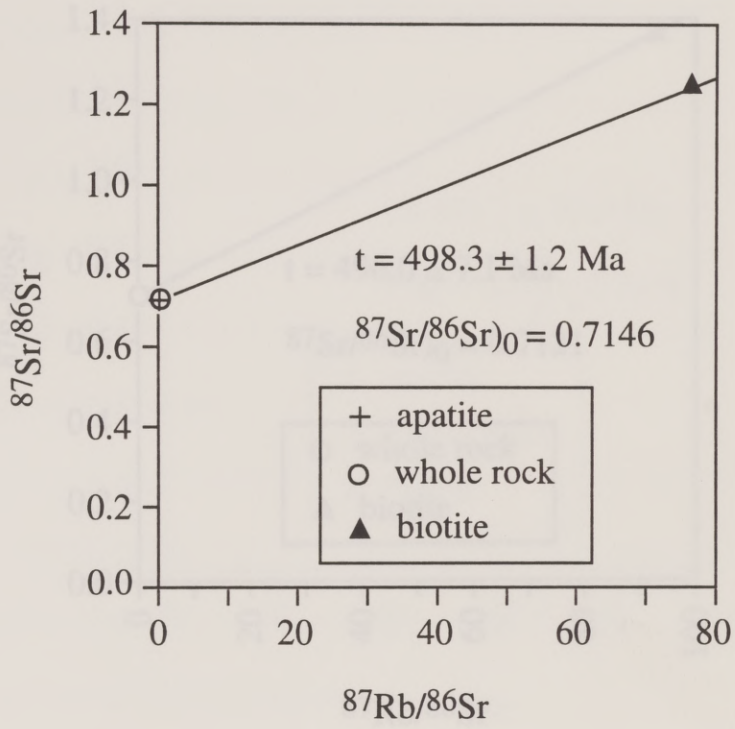

Figure 42. DSR-4 Rb-Sr mineral-whole-rock isochron diagram.

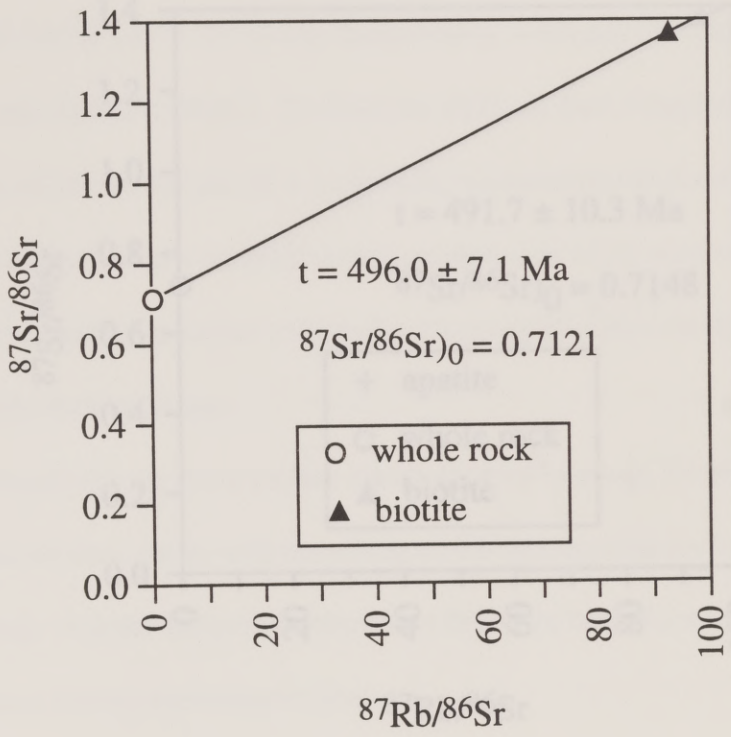

Figure 43. DSR-13 Rb-Sr biotite-whole-rock isochron diagram.

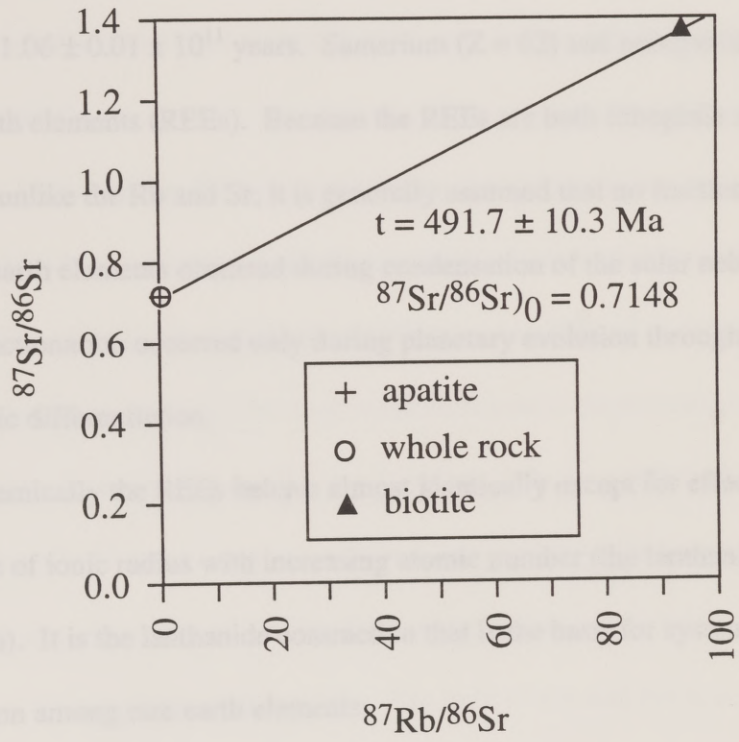

Figure 44. DSR-25 Rb-Sr mineral-whole-rock isochron diagram.

Sm-Nd ISOTOPE CHEMISTRY

Geochemistry of Sm and Nd

Principles of the Sm-Nd method are analogous to those of the Rb-Sr method. The Sm-Nd method is based on the α-decay of ^{147}Sm to ^{143}Nd with a half-life of $1.06 \pm 0.01 \times 10^{11}$ years. Samarium (Z = 62) and neodymium (Z = 60) are rare earth elements (REEs). Because the REEs are both lithophile and highly refractory, unlike the Rb and Sr, it is generally assumed that no fractionation of these rare earth elements occurred during condensation of the solar nebula. Instead, fractionation occurred only during planetary evolution through processes of magmatic differentiation.

Chemically the REEs behave almost identically except for effects related to decrease of ionic radius with increasing atomic number (the lanthanide contraction). It is the lanthanide contraction that is the basis for systematic fractionation among rare earth elements.

Abundances of REE are generally plotted by atomic number (i.e., element by element), the abundance data being normalized to average abundances in chondritic meteorites (known as CHUR: CHondritic Uniform Reservoir (DePaolo and Wasserburg, 1976)). Partial melts are generally enriched in REEs, with elevated patterns relative to CHUR. Granites typically are much more enriched in light rare earths (LREEs) than the other REEs, and therefore the plots tend to have

both high y-intercepts and steep slopes. Sm and Nd are both light rare earths (LREEs) and the Sm/Nd ratio generally reflects the overall abundance of LREEs in a sample (low Sm/Nd- enriched in LREE, high Sm/Nd- depleted in LREE). The range of abundances of Sm/Nd in rocks is very narrow (0.1 to 0.5 by weight) compared to variations of parent/daughter of most other isotope systems of geologic interest.

The advent of Sm-Nd as a useful dating tool depended on two technological advancements: (i) the development of ion exchange methods to separate REEs effectively, and (ii) the development in 1969 of computer-interfaced mass spectrometers making possible dramatic improvements of precision of isotope abundance ratio measurement. The ion exchange and computer interfaced mass spectrometry were first combined by Lugmair (1974).

A major advantage of the Sm-Nd isotope system over Rb-Sr or U-Th-Pb is that Sm and Nd are relatively immobile. The bulk of Sm and Nd is contained in major minerals such as pyroxene and plagioclase that are less susceptible to leaching than are the smaller grains of trace phases. In addition, the decay of ^{147}Sm does not cause as much structural damage to the crystal as does U decay. The energy released by the decay of U can be about 2000 times greater than that produced by Sm decay (DePaolo, 1988). Furthermore, Sm and Nd naturally

occupy the same structural sites (there is no "misfit" of daughter atoms in the crystal lattice as there is with Sr, and especially with Pb).

Age Determinations. The principles of the Sm-Nd and Rb-Sr isochrons are analogous. In a Sm-Nd isochron, the *y*-axis is $^{143}Nd/^{144}Nd$; the *x*-axis is $^{147}Sm/^{144}Nd$.

Most magmas are well enough mixed to cause the minerals to crystallize with the same initial $^{143}Nd/^{144}Nd$, at least at the scale of sample size. High-grade metamorphism can cause rehomogenization of $^{143}Nd/^{144}Nd$, effectively resetting the system at some time later than $t_{crystallization}$. The reasoning here for the Rb-Sr and Sm-Nd systems is the same.

Determination of a mineral isochron is improved if there are relatively large differences in $^{147}Sm/^{144}Nd$ amongst the samples. Feldspars, apatite, and monazite all incorporate low Sm/Nd ratios. Pyroxene, garnet, titanite, zircon, and amphibole have higher Sm/Nd. Because there are no common minerals in which $^{147}Sm/^{144}Nd$ is near zero (no data points near the *y*-intercept on an isochron diagram), the initial $^{143}Nd/^{144}Nd$ ratio is difficult to obtain precisely.

Whole-rock isochrons can be measured with acceptable precision on suites characterized by a sufficient range of $^{143}Nd/^{144}Nd$. This method is advantageous because large sample sizes reduce the impact of geochemical disturbance due to

postcrystallization isotopic re-equilibration. Just as for the Rb-Sr isochron, violations of underlying assumptions invalidate a straightforward interpretation of the Sm-Nd isochron.

Notation and Sm-Nd Model Ages. Variations of $^{143}Nd/^{144}Nd$ are so small (largely because of the long half-life of ^{147}Sm) that comparisons are facilitated by representing ratio data in terms of deviations from a standard value. The $^{143}Nd/^{144}Nd$ of any rock sample at time T may be represented by ε_{Nd} (T) which is defined as:

$$\varepsilon_{Nd}(T) = 10^4\left[\frac{^{143}Nd/^{144}Nd_{sample}(T) - {}^{143}Nd/^{144}Nd_{CHUR}(T)}{^{143}Nd/^{144}Nd_{CHUR}(T))}\right]$$

$\varepsilon_{Nd}(T)$ is the deviation of a ratio from that of CHUR in parts per 10^4. An approximate sample age can be derived from $\varepsilon_{Nd}(0)$ using the relationship:

$$\varepsilon_{Nd}(T) = \varepsilon_{Nd}(0) - 25.13 b.y.^{-1} f_{Sm/Nd} T$$

$f_{Sm/Nd}$ is the chemical fractionation parameter, defined as the difference between $^{147}Sm/^{144}Nd$ ratios of the sample and of CHUR, divided by the $^{147}Sm/^{144}Nd$ ratio of CHUR. If a typical crustal rock value of -0.4 is assumed for this factor, and assuming $\varepsilon_{Nd}(T) = 0$, then the epsilon value at time = 0 can be roughly equated to a crystallization age (T) by $\varepsilon_{Nd}(0) = -10.05$ T.

The CHUR model provides the basis for further modeling of the evolution of Nd in the crust and mantle. As mentioned, the decay of ^{147}Sm to ^{143}Nd causes the $^{143}Nd/^{144}Nd$ in CHUR to increase through time, at a rate proportional to the Sm/Nd ratio. Suppose that at some time (T1) in the past, partial melting of a portion of the reservoir occurred to form ancient crust. This crust would be enriched in LILs and a counterpart zone in the mantle would be depleted in these elements relative to CHUR. Moreover, typically crust is enriched in Nd relative to Sm. Further growth of the $^{143}Nd/^{144}Nd$ ratio in the crust would therefore be slower than in CHUR. Conversely, Sm/Nd would be higher in the depleted zone (depleted mantle), and the $^{143}Nd/^{144}Nd$ ratio would evolve more rapidly than in CHUR.

Much of the crust is assumed to be derived from zones in the upper mantle that were previously depleted in LILs. A theoretical "crust formation age" can be calculated relative to the mantle evolution curve because, after the event of differentiation, radiogenic Nd continues to grow in the crustal and mantle reservoirs at different rates. A depleted mantle model age (T_{DM}) is a calculation of the time when the Sm-Nd system within a crustal sample had separated from the depleted mantle reservoir. It corresponds to the projected intersection of sample data with the depleted mantle curve (Fig. 45). The depleted mantle model

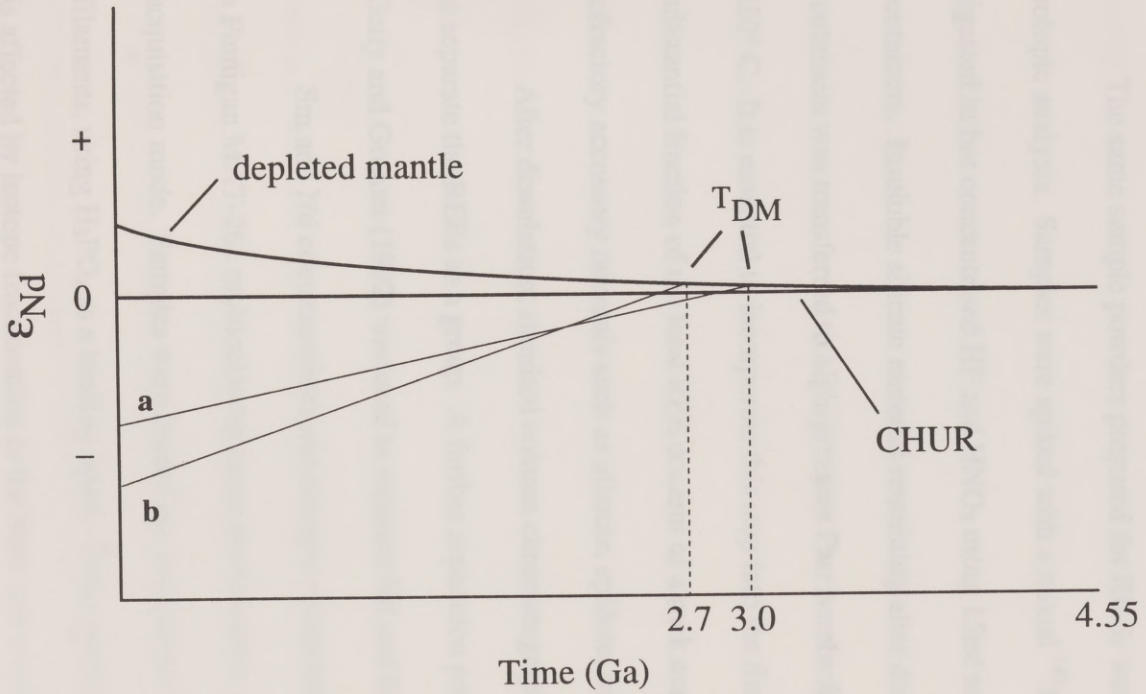

Figure 45. A graphic representation of a Sm-Nd depleted mantle model age (T_{DM}). The T_{DM} is calculated from present-day ε_{Nd} and Sm and Nd concentrations. It is illustrated as the intersection of a diagonal sample line with the depleted mantle curve and represents the time at which a sample would have separated from a hypothetical depleted mantle reservoir. Sample **a** and sample **b** represent two rocks with different present-day ε_{Nd} and Sm and Nd concentrations. Note the dependence of theT_{DM} on both the intercept and slope of the line.

age (T_{DM}) is calculated from Sm and Nd concentrations and $^{143}Nd/^{144}Nd$ and the depleted mantle curve of DePaolo (1981).

Analytical Technique

The same sample powders prepared for Rb-Sr were used for Sm-Nd isotopic analysis. Samples were spiked with a mixed ^{147}Sm-^{146}Nd spike and digested in hot concentrated HF and HNO_3 using 15ml screw-top Teflon containers. Insoluble silicate material remaining after dissolution in the screw-top containers was transferred to high-pressure Parr bombs for total dissolution at 230° C. It is essential to incorporate this step into the Sm-Nd procedure because a substantial fraction of the total REE content of a rock may be bound up in refractory accessory minerals such as allanite, epidote, or titanite.

After dissolution, standard column chromatography techniques were used to separate the REEs as a group. A further separation procedure similar to that of Getty and Gromet (1992) was used to separate Nd and Sm.

Sm and Nd concentrations and isotopic compositions were measured using a Finnigan MAT-261 multicollector mass spectrometer, operated in static acquisition mode. Samples were loaded on, and ionized with, double Re filaments, using H_3PO_4 as a binding agent. Determination of isotope abundance is affected by isotope fractionation in the mass spectrometer. Laboratories use a

number of different ratios of nonradiogenic Nd isotopes to correct for this problem. In the procedure used at the University of Texas, the measured values were corrected for fractionation with $^{146}Nd/^{142}Nd = 0.636151$ (Wasserburg and others, 1981). Other details of the analytical technique can be found in Awwiller (1992).

Sm-Nd Whole-rock Geochemistry

Data from six whole-rock samples provide a Sm-Nd isochron apparent age of ~1.1 Ga, which is inconsistent with field evidence for late Brasiliano emplacement (Fig. 46). The anomalous Sm-Nd data ("fictitious" isochron) indicate that initial Nd ratios were also inhomogeneous, just as Sr initial ratios were. Note that the datum from the Serra facies sample (DSR-25) plots off the trend defined by the epidote-bearing facies samples and the MME. The Serra data point was not included in the isochron calculation.

The Sm-Nd data are shown in Table 7 with epsilon values and depleted mantle model ages. The strongly negative values of $\varepsilon Nd_{0.6\ Ga}$ (-18 to -21) imply that the source was relatively enriched in Nd, a characteristic of continental crust. The longer a Sm-Nd system resides in a crustal reservoir before partial melting produces granitic magma, the more negative the value of ε_{Nd} becomes.

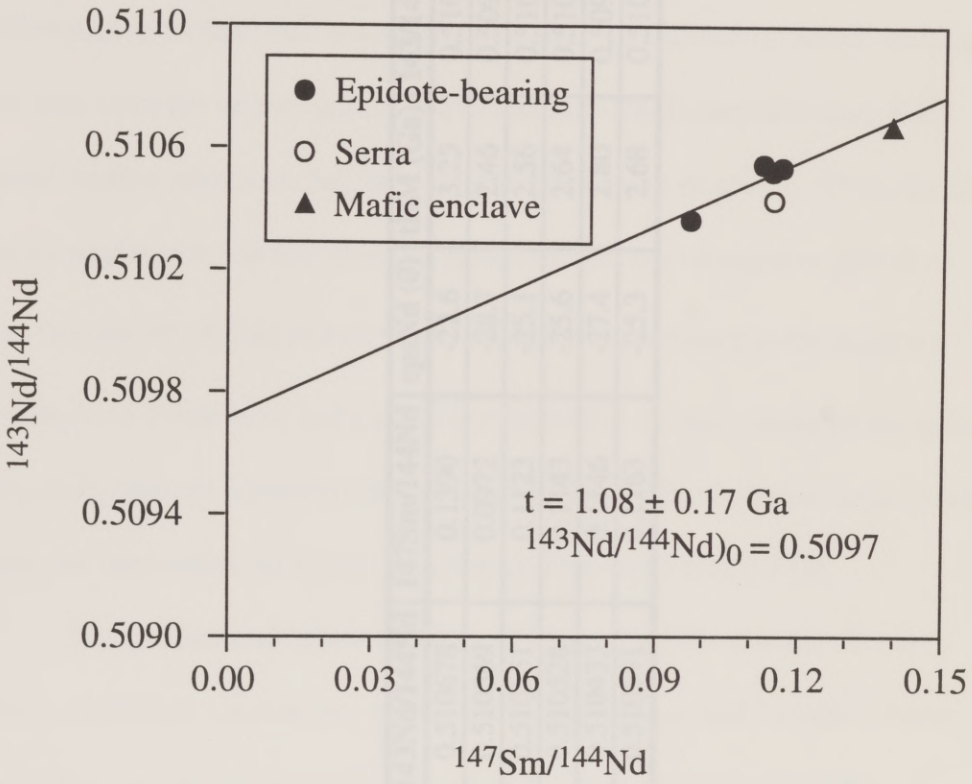

Figure 46. Sm-Nd whole-rock isochron diagram.

Table 7. Sm-Nd isotopic data.

Sample ID	ppm Nd	ppm Sm	143Nd/144Nd	147Sm/144Nd	epsNd (0)	tDM (Ga)	143/144(0.6)	epsNd (0.6)
DSR-3	52.96	12.178	0.510678	0.1390	-22.6	3.25	0.510131	-18.2
DSR-4	12.89	2.072	0.510369	0.0972	-28.7	2.46	0.509987	-21.1
DSR-13	18.29	3.398	0.510551	0.1123	-25.1	2.56	0.510109	-18.7
DSR-24	20.19	3.817	0.510528	0.1143	-25.6	2.64	0.510079	-19.3
DSR-25	12.02	2.277	0.510433	0.1146	-27.4	2.80	0.509982	-21.1
DSR-29	17.10	3.289	0.510541	0.1163	-25.3	2.68	0.510084	-19.2

This precursor time interval is estimated by calculation of a depleted mantle model age (T_{DM}). According to the DePaolo (1981) model, the São Rafael source separated from the depleted mantle reservoir at a minimum age of 2.7 ± 0.3 Ga. The calculated age is a minimum because there have actually been two differentiation events: first when the source rock was formed by partial melting, and later when the source rock melted to make the São Rafael batholith. Each partial melting event enriched the melt in Nd relative to its source. Thus, the São Rafael source rock was less enriched in Nd (smaller rate of negative growth of ε_{Nd}) than the São Rafael batholith, and the line projected back to the depleted mantle curve would have had a shallower slope than the line calculated using the present-day isotope compositions from the batholith. The shallower slope would cause the intersection (at T_{DM}) to be at an age even older than 2.7 Ga.

The geochemical behaviors of the Rb-Sr and Sm-Nd systems lead to several consistent conclusions: (i) the anomalous ages yielded by both systems due to inhomogeneous initial ratios provide two lines of evidence for the formation of the São Rafael magma by incomplete mixing of two or more partial melts with distinctive isotopic characters; (ii) the isotopic behavior of the Serra samples is also consistently different from that of the epidote-bearing facies; (iii) the strongly negative $\varepsilon Nd_{0.6\ Ga}$ values, 2.7 Ga minimum depleted mantle model

ages, and the high initial Sr ratios of the pluton (at 0.6 Ga) all suggest that the São Rafael source rock was ancient crust. This last conclusion is also consistent with the existence of Archean basement in northeastern Brazil.

U-Pb ZIRCON GEOCHRONOLOGY

Preliminary Results

U-Pb analyses of a single zircon sample are in progress in an attempt to pinpoint the precise crystallization age of the São Rafael batholith. DSR-13, a very fresh rock collected from a quarry, was chosen as the most representative sample. Zircons were separated from the bulk rock by using a Wilfley table, heavy liquids, and magnetic separation, then hand picked, and three fractions based on grain size and morphology were isolated.

Thus far, only one fraction composed of large multi-faceted clear grains has been partially analyzed. Some grains with visible cores were discarded. Prior to dissolution in a Parr bomb the sample was air-abraded for >3 days.

This fraction is highly discordant (44% Pb loss), with a $^{207}Pb/^{206}Pb$ age of 2.0 Ga (Table 8). Two possible interpretations are: (i) the rock crystallized at 2.0 Ga and has experienced drastic lead loss (or much less likely, uranium gain), or (ii) relict cores are present containing an inherited component whose age is older than 2.0 Ga.

Table 8. Preliminary U-Pb results for DSR-13.

U (ppm)	204.60
Pb total (ppm)	43.77
Pb rad (ppm)	43.73
$^{206}Pb/^{238}U$	0.20175
$^{207}Pb/^{235}U$	3.36334
$^{207}Pb/^{206}Pb$	0.12091
$^{208}Pb/^{206}Pb$	0.1105
Model : Th (ppm)	44.78
Model : Th/U	0.219
$^{206}Pb/^{238}U$ age (Ma):	1184.69
$^{207}Pb/^{235}U$ age (Ma):	1495.90
$^{207}Pb/^{206}Pb$ age (Ma):	1969.71

Model i is not favored because a 2.0 Ga primary age is inconsistent with all of the field evidence, and there is no textural evidence (such as foliation) for a metamorphic event that could have caused lead loss (uranium gain). Moreover, such extreme discordance is much higher than that caused by diffusion of lead, for which typical values are only a few per cent. The crystals are very clear, lacking any indication of radiation damage. As mentioned, the rock sample was freshly quarried, not collected from a weathered outcrop.

A more plausible hypothesis is that part of the zircon is neoformed, and part contains an inheritance of old Pb from the source rock. In this interpretation, the position of the data point on a concordia diagram lies on a mixing line whose upper intercept corresponds to the age of the precursor, and whose lower intercept

provides the crystallization age of the São Rafael pluton. Figure 47 shows a possible mixing line. If the age of crystallization is assumed to be ~0.6 Ga (which actually is begging the question considering our present knowledge) the upper intercept of discordia is ~2.4 Ga, a not unreasonable age for the precursor rock based on the regional geology and Rb-Sr and Sm-Nd isotope data. In order to establish or discredit the hypothesis of inheritance, more zircon fractions will have to be analyzed. They will need to be variably abraded in order to obtain a dispersion of data points arrayed along the mixing line.

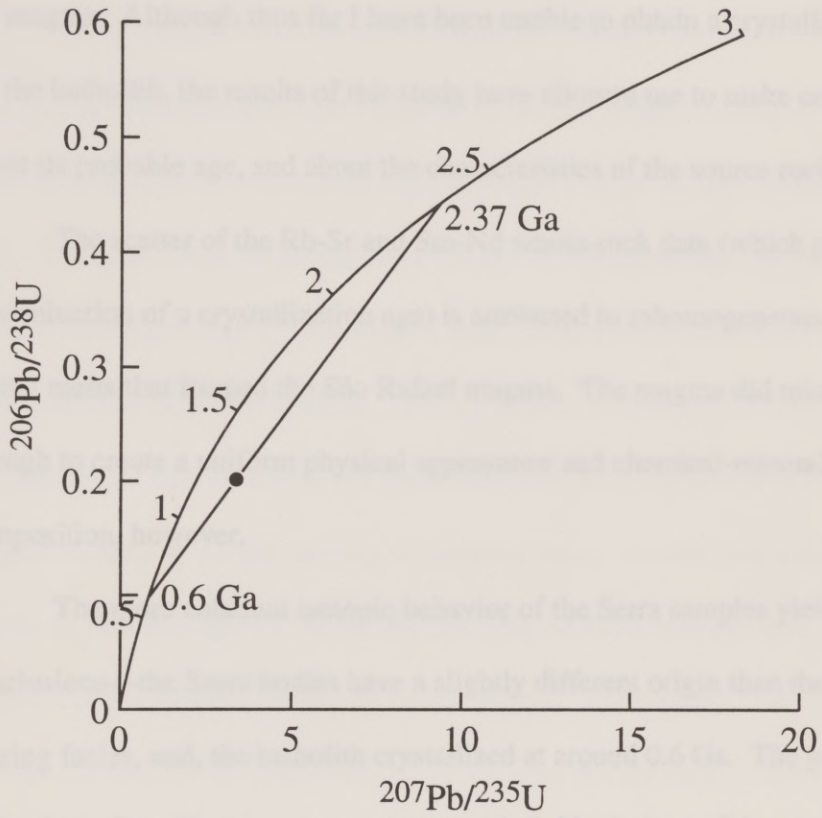

Figure 47. Concordia plot of preliminary U-Pb zircon data for DSR-13. The straight line represents a hypothetical mixing line, assuming a crystallization age of 0.6 Ga for the São Rafael batholith.

CONCLUDING REMARKS

The intent of this study was to date the São Rafael batholith by the Rb-Sr and Sm-Nd methods, and to characterize isotopic properties of the source rock of the magma. Although thus far I have been unable to obtain a crystallization age for the batholith, the results of this study have allowed me to make conclusions about its probable age, and about the characteristics of the source rock.

The scatter of the Rb-Sr and Sm-Nd whole-rock data (which precludes the determination of a crystallization age) is attributed to inhomogeneous mixing of partial melts that formed the São Rafael magma. The magma did mix well enough to create a uniform physical appearance and chemical-mineralogical composition, however.

The more coherent isotopic behavior of the Serra samples yields two conclusions—the Serra bodies have a slightly different origin than the epidote-bearing facies, and, the batholith crystallized at around 0.6 Ga. The poorly defined late Brasiliano age is consistent with field relations of the pluton, and is currently the best estimate of the crystallization age. On the isochron diagram, data for the Serra sample analyzed by the Sm-Nd method also plots off the trend of the epidote-bearing facies; this too supports a different origin for the Serra samples.

Mineral-whole-rock isochrons for the epidote-bearing facies and the Serra facies yield consistent cooling ages of 0.49 ± 0.01 Ga. These ages correspond well with other Rb-Sr and K-Ar cooling ages for the region (650-450 Ma).

ε_{Nd} and depleted mantle model ages calculated from whole-rock Sm-Nd data provide valuable information about the source of the São Rafael magma. They both lead to the conclusion that the source was an ancient enriched (crustal) rock. Sr initial ratios, assuming a 0.6 Ga age of crystallization, also support an ancient radiogenic source. Although a high initial Sr ratio is one of the characteristics of S-type granites, I favor an igneous source rock (I-type) because the São Rafael batholith does not show any other major characteristics of a magma formed by partial melting of metasediments. In addition, there was a source of Archean igneous rocks, for example Archean orthogneisses in the nearby Caicó Complex, basement to the foldbelt. Preliminary U-Pb zircon data also do not rule out the possibility of an Archean source rock. I interpret the discordance of the data point as reflecting the presence of relict zircon cores with inherited Pb from a rock with an age >2.0 Ga.

A possible scenario for the formation of the São Rafael batholith is as follows: At approximately 2.7 Ga, a crust formation event occurred, causing partial melting of a hypothetical depleted mantle reservoir, and enriching the melt in Nd. During the next 2 billion years this body of rock resided in the middle to

upper crust, becoming enriched in radiogenic Sr and Nd. At around 0.6 Ga, heat associated with the latter stages of the Brasiliano tectono-thermal event caused anatexis of the source body and emplacement of the São Rafael batholith. During this second partial melting event, the magma inherited a high initial Sr ratio from the source and there was also further enrichment of Nd relative to Sm. The magma, however, was comprised of partial melts with different isotopic characters which failed to mix completely. Cooling of the batholith had occurred by 0.49 Ga.

APPENDIX

Table A. Trace element analyses for epidote-bearing facies (ppm). From Souza (unpublished thesis); method of analysis unknown.

Element	KSR-2	KSR-3	KSR-4	KSR-5	KSR-7	KSR-8	KSR-9	KSR-10	KSR-11	KSR-13
Ba	1040	1130	1290	1280	1190	1340	1270	1190	1220	1620
Sr	10	660	860	820	810	760	920	710	510	610
Rb	47	47	58	42	75	60	49	58	39	74
Nb	36	<20	<20	20	<20	<20	<20	<20	<20	<20
Zr	160	250	106	160	60	220	59	220	240	250
Y	<10	12	10	12	<10	<10	<10	14	<10	12
Ta	<15	<15	<15	<15	<15	<15	<15	<15	<15	<15
Th	<15	<15	<15	<15	<15	<15	<15	<15	<15	<15
Hf	<200	<200	<200	<200	<200	<200	<200	<200	<200	<200

Element	KSR-5A	KSR-8A	KSR-9A	KSR-12A
Ba	2660	2620	1320	2680
Sr	800	370	660	750
Rb	87	100	89	99
Nb	<20	36	20	20
Zr	138	190	160	160
Y	12	61	18	25
Ta	<15	<15	<15	<15
Th	<15	<15	<15	<15
Hf	<200	<200	<200	<200

Table B. Trace element analyses for the Serra samples and DSR-29 epidote-bearing facies sample (ppm).

	DSR-20	DSR-25	DSR-26	DSR-28	DSR-29
BaO	994	814	1599	856	1368
Ce	38	23	26	27	33
Co	101	71	47	104	76
Cr2O3	33	40	25	28	76
Cu	40	35	71	18	55
Ga	16	16	16	16	17
Nb	12	12	10	10	12
Ni	36	30	18	7	36
Pb	33	22	21	21	26
Rb	68	50	50	51	63
Sr	352	411	484	439	707
Sc	5	5	1	6	4
Th	16	10	11	10	14
U	7	7	7	7	10
V	27	12	23	17	24
Y	16	15	9	12	16
Zn	33	40	42	38	38
Zr	87	113	115	103	122

Table C. REE abundances for the epidote-bearing facies (ppm). Analyzed by ICP. From Souza (unpublished thesis).

ELEMENT	KSR-2	KSR-3	KSR-5	KSR-7	KSR-9	KSR-11
La	16.57	17.44	22.59	16.99	17.75	16.02
Ce	34.36	34.89	47.13	33.25	37.82	32.91
Pr	-	-	-	-	-	-
Nd	14.66	15.53	21.58	15.37	17.38	14.00
Sm	2.43	2.47	3.58	2.56	3.16	2.17
Eu	0.77	0.75	1.06	0.78	0.93	0.70
Gd	1.74	1.88	2.79	1.90	2.27	1.59
Tb	-	-	-	-	-	-
Dy	1.63	1.45	2.52	1.73	2.11	1.00
Ho	0.31	0.30	0.52	0.35	0.42	0.23
Er	0.90	0.85	1.41	1.03	1.19	0.68
Tm	-	-	-	-	-	-
Yb	0.78	0.81	1.06	1.06	0.95	0.66
Lu	0.13	0.15	0.16	0.16	0.14	0.15

BIBLIOGRAPHY

Almeida, F. F. M., Hasui, Y., de Brito Neves, B. B., and R. A. Fuck, 1981. Brazilian structural provinces: an introduction: Earth Sci. Rev., v. 17, p. 1-29.

Anders, E. and N. Grevesse, 1989. Abundances of the elements: Meteoritic and solar: Geochim. et Cosmochim. Acta, v. 53, p. 197-214.

Archanjo, C. J., 1988. A deformação constrictional nos conglomerados da faixa Seridó: Anais XXV Congr. Bras. Geol., Belém, Brasil, v. 5, p. 2240-2247.

Awwiller, D. N., 1992. Geochemistry, mineralogy, and burial diagenesis of Wilcox Group shales, Texas gulf coast basin, unpubl. Ph.D. diss., The University of Texas at Austin, Austin, Texas, 239 p.

Blundy, J. D. and T. J. Holland, 1990. Calcic amphibole equilibria and a new amphibole-plagioclase geothermometer: Contrib. Miner. Petrol., v. 104, p. 208-224.

Brito Neves, B. B. de, Kawashita, K., and Pessoa, R. R., 1975. A posição estratigráfica do complexo Caicó: Proc VII Simp. Geol. Nord. Soc. Bras. Geol., p. 289-297.

Caby, R., Sial, A. N., Arthaud, M., and A. Vauchez, 1991. Crustal evolution and the Brasiliano orogeny in northeast Brazil in The West African Orogens and Circum-Atlantic Correlatives, Dallmeyer, R. D. and J. P. Lécorché, eds., Springer-Verlag, p. 373-397.

Caby, R., 1989. Precambrian terranes of Benin-Nigeria and northeast Brazil and the Late Proterozoic south Atlantic fit: GSA Special Paper #230, p. 145-158.

Castaing, C., Triboulet, C., Feybesse, J. L., and P. Chèvremont, 1993. Tectonometamorphic evolution of Ghana, Togo and Benin in the light of the Pan-African/Brasiliano orogeny: Tectonophysics , v. 218, p. 323-342.

Chappell, B. W. 1984. Source rocks of I- and S-type granites in the Lachlan Fold Belt, southeastern Australia. Phil. Trans. Royal Soc. London, v. A310, p. 693-707.

Chappell, B. W., and A. J. R. White, 1974. Two contrasting granite types: Pacific Geology, v. 8, p. 173-174.

Chappell, B. W., and A. J. R . White, 1992. I- and S-type granites in the Lachlan Fold Belt: Trans. Royal Soc. of Edinburgh: Earth Sciences, v. 83, p. 1-26.

Corsini, M., Vauchez, A., Archanjo, C., and E. F. J. de Sá, 1991. Strain transfer at continental scale from a transcurrent shear zone to a transpressional fold belt: The Patos-Seridó system, northeastern Brazil: Geology, v. 19, p. 586-589.

Dawes, R. L., and B. W. Evans, 1991. Mineralogy and geothermobarometry of magmatic epidote-bearing dikes, Front Range, Colorado: Geol. Soc. America Bull., v. 103, p. 1017-1031.

DePaolo, D. J., 1981. Neodymium isotopes in the Colorado Front Range and crust-mantle evolution in the Proterozoic: Nature, v. 291, no. 5812, p. 193-196.

DePaolo, D. J., 1988. Neodymium isotope geochemistry: An introduction. Springer-Verlag, 197 p.

DePaolo, D. J. and G. J. Wasserburg, 1976. Nd isotopic variations and petrogenetic models: Geophys. Res. Letters, v. 3, p. 249-252.

Getty, S. R. and L. P. Gromet, 1992. Geochronological constraints on ductile deformation, crustal extension, and doming about a basement-cover boundary, New England Appalachians: Am. Jour. Sci., v. 292, p. 359-397.

Hammarstrom, J. M. and E-an Zen., 1986. Aluminum in hornblende: An empirical igneous geobarometer: Am. Mineral., v. 71, p. 1297-1313.

Hine, R., Williams, I. S., Chappell, B. W., A. J. R. White, 1978. Contrasts between I-type and S-type granitoids of the Kosciusko batholith: J. Geol. Soc. Australia, v. 15, p. 219-234.

Hollister, L. S., Grissom, G. C., Peters, E. K., Stowell, H. H., and V. B. Sisson, 1987. Confirmation of the empirical correlation of Al in hornblende with pressure of solidification of calc-alkaline plutons: Am. Mineral., v. 72, p. 231-239.

Irvine, T. N., and W. R. A. Baragar, 1971. A guide to chemical classification of the common volcanic rocks: Can. Jour. Earth Sci., v. 8, no. 5, p. 523-548.

Jardim de Sá, E. F., and J. M. Sá, 1987. Proterozoic granitoids in a polycyclic setting: A field excursion in the Seridó region, NE Brazil: International Symposium on Granites and Associated Mineralizations, Salvador, Bahia, Brazil, January 21-31, 1987 Excursion Guide, p. 33-45.

Jardim de Sá, E. R., and J. Salim, 1978. Reavaliação dos conceitos estratigráficos na região do Seridó (RN-PB): Congr. Bras. Geol.,v. 30, Recife. 1978. Bol. Recife. SBG. p. 125.

Jardim de Sá, E. F., Macedo, M. H. F., Legrand, J. M., McReath, I., Galindo, A. C. and J. M. Sá, 1987. Proterozoic granitoids in a polycyclic setting: The Seridó region, NE Brazil: International Symposium on Granites and Associated Mineralizations, Salvador, Bahia, Brazil, January 21-31, 1987 Extended Abstracts, p. 103-109.

Johnson, M. C. and M. J. Rutherford, 1989. Experimental calibration of the aluminum-in-hornblende geobarometer with application to Long Valley caldera (California) volcanic rocks: Geology, v. 17, p. 837-841.

Johnston, A. D. and P. J. Wyllie, 1988. Constraints on the origin of Archean trondhjemites based on phase relationships of Nuk gneiss with H_2O at 15 kbar: Contrib. Miner. Petrol., v. 100, p. 35-46.

LeMaitre, R. W., 1989. A classification of igneous rocks and glossary of terms: Recommendations of the International Union of Geological Sciences on the systematics of igneous rocks, Blackwell Scientific Publ., Oxford, 193 p.

Lima, E. A. M., Torres, A. G., Wanderley, A. A., Brito, A. L. F., Vieira, A. T., Pereira, A. C. S., Medina, A. I. M., Barbosa, A. J., Vasconcelos, A. M., Aguiar, C. B. J., Jaeger, C. R. S., Amaral, C. A., Sato, E. Y., Silva, E. H. R. O., Fortes, F. P., Benevides, H. C., Leite, J. F., Moraes, J. F. S.,

Ribeiro, J. A., Nesi, J. R., Angelim, L. A. A., and M. E. V. Calheiros, 1980. Schemata do Seridó. Recife, DNPM/CPRM, v. 1-5, 1284p.

Lima, E. S. de, 1987. Evolução termobarométrica das rochas metapelíticas da região do Seridó, Nordeste Brasileiro: Rev. Bras. Geoc., v. 17, p. 315-323.

Lima, E. S. de, 1989. Evolução tectono-metamorfica durante o Proterozóico do segmento mediano do Dominio Estrutural Central, Nordeste do Brasil, Recife. Universidade Federal de Pernambuco, 137 p.

Liou, J. G., 1973. Synthesis and stability relations of epidote, $Ca_2Al_2FeSi_3O_{12}(OH)$: Jour. Petrol., v. 14, p.381-413.

Loiselle, M. C. and D. R. Wones, 1979. Characteristics and models for the origin of A-type granites. 54 p. (unpublished manuscript).

Lugmair, G. W., 1974. Sm-Nd ages: a new dating method: Meteoritics, v. 9, p. 369.

Macedo, M. H. F., Jardim de Sá, E. F., and J. M. Sá, 1984. Datação Rb-Sr em othogneisses e a idade do Grupo Seridó: Proc. XI Simp. Geol. Nord, Soc. Bras. Geol., p. 253-257.

McMurry, J., 1982. Petrology and Rb-Sr geochemistry of the Monte das Gameleiras and Dons Inês plutons, northeastern Brazil, unpubl. Master's thesis, University of Texas at Austin, 180 p.

Moench, R. H., 1986. Comment on "Implications of magmatic epidote-bearing plutons on crustal evolution in the accreted terranes of northwestern North America" and "Magmatic epidote and its petrologic significance": Geology, v. 14, p.187-188.

Naney, M. T., 1983. Phase equilibria of rock-forming ferromagnesian silicates in granitic systems: Am. Jour. Sci., v. 283, p. 993-1033.

O'Neil, J. R. and B. W. Chappell, 1977. Oxygen and hydrogen isotope relations in the Berridale Batholith: Jour. Geol. Soc. London, v. 133, p. 559-571.

Pessoa, R. R., Brito Neves, B. B. de, Kawashita, K., Pessoa, D. R., and A. R. Fuck, 1986. Contribuição ao estudo da evolução geocronológica do

maciço de Tróia, CE: Proc. XII Simp. Geo. Nord., Soc. Bras. Geol., João Pessoa, p. 75-93.

Poli, S. and M. W. Schmidt, 1992. A comment on "Calcic amphibole equilibria and a new amphibole - plagioclase geothermometer" by J. D. Blundy and T. J. B. Holland (Contrib. Mineral. Petrol. (1990) 104: 208-224). Contrib. Miner. Petrol., 111, p. 273-278.

Rutter, M. J., Van der Laan, S. R., and P. J. Wyllie, 1989. Experimental data for a proposed empirical igneous geobarometer: Aluminum in hornblende at 10 Kbar pressure. Geology, 17, p. 897-900.

Santos, E. Jose dos, 1964. Geologic map, Açu, RN quadrangle (SB-24-L-111).

Santos, E. Jose dos, and B. B. de Brito Neves, 1984. Província Borborema in O Pré-Cambriano do Brasil, Fernando F. M. de Almeida and Yociteru Hasui eds., Edgard Blucher Ltd., p. 123-186.

Santos E. J., Coutinho, M. G. N., Costa, M. P. A. and R. Ramalho, 1984. A direção de dobramentos Nordeste e a Bacia do Parnaíba, incluindo o craton de São Luiz e as bacias marginais in Geologia do Brasil, Schobbenhaus, C., Almeida Campos, D., Derze, G.R. and Asmus, H.E. eds., Dept. Nac. Prod. Mineral (SNPM), p. 131-189.

Schmidt, M. W., 1992. Amphibole composition in tonalite as a function of pressure: an experimental calibration of the Al-in -hornblende barometer. Contrib. Miner. Petrol., 110, p. 304-310.

Shand, S. J., 1951. The study of rocks. London, Thomas Murby and Co., 236 p.

Sial, A. N., 1987. Granitic rocks of northeast Brazil: International Symposium on Granites and Associated Mineralizations, Salvador, Bahia, Brazil, January 21-31, 1987 Extended Abstracts, p. 61-69.

Sial, A. N., 1990. Epidote-bearing calc-alkalic granitoids in northeast Brazil: Rev. Bras. Geoc., v. 20, p. 88-100.

Sial, A. N. and V. P. Ferreira, 1990. Granitoids in northeastern Brazil: Oxygen and sulfur isotope compositions and depths of emplacement: Jour. S. Am. Earth Sci., v. 3, p. 103-112.

Sial, A. N., Ferreira, V. P., and L. E. Long, in press. High $\delta^{18}O$, high Al-hornblende, epidote-bearing granitoids in northeast Brazil.

Souza, K. de. Petrologia e geoquímica do batólito granítico cálcio-alcalino Brasiliano de São Rafael (RN) e o significado barométrico de epidoto magmático, unfinished Master's thesis, Federal University of Pernambuco, Recife, Brazil.

SUDENE, 1985. Topographic map, Açu, RN quadrangle (SB.24-X-D-V, MI-975), Diretoria de Serviço geográfico.

Tulloch, A. J., 1979. Secondary Ca-Al silicates as low-grade alteration products of granitoid biotite: Contrib. Miner. Petrol., v. 69, p. 105-117.

Tulloch, A. J., 1986. Comment on "Implications of magmatic epidote-bearing plutons on crustal evolution in the accreted terranes of northwestern North America" and "Magmatic epidote and its petrologic significance": Geology, v. 14, p. 186-187.

Vance, J. A., 1969. On synneusis: Contrib. Miner. Petrol., v. 24, p. 7-29.

Wasserburg, G. J., Jacobsen, S. B., DePaolo, D. J., McCulloch, M. T., and T. Wen, 1981. Precise determinatin of Sm/Nd ratios, Sm and Nd isotopic abundances in standard solutions: Geochim. et Cosmochim. Acta, v. 45, p. 2311-2323.

Wernick, E., 1981. The Archean of Brazil: Earth Sci. Rev., v. 17, p. 31-48.

Zen, E-an, 1985. Implications of magmatic epidote-bearing plutons on crustal evolution in the accreted terranes of northwestern North America: Geology, v. 13, p. 266-269.

Zen, E-an, 1989. Plumbing the depths of batholiths: Am. Jour. Sci., v. 289, p. 1137-1157.

Zen, E-an and J. M. Hammarstrom, 1984. Magmatic epidote and its petrologic significance: Geology, v. 12, p. 515-518.

Zen, E-an and J. M. Hammarstrom, 1986. Reply on "Implications of magmatic epidote-bearing plutons on crustal evolution in the accreted terranes of northwestern North America" and "Magmatic epidote and its petrologic significance": Geology, v. 14, p. 188.

The vita has been removed from the digitized version of this document.